ENERGY USE FORECAST AND MODEL PREDICTIVE CONTROL OF BUILDING COMPLEXES

BY SEYEDABOLFAZL TAGHIZADEHVAGHEFI

A dissertation submitted to the

Graduate School—New Brunswick

Rutgers, The State University of New Jersey

in partial fulfillment of the requirements

for the degree of

Doctor of Philosophy

Graduate Program in Industrial and Systems Engineering

Written under the direction of

Mohsen A. Jafari

and approved by

_____

_____

_____

_____

_____

New Brunswick, New Jersey

October, 2014

ABSTRACT OF THE DISSERTATION

ENERGY USE FORECAST AND MODEL PREDICTIVE CONTROL OF BUILDING COMPLEXES

by SEYEDABOLFAZL TAGHIZADEHVAGHEFI

Dissertation Director: Mohsen A. Jafari

U.S. households and commercial buildings consume approximately 40 percent of total energy conversion in the U.S. and account for 72 percent of total U.S. electricity consumption. Commercial building energy demand, in particular, doubled between 1980 and 2000 and has increased 50 percent since then. Developing innovative technologies and building energy-efficiency methods are therefore essential for U.S. national interests and a sustainable energy future.

In this thesis, an optimal framework for forecasting and optimization of energy consumption for building complexes is developed. For forecasting purposes, a hybrid time series-regression model is introduced to combine regression models and seasonal autoregressive moving average models to accurately forecast energy usage at both the building and the community/campus level. For optimization purposes, this thesis proposes an optimal control strategy at the building level, which consists of two main phases. In the first phase, a set of offline data either generated by a whole building simulation platform or measured from a real building is used to develop models that capture the dynamic behavior of building energy usage. In the second phase, the models are fed

into an optimization model that computes the optimal control variables of the building. The optimization model is a Multi-objective Dynamic Programing model that minimizes total operating energy cost and demand charges as well as total deviation from thermal comfort bounds. In addition, the proposed control strategy is adaptive, so that it updates both the estimation and the optimization steps as soon as it receives new measured data.

A data-driven risk-based framework is also proposed to predict and control industrial loads in non-residential buildings. In this framework, a set of predictive analysis tools are employed to allocate industrial load profiles into a particular set of classes. Load profiles within the same class have lower variance and follow the same pattern. Then, a generalized linear model (GLM) is used to predict the probability of having stochastic industrial loads coming online over rolling time windows. Finally, for controlling demand response to avoid demand charges, the proposed framework provides the necessary tools to institute load shedding or load shifting strategies.

Acknowledgements

It would have been almost impossible to accomplish this dissertation without the help and support of many people. I am greatly humbled for all their support and assistance. First and foremost, I wish to express my sincerest gratitude to my advisor, Professor Mohsen Jafari, who has been an exemplary mentor and an awesome character in all aspects. He is such a creative academician, a profound thinker and more importantly, an extremely committed person to human and ethic core values. He is a lifetime friend whom I can always trust.

I have been so grateful to have valuable comments, great support, and friendship of my co-advisor Professor Jack Brouwer and my committee members Dr. Yan Lu, Dr. Melike Baykal-Gursoy and Dr. Myong-K. Jeong. I would like to thank all of you for your constructive suggestions, technical comments and continuous support.

During my course of study, I have been privileged to receive several Awards and Scholarships. I would like to thank CAIT for their continuous support during my Ph.D. years. I was particularly honored to receive Professor Tayfur Altioks Scholarship and would like to take this opportunity to thank Professor Tayfur Altioks family for their support. I will never forget the unique personality of Professor Altiok, his manner and his integrity. I also have to thank the Department of Industrial and Systems Engineering, Siemens Research Corporate as well as the Advanced Power & Energy Program (APEP) in University of California, Irvine for all their support.

I am very lucky to be surrounded by so many brilliant and talented friends, whose support, ideas, and academic suggestions have inspired me in my research career and I thank all of them. I am particularly thankful to Majid Eyvazian and Ali Nouri for their generosity. I would like also thank Helen Pirrello for her great help and support.

Last, but by no means least, I would like to send special thanks to my lovely family and extraordinary wife, Saeide, for their unconditional love and support and encouragement. I am blessed with having the warmest and friendliest parents, brothers and sister ever, whom I shared the best time of my life with in Iran. Aziz, my beloved grandmother, I first started my journey with you, when I was in my first year of school in Iran. I still remember how you solved my problem when I could not find a 12 colored pencil set and you bought two 6 colored ones for me! Saeide, thank you so much for always being there for me, during all those happy times with love and laughter, during hard times, with never-failing sympathy and encouragement during busy times with patience and support. Lets keep appreciating all the little things and living in the moment.

Table of Contents

Chapter 1

Introduction

1.1 Motivation

With 19% share of the global energy usage in 2010 the United States is the second largest energy consumer in the world. U.S. households and commercial buildings, in particular, account for 41% of all energy consumed in the country. This is 44% more than the transportation sector and 36% more than the industrial load. In other words, approximately 7% of the worlds primary global energy is solely consumed in the U.S. by residential and nonresidential buildings [1]. In addition, commercial building energy demand doubled between 1980 and 2000 and has increased by 50 percent since then [2]. Therefore, developing innovative engineering methods and energy-efficient building technologies are necessary more than ever as the country faces dwindling non-renewable energy sources [3]. Among all building services and electric appliances, the amount of energy consumed by cooling and heating systems, at about 50 percent, has the major contribution [4].

This motivates many researchers and practitioners to pay higher attention to developing novel technologies and methods for improving building cooling and heating systems. Heating, Ventilation and Air Condition (HVAC) systems, for example, have increasingly been moving toward energy-efficient technologies since the 1980s. Combined Cooling, Heating and Power (CCHP) is another example, which is often identified as an alternative for solving energy-related and environmental issues [5]. Although new technologies and innovative methods have been significantly contributing to improving energy consumption, there are still many potentials for energy-use reduction. The problem is that most commercial or residential building loads are highly dynamic

and complicated, making the existing systems less cost effective and less attractive to end-users.

With this background in mind, we are motivated to propose a novel framework to model, forecast and optimally control the dynamic behavior of building electrical, heating and cooling loads under certain operational constraints. The existing control strategies have often been driven by two approaches: High fidelity models that are based on physical characteristics of buildings and load dynamics of the cooling/heating system. These models are often too complex to be analytically solved or implemented in real cases. Therefore, researchers often make restrictive assumptions in order to obtain approximate solutions [8, 9]. In the second approach, an individual metamodel is developed for whole-building energy consumption using statistical or soft computing techniques. These models discover and capture the relationship between the energy consumption and a set of environmental or physical variables. However, the problem is that such approximate models may not adequately capture a considerable portion of energy dynamics, as the physical relationships between building components and environmental variables are complex [6].

To address these problems, our proposed framework utilizes the advantages of both approaches and propose a combined physical/statistical model for capturing energy dynamics separately for each zone. The zonal decomposition significantly simplifies the calculation of the heat balance equations and building load dynamics. The zonal calculations are fed into a statistical model that represents the total building energy use. The same approach is also used for optimization and control purposes, so that state variables are defined and updated independently for each zone, but the energy minimization is carried out over the whole building.

A data-driven risk-based framework is also proposed in Chapter 5 to predict and control industrial loads in non-residential buildings. The proposed framework consists of two major steps: In the first step, it employs a set of predictive analytics tools to capture and predict the patterns of industrial load profiles. These tools can also estimate the probability of the day-ahead load pattern. Once the patterns of industrial loads are

determined, a risk analysis method is used to evaluate the worst-case, best-case, and most-likely estimations of energy cost. Any demand response programs can be analyzed for worst-case, best-case, and most-likely scenarios and the best action can be selected accordingly.

1.2 Synopsis of Contributions

1.2.1 Modeling and Forecasting Cooling and Electricity Load Demands

In Chapter 2, the main objective is to extend a statistical approach to effectively provide look-ahead forecasts for cooling and electricity demand load over time. The statistical model proposed in this chapter is a generalized form of the CochraneOrcutt estimation technique that combines a multiple linear regression model and a seasonal autoregressive moving average (ARMA) model. It simultaneously fits a linear regression and a time series model to the load data while maintaining LSE (least square estimate) conditions. The proposed model is adaptive so that it updates residual and forecast values every time new information on cooling and electricity load are received. Therefore, the model can simultaneously take advantage of two powerful statistical methods, time series, and linear regression in an adaptive way. The performance of the proposed model is shown through two real examples.

1.2.2 Optimal Control Strategy for Building Cooling/Heating Systems

In Chapter 3, we propose a framework for modeling, forecasting and optimization of building cooling/heating systems. This framework integrates a physics-based model with a data driven time-series model to forecast and optimally manage building energy. To do this, first a zonal cooling/heating model is proposed based on the energy balance equations and the least squares estimation (LSE) technique is employed to analytically estimate the model parameters. The data required to obtain estimation values are

either collected from an actual building or generated by a whole-building simulation model. The zonal cooling/heating model is then fed into a forecast model to provide the look-ahead forecast values of total building energy consumption. The forecast model is similar to the model presented in Chapter 2. The forecast values are finally used to find the optimal building set point values for a finite horizon. The optimization model is a multi-objective mathematical programing that minimizes total operating energy cost and demand charges as well as total deviation from thermal comfort bounds. In addition, the optimization model is an adaptive dynamic control, so that the forecast values are updated and optimization process is repeated, every time that new data on energy or internal temperature is received. The novelty of the proposed framework is on the specific combination and application of data-driven methods to optimize energy control of large buildings, which are subject to stochastic externalities. In particular, the methodology integrates a physics-based zonal model with an advanced time series model to ensure enhanced accuracy and sensitivity of energy forecasts to incremental changes in control variables.

1.2.3 Extensions of Optimal Control Strategy for Building Cooling/heating Systems

In Chapter 4, several extensions are provided to improve the performance of the optimal control strategy and to adjust it to a wider range of practical cases. Instead of using a physical/statistical model, in this chapter, a regression model is proposed to find the correlation between required cooling/heating power for each zone and a number of input variables including the current and past zone internal temperatures, external temperature, and time-related variables. By relaxing the physical form of the heat balance equations, and by adding time-related variables, the proposed model can appropriately fit with data and can provide accurate forecast values. In addition, we improve the structure of our multi-objective dynamic programing to be able to adequately consider daily as-used demand charge. In the kth step of the dynamic programing algorithm, the maximum energy used in previous hours is obtained based on the highest energy

usage from time t to t+k, given the optimal cost-to-go at step k.

1.2.4 Predictive Analytics Approach to Modeling Building Industrial Loads

A predictive analytics approach is proposed in Chapter 5 to capture the behavior of non-stationary industrial loads in non-residential buildings. The proposed approach consists of an *exploratory data analysis* (EDA) to better understand the main characteristics of industrial load data and to select appropriate statistical tools. It also includes a high-dimensional clustering method to assign industrial load profiles into smaller groups with less variability and same patterns. This approach employs a classification method to estimate the best class that matches with any new load profiles. Ultimately, once the appropriate classes of future load profiles are determined, the proposed approach provides a cost-based risk analysis to calculate and evaluate the total risk of energy decisions for the next day. This is coupled with a utility function structure to help decision makers to take best demand-side actions.

1.3 Brief Overview of Thesis Accomplishments

The proposed work intends to address the following problems:

1. Statistical modeling and forecast of cooling and electricity demand loads in both building and community levels. The following models and tools are introduced and applied:

   (a) A hybrid time series-regression model is proposed based on a generalized Cochran-Orcutt estimation technique to forecast the campus/building energy consumption.

   (b) A set of data visualization techniques, such as box plot, scatter plot, auto-correlation function (ACF) and partial auto-correlation function (PACF) plots, are employed to extract the existing patterns of energy data and to discover useful knowledge and information used for forecast proposes.

2. Optimal control of building cooling/heating systems to minimize building total cost of energy as well as total deviation from thermal discomfort. The following models and tools are introduced and applied:

   (a) A zonal cooling/heating model is proposed based on the energy balance equations and the least squares estimation (LSE) technique to forecast the zonal internal temperature and the effective power rate.

   (b) An energy forecast model is built to provide the k-hour-look-ahead forecasts ($k = 1, 2, ..., 24$) for the total building energy use. The models inputs are the effective cooling power and the external temperature and the output is the forecasted as total energy consumption.

   (c) A Multi-objective Dynamic Programming problem that is formulated to minimize total operating energy cost, demand charge as well as total deviation from thermal comfort bounds.

   (d) The weighted l_p metric method is implemented to combine both objective functions of the Multi-objective Dynamic Programming problem (total cost of energy and total deviation from thermal comfort).

3. Extended optimal control strategy to improve the performance of the proposed heating/cooling forecast model and the optimal control strategy. The following revised models and extensions are considered in Chapter 4:

   (a) The extended cooling/heating model, including time-related indicator variables and smaller time slots is proposed to capture more variability within building cooling/heating data.

   (b) The dynamic programing is revised to improve the performance of the optimal control strategy.

4. The data-driven risk analysis approach to predict the industrial load patterns and to evaluate and select the best demand response program(s). The following predictive analytics and risk-based tools are developed or used in Chapter 5:

(a) Predictive analytics methods are proposed to capture the industrial load patterns and to estimate the probability of having specific pattern.

(b) Cost-based risk analysis is also developed to obtain the most likely, pessimistic and optimistic estimations of the building energy cost.

(c) A utility-based approach is proposed to evaluate the risk of different demand response programs and to select the best scenario based.

Chapter 2

Modeling and Forecasting of Cooling and Electricity Load Demand

2.1 Introduction

The objective of this chapter is to extend a statistical approach to effectively provide look-ahead forecasts for cooling and electricity demand load. The statistical model proposed in this chapter is a generalized form of a CochraneOrcutt estimation technique that combines a multiple linear regression model and a seasonal autoregressive moving average model. The proposed model is adaptive so that it updates forecast values every time that new information on cooling and electricity load is received. Therefore, the model can simultaneously take advantage of two statistical methods, time series, and linear regression in an adaptive way. The effectiveness of the proposed forecast model is shown through two use cases. The first example utilizes the proposed approach for economic dispatching of a combined cooling, heating and power (CCHP) plant at the University of California, Irvine. In the second case, the proposed model is treated as an approximation to EnergyPlus for the APEP building at the University of California, Irvine. The results reveal the effectiveness of the proposed forecast model. The forecast values of cooling and electricity demand load can be fed into any optimization model to minimize the total energy consumption.

Combined Cooling, Heating and Power (CCHP) systems can significantly contribute to reduction in buildings energy use, curtail pollutant and carbon emission, and help to reduce risks of blackouts and brownouts in the utility grid [5-7]. CCHP technology integrates processes of production and simultaneous use of cooling, heating, and power at a single site. However, since most commercial and industrial electrical loads

are highly dynamic and typically not synchronized with local heating and cooling demands, advanced control strategies will be imperative to economic dispatch of CCHP resources. A wide range of optimal control strategies has been proposed to improve the CCHP operation based on different objectives including power flow, capacity, operation, energy-use and environmental considerations [8-17]. A common element in almost all optimal control strategies is to have an accurate estimation of cooling, heating, and electricity load demands. Some researchers assume that load demands are known and available over a specific period [11, 14].The existing works in the literature typically assume that cooling and electricity demand forecasts are exogenously given [14]. However, cooling and electricity demands are typically difficult to model mainly because of the complex interactions between plant facilities and equipment, e.g. HVAC (heating, ventilation, and air conditioning), chillers and turbines yields. Ref. [11] points out that in practical applications, the exact future load profile does not exist; and forecasting methods should be taken into consideration by researchers.

A number of researchers employ building simulation platform to generate building load demand based on its physical characteristics and other dynamic input variables such as occupancy, weather, and time information. The cooling and electricity load demands are outputs of running the simulation and are then fed into the optimization model [15-17]. However, the quality of results highly depends on quality of the simulation models and their inputs. In addition, for any CCHP optimization, a detailed building simulation model needs to be accordingly built and run repeatedly. Another way to deal with this problem is to consider uncertainty in CCHP optimization model. Hu and Cho [15] for instance, propose an optimization model with some probabilistic constraints to guarantee that the model is reliable to satisfy the stochastic load demand. They assume load demands are independent and follow normal distributions in which 95% of the area is within the range of 20% of the average load demands. Another approach to this problem is to develop a forecasting model and embed it into the optimization model. This is the main motivation of this work. In this chapter, CochraneOrcutt estimation technique is used as an effective linear model to provide look-ahead forecasts

for cooling and electricity demand load. It simultaneously fits a regression model and a time series to the data while maintaining least square estimate (LSE) conditions. In addition, the forecast values are modified when a new data is received from the real system. The proposed model is currently working as a part of an integrated optimal dispatch for CCHP plant at the University of California, Irvine and providing accurate forecasts for the entire campus cooling and electricity load demand.

2.2 Background Study

In most real cases, cooling and electricity load demands are highly dynamic oscillating within a wide range of values during course of a day. This is mainly because several physically explicit or latent factors can instantaneously influence cooling and electricity demand patterns. These factors can be any one of the following types: (i) Static factors that are usually set at the design stage and only change due to ageing wear and tear. Building characteristics, CCHP components, chiller types and generator nominal capacities are examples of such factors; (ii) Environmental variables extrinsic to the building, such as climate and weather data; (iii) operational variables, e.g. cooling/heating set point values, lighting, time schedule to operate various equipment and system components within plant or building; and (iv) uncontrollable dynamical variables, such as number of occupants at any time, noise due to structural variations etc. It is ideal to know all these factors and their impacts on energy dynamics in order to optimally forecast and control cooling and electricity demands for single building or a cluster of buildings. However, a complete forecast model is not practically attainable due to unknown significant dynamical variables, lack of tools to measure their effects, or that some of these variables are uncontrollable. Therefore, a wide range of different methods has been proposed to model and forecast load dynamics. In overall, these methods can be categorized into three general approaches.

In the first approach, a linear or nonlinear statistical model is used to explain the variability of response (load or energy dynamics) over time. The most popular example of such statistical models is Box and Jenkins time series paradigm where load demands

are estimated based upon a linear combination of their past values [18-20] There are a large family of different models in this category that can deal with many special cases including seasonality, non-stationary, and non-homogeneity of variances (see e.g. [21, 22]). The major drawback of such models is that the future values are typically forecasted based upon the past and present values of cooling and electricity load demands without considering any exogenous factors in the model [23-25].

Another example of statistical approach is using regression models (metamodel) where the variability within response is modeled via a number of exogenous factors [26-30]. The major problem of such models is that they often ignore the complex interactions between exogenous factors, which may result in less accurate forecast values. To overcome this problem, a number of studies use a hybrid approach, which employs the main components of both above-mentioned approaches [31-33]. Autoregressive with exogenous variable (ARX) and autoregressive moving average with exogenous variable (ARMAX) are two examples of this approach. Although these models perform effectively in many cases, they have many parameters to be estimated since all input and output variables with their past and current values should appear in the forecast model.

The second approach employs artificial intelligence to find the k-step ahead forecasts for load demand. A broad range of numerical methods can be included in this category. Refs. [34] and [35] a comprehensive review of AI techniques in some areas of energy. Although their techniques are not directly related to load forecasting, however, they can easily be used with minor changes. Artificial neural network (ANN) is among most frequent AI techniques and has been widely used in load or energy forecasting. ANNs have particularly evolved based upon different settings of neuron arrangement, neuron connections, training techniques, and internal layers and become a powerful competitor for statistical methods [36-40]. They can be designed to include both past observation of cooling and electricity demands and associated exogenous factors. The main disadvantage of AI approach is that they are often black box and do not show any explicit relationship between response an input variables. For example, the hidden layers of ANNs are difficult to explain and cannot be appeared in an explicit forecasting

equation [41].

In addition, by developing computational methods, a third approach has recently been developed which is a combination of any abovementioned techniques. The main purpose of this hybrid approach is to improve the accuracy of the forecast values by combining different numerical-analytical methods. Some hybrid methods also partially include the physical aspects of the real system in their computation and come up with a mixed physical-numerical method, which is often referred to as grey models [41]. A few applications of hybrid models in the area of energy can be found in [42, 43].

The proposed model can be classified in the statistical groups. It first fits a linear regression to find the correlation between the cooling and electricity load demands and exogenous factors. Any variability that cannot be explained by regression models can be aggregated in residual terms. Then, a seasonal time series model is applied to the residuals to express the remaining variability. Since, the regression parameters should be estimated using least square error method, the process of parameters estimation is applied iteratively and simultaneously. Further details will be explained in the next section.

2.3 Problem Statement

The common assumption of uncorrelated random error terms ε's made in basic regression models is not appropriate to forecast building energy consumption. Historical data shows that error terms are frequently correlated (often positively) over time [44]. In particular, this typically happens when there are some uncontrollable, unknown, or non-measurable input variables. A special case for the regression model with auto-correlated data can be shown as follows:

$$y_t = \sum_{j=0}^{k} \beta_j x_{tj} + \varepsilon_t,\ \varepsilon_t = \xi(\varepsilon_{t-1}, ..., \varepsilon_{t-q}) + \alpha_t, \tag{2.1}$$

where $\xi(.)$ is a function of previous error terms ε's, y_t is the power consumed at time t and x_{tj} is the jth input variable affecting the building energy consumption at time t and α_t is a white noise. The error terms are typically modeled using Box

and Jenkins model as a first order auto-regressive model. A preliminary study of our historical data on cooling and electricity load demands indicates a seasonal pattern with lag of 24 hours. Therefore, the error terms in Equation (2.1) is generalized to include seasonal patterns. To do this, assume that p, q, P and Q are the order of non-seasonal and seasonal autoregressive and moving range parts respectively, and s is the seasonal order. Then a general ARMA model for error terms can be written as follows:

$$\phi_p(B)\Phi_P^s(B)\varepsilon_t = \theta_q(B)\Theta_Q^s(B)\alpha_t, \tag{2.2}$$

where ϕ_p and Φ_P^s are autoregressive operators, θ_q and $\Theta_Q^s(B)$ are moving average operators and B is backward operator. s is set equal to 24 showing the significance of autocorrelation between loads of same time in two consecutive days. Let

$$\phi_p(B)\Phi_P^s(B) = 1 - \Psi(B),$$

then

$$\varepsilon_t = \Psi(B)\varepsilon_t + \theta_q(B)\Theta_Q^s(B)\alpha_t, \tag{2.3}$$

Furthermore, Equation (2.2) can be written as follows:

$$y_t = \sum_{j=0}^{k}\beta_j x_{tj} + \varepsilon_t \sum_{i=0}^{p}\sum_{j=0}^{P}(-1)^{i+j-1}\phi_i\varphi_j B^{i+s\times j} + \alpha_t \sum_{i=0}^{q}\sum_{j=0}^{Q}(-1)^{i+j}\theta_i\Theta_j B^{i+s\times j}. \tag{2.4}$$

Note that $\phi_0 = \varphi_0 = 0$ and $\theta_i = \Theta_j = 0$. For example, for the ARMA$(1,0)(1,0)_n$ we have

$$\begin{aligned} y_t &= \sum_{j=0}^{k}\beta_j x_{tj} + \varepsilon_t(\phi B + \varphi_1 B^{24} - \phi.\varphi_1 B^{25}) \\ &= \sum_{j}\beta_j x_{tj} + \phi\varepsilon_{t-1} + \varphi_1\varepsilon_{t-24} - \phi.\varphi_1\varepsilon_{t-25} \end{aligned} \tag{2.5}$$

The main significance of Equation (2.4) is that it includes seasonal error and tends to capture statistical similarities between two periods, which are n hours apart. The major problem of multiple linear regression with auto-correlated error terms is the estimation of coefficients. With auto-correlated error terms, the ordinary least square

(OLS) procedures can be misleading and does not guarantee estimation with the minimum variance [44]. To overcome this problem, Cochrane and Orcutt [45] proposed a transformation when error terms follow a first order autoregressive process. According to Cochrane-Orcutt model, one should transform the response values in such a way that $\acute{y_t} = \varphi_p(B)\Phi_P^s(B)Y_t$, $\acute{\mathbf{x}_t} = \phi_p(B)\Phi_P^s(B)\mathbf{x}_t$ and $\acute{\beta_0} = \phi_p(B)\Phi_P^s(B)\beta_0$, Therefore, Equation (2.4) can be replaced by:

$$y'_t = \beta'_0 + \mathbf{x'}_t\beta'_t + a_t \tag{2.6}$$

Equation (2.6) is an ordinal multiple linear regressions with independent error terms and can be calculated via OLS estimation method. As a result, the fitted linear function $\acute{y_t} = \beta'_0 + \mathbf{x'}_t\beta'_t$ can eliminate the autocorrelation structure of the error terms. The following algorithm summarizes our approach:

2.3.1 Algorithm

Step 1 Divide the original dataset into two subsets: training dataset and testing dataset, which are used for model estimation and model verification respectively and denoted by Ω_1 and Ω_2. Set i=0.

Step 2 Fit a multiple regression model to training subset and estimate vector of $\hat{\boldsymbol{\beta}}^i$ in $\mathbf{y'}^i{}_1 = \mathbf{X}_1\hat{\boldsymbol{\beta}}^i$, where $\mathbf{y}_1, \mathbf{X}_1 \in \Omega_1$ are response (cooling or electricity load demand) and independent variables (exogenous variables). Then calculate initial residual values by $\hat{\varepsilon}^i = \mathbf{y}_1 - \mathbf{y'}^i{}_1 = \mathbf{y}_1 - \mathbf{X}_1\hat{\beta}^i$.

Step 3 If $\hat{\boldsymbol{\varepsilon}}^i$'s are correlated then fit an ARMA model, i.e. $\hat{\varphi}_p^i(B)\hat{\Phi}_P^{si}(B)\varepsilon_t^i = \hat{\theta}_q^i(B)\hat{\Theta}_Q^{si}(B)\alpha_t$, and find estimation values for $\hat{\varphi}_p^i(B)$, $\Phi_P^{si}(B)$, $\hat{\theta}_q^i(B)$ and $\hat{\Theta}_Q^{si}(B)$ using least square error technique or other estimators (See [14] for further details about estimation procedures).

Step 4 Apply following transformations $\acute{y}_{1t}^i = \varphi_p^i(B)\Phi_P^{si}(B)y_1$, $\acute{\mathbf{x}_{1t}} = \phi_p^i(B)\Phi_P^{si}(B)\mathbf{x}_{1t}$ on $\mathbf{y}_1, \mathbf{X}_1 \in \Omega_1$.Then fit a new multiple regression model to transformed subset and estimate vector $\hat{\boldsymbol{\beta}}'^i$ where $\mathbf{y'}^i{}_1 = \mathbf{X'}^i{}_1\hat{\boldsymbol{\beta}}'^i$.

Step 5 Check $[\left|\hat{\boldsymbol{\beta}}'^{i} - \hat{\boldsymbol{\beta}}'^{i-1}\right| < \delta$; if true then set $\hat{\boldsymbol{\beta}}' = \hat{\boldsymbol{\beta}}'^{i}$ and go to Step 6. Otherwise, calculate the residual values by $\hat{\boldsymbol{\varepsilon}}^{i} = \mathbf{y}_1 - \mathbf{y}'^{i}{}_1 = \mathbf{y}_1 - \mathbf{X}'^{i}{}_1\hat{\boldsymbol{\beta}}'^{i}$ and go to Step 3.

Step 6 Apply anti-transformations $\beta'_0 = \varphi_p(B)\Phi^s_P(B)\beta_0$ for and $\hat{\beta}_{\neq \mathbf{0}} = \hat{\beta}'_{\neq \mathbf{0}}$ and use them in Equation (2.1).

It is quite common to use the estimated parameters as well as subset Ω_2 to check the adequacy of the given model. In this study, we employ coefficient of determination R^2 and adjusted coefficient of determination R^2_{adj} as measures for model adequacy checking. These measures can be calculated as follows:

$$R^2 = \frac{\hat{\boldsymbol{\beta}}'^{T}\mathbf{X}'^{T}{}_2(I-H)\mathbf{X}'_2\hat{\boldsymbol{\beta}}'}{\mathbf{y}'^{T}{}_2\left(I-(1/n)J\right)\mathbf{y}'_2} \tag{2.7}$$

and

$$R^2_{adj} = \frac{\hat{\beta}'^{T}\mathbf{X}'^{T}{}_2(I-H)\mathbf{X}'_2\hat{\beta}'/k-1}{\mathbf{y}'^{T}{}_2\left(I-(1/n)J\right)\mathbf{y}'_2/n_2-k} \tag{2.8}$$

where k is number of exogenous variables, n_2 is sample size for testing dataset , I is identity matrix and H can be calculated by $H = \mathbf{X}_2(\mathbf{X}^T{}_2\mathbf{X}_2)^{-1}\mathbf{X}^T{}_2$ as well. R^2 and R^2_{adj} are both between 0 and 1 and explain the percentage of variation that is explained by model. A closer value to 1 depicts a better model.

2.4 Case studies and Experimentation

In this section, the forecast model is employed as a part of optimal dispatching of a CCHP plant at the University of California, Irvine. Cooling and electricity forecast values are fed into an optimal control strategy, which searches for optimal set points for 24 hours ahead. The forecast model then is used to compute optimal control values to minimize energy consumption during course of a day in a building.

2.4.1 Combined Cooling, Heating and Power System

The UC Irvine Central Plant consists of eight electric chillers, providing cold water, a 13.5 MW gas turbine (GT), a 5.7 MW steam turbine (ST), thermal energy storage (TES) tank, and a heat recovery steam generator (HRSG). It provides heating and cooling loads for the entire campus as well as the majority of the campus electric loads. The chillers are able to supply as much as 14500 tons (51 MW) and the steam driven chiller can provide an additional 2000 tons (7 MW). The TES tank capacity is 60000 ton-hour (211 megawatt-hour) which is able to shift, on average, 65% of the cooling load during the day to the night when electricity prices are lower and temperature is cooler.

Figure 2.1 provides a schematic of the plant, where GT is the primary source of electric power providing electricity for the campus and for the chillers. As a byproduct, the gas turbine generates the exhaust gas, which can be source of extra thermal energy. Such energy is then used to produce steam using HRSG unit. HRSG can supply 23500 kg/hour and 54000 kg/hour without and with duct fire, respectively. The generated steam drives the steam turbine (ST). The steam can also be used to produce hot water for the campus needs. A portion of the produced steam is also transferred to use in a steam chiller unit. GT and ST supply about 85% of the total electrical needs on the campus with the balance being served by utility import (14%) and an 893 kW-fixed panel solar photovoltaic (1%).

As mentioned, the electricity produced by two generators are either sent directly to the campus to satisfy electricity demand or supplied as the energy input to the electrical chiller (see [14] for more details), which is mainly responsible to provide cold water. Cold water can be either directly supplied to the campus to meet campus cooling needs or stored in the TES tank for later use. Hence, the chillers and the TES together are the main sources for the campus cooling demands. Any additional electricity demand is provided from the grid.

Such a CCHP system is able to produce thermal energy along with electricity over

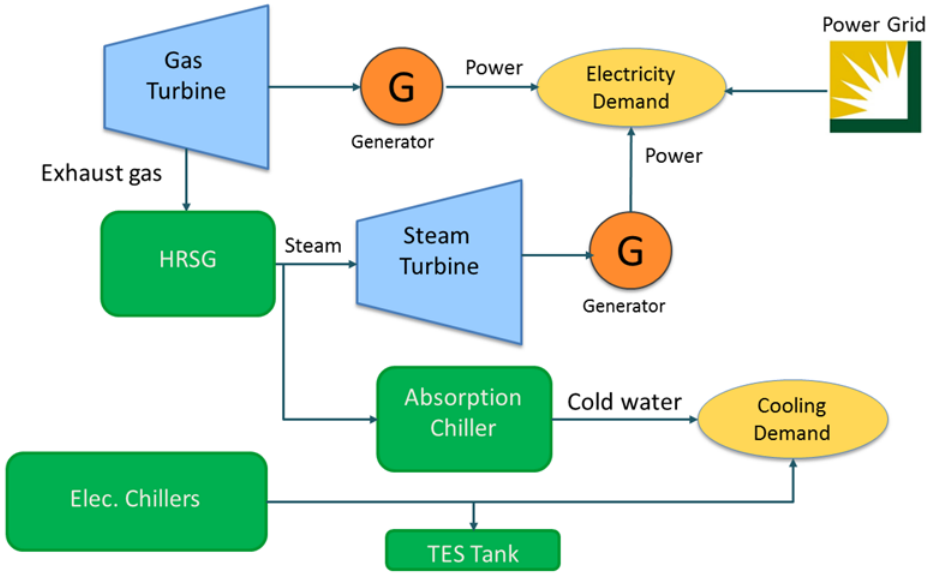

Figure 2.1: Schematic Framework of CCHP plant at University of California, Irvine

time. The Thermal Energy Storage (TES) is a flexible component of the plant, which allows the campus to reshape the cooling demand particularly in peak hours. There are many examples of CCHP supervisory control systems in literature ([8], [9], and [15]). A key element for such optimal control is to have accurate information about the power (electricity and cooling) demand over the course of a day, which is the central focus of this study.

Suppose that W_{CHC}^k is the cooling load generated by the k^{th} chiller (kW), and that is the power consumed by the kth chiller (kW) to generate units of cooling load. Then W_{CHC}^k is proportional with as follows:

$$W_{CHW}^k = w_{CHC}^k / COP^k \tag{2.9}$$

where COP^k is the coefficient of performance for the k^{th} chiller which is the ratio between efficient energy acquired by and supplied to the chiller; this is typically determined by the chiller manufacturer. In this study, COP^k is fixed and given by the chillers manufacturer. However, in reality, it is a function of the real operating temperature and reliability of the absorption chiller. This information is not often available.

Therefore, any variation due to change in COP^k is appeared in error term of Equation (2.1) and should be modeled via time series part of the proposed model. W^k_{CHW} presents the actual power (electricity) consumed by the k^{th} chiller to produce W^k_{CHC}. The total power consumed by all chillers is given by:

$$W_{CHW} = \sum_{k=1}^{8} W^k_{CHW} \tag{2.10}$$

Note that W^k_{CHW} values do not reflect the cooling power *supplied* to the campus. A portion of cooling load produced by the chillers is sent to the TES tank and stored for peak hours. Thus, W^k_{CHW} values cannot be a good measure for determining the total cooling demand of campus at any time. Instead, the amount of cooling supplied to the campus can be expressed as follows:

$$Q_{cooling} = \dot{m}_{chw} \times c_w \times (T_{CHRw} - T_{CHSw}), \tag{2.11}$$

where $Q_{cooling}$ is the total amount of cooling (kW) provided by the chillers and supplied to the campus to meet cooling demands, T_{CHRw} is the temperature of returned water to chillers (K), T_{CHSw} is the supply water temperature from chillers (K), $\dot{m}_{chw}$ is the chilled water mass flow rate (kg/s) and is the specific heat capacity of water (kJ/kg-K) [14]. All above parameters are known and available in the plant. This allows us to accurately estimate the actual cooling load demands.

Similar to the cooling load, the direct values for the electricity load demand are not available. However, this can be calculated from the hourly power consumption by the chillers, the total power generated by gas and steam turbines, and the power provided by grid. The electricity load at time t is therefore:

$$W^t_{electricity} = W^t_{grid} + W^t_{GT} + W^t_{ST} - w^t_{CHW}, \tag{2.12}$$

Where W_{GT} and W_{ST} are the power produced by gas and steam turbines, respectively, and W_{grid} is the power purchased from grid at any time. w_{CHW} is the total power consumed by all chillers, which is calculated in Equation (2.10), and $W_{electricity}$ is the electricity load demand at time *t*. In this study, due to lack of data, we ignore the power consumption by pumps and chiller compressors, which account for a relatively

negligible portion of the power consumption throughout the campus. The proposed forecast model is used to forecast both $Q_{cooling}$ and $W_{electricity}$ using a set of weather and time variables as well as historical cooling and electricity data.

2.5 Results for the CCHP Plant Data

In this section, the performance of the proposed method is discussed using the CCHP plant data collected from the UCI campus. In this example, one year (September 2009 through September 2010) and 4 months data (September 2009 through December 2009) are used for building the forecast models for the cooling and electricity load demands, respectively. Both datasets are provided by the UCI campus plant based on actual values of the cooling and electricity consumption. Each dataset is divided into two subsets. The first set is used for model building and estimation purposes (training dataset). The rest of the data is used for validation purposes (testing dataset). In this work, Matlab is employed for creating and testing the proposed forecast model and plotting and visualization is done by Minitab and R. In this phase, Equations (2.7) and (2.8) are used to investigate the performance of the forecast models. The testing subset does not share any information with the training dataset.

Before building the forecast model, an exploratory data analysis is performed to capture the behavior of data over time. Figure 2.2 depicts the 95% confidence interval plots for the cooling and electricity load demands categorized by weekdays. It is observed that both the cooling and the electricity load demands are higher in working days than weekends.

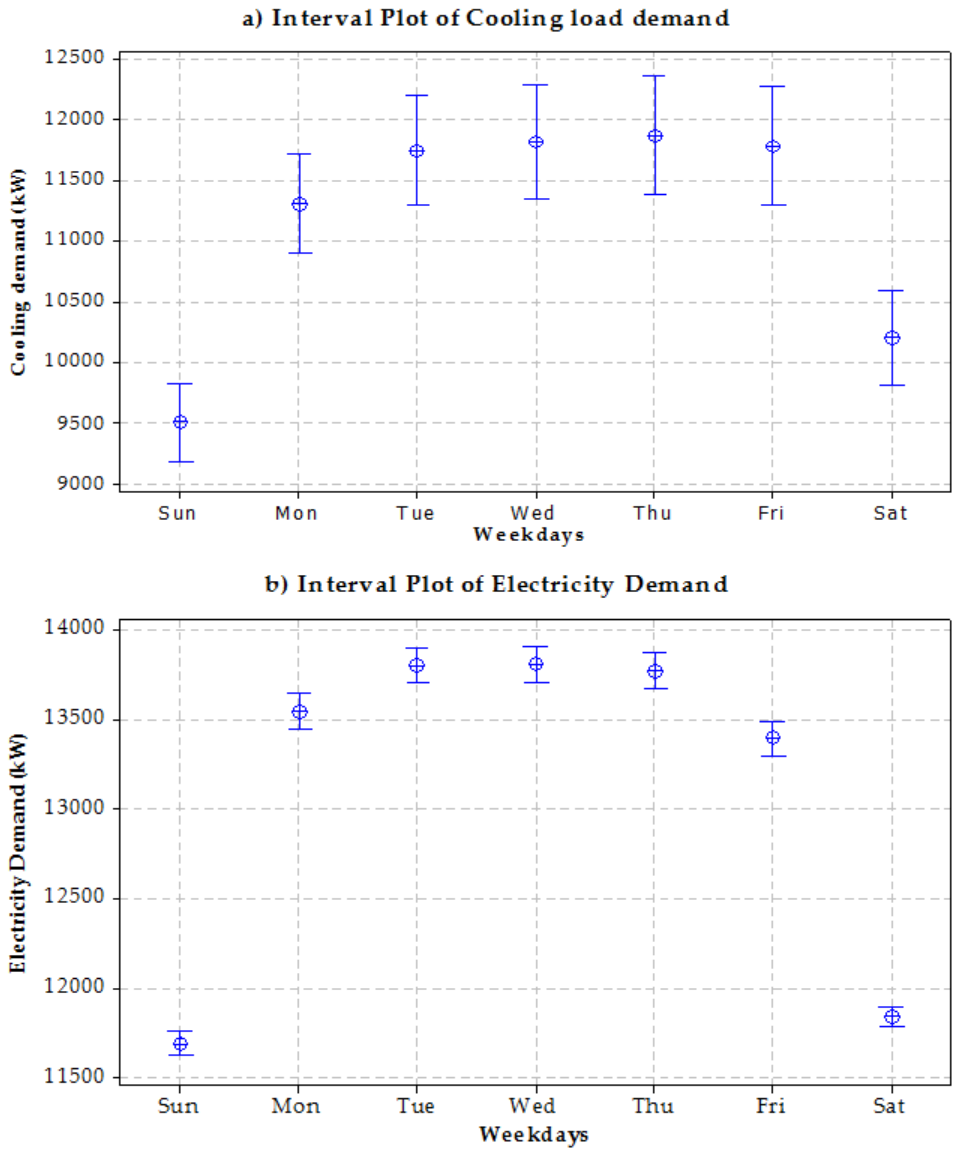

Figure 2.2: 95% Confidence Interval Plots Categorized by Weekday for a) Cooling Load Demand b) Electricity Load Demand

This is particularly obvious for the electricity load demand that is less than 12000 (kW) in weekends and more than 13000 (kW) for weekdays. This implies that mixing all data and building a global forecast model without considering the factor of day may result in a less powerful model. Thus, in this work, two different models are constructed for weekdays and weekends.

Figure 2.3 presents the 95% confidence interval plots for the cooling and the electricity

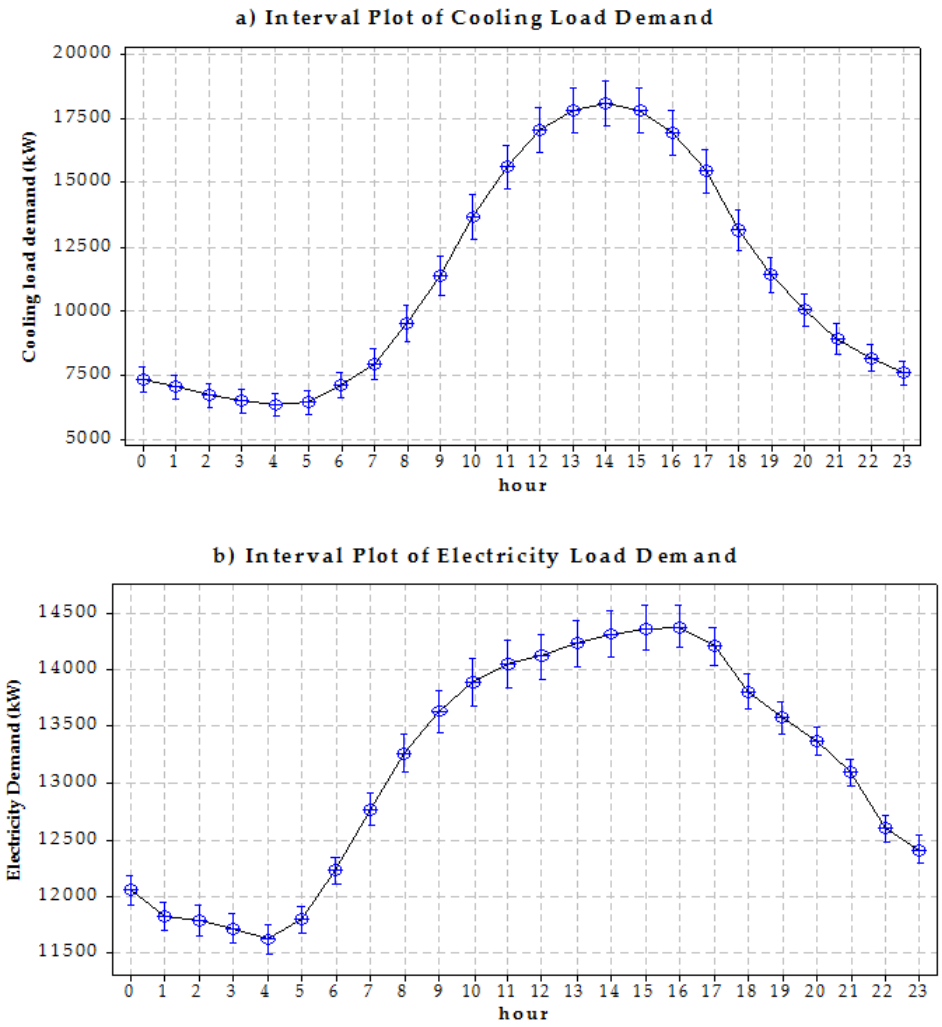

Figure 2.3: 95% Confidence Interval Plots Categorized by Hours for a) Cooling Load Demand b) Electricity Load Demand

load demands categorized by 24 hours of the day. For example, 17 in x-axis means the 95% confidence interval for the cooling and electricity load demands at time 17:00, which is constructed by all data collected at this particular time slot. This figure can easily represent peak time for the cooling and electricity load demands.

For cooling, the load demand increases constantly from 6:00 and reaches its maximum value at time14:00 then decreases until end of the day. The peak hours for the cooling load demand are between 11:00 to 17:00. This also implies that the cooling demand load is highly correlated with the ambient temperature. Similarly, the peak hours for electricity load demand are between 9:00 to 19:00 as well.

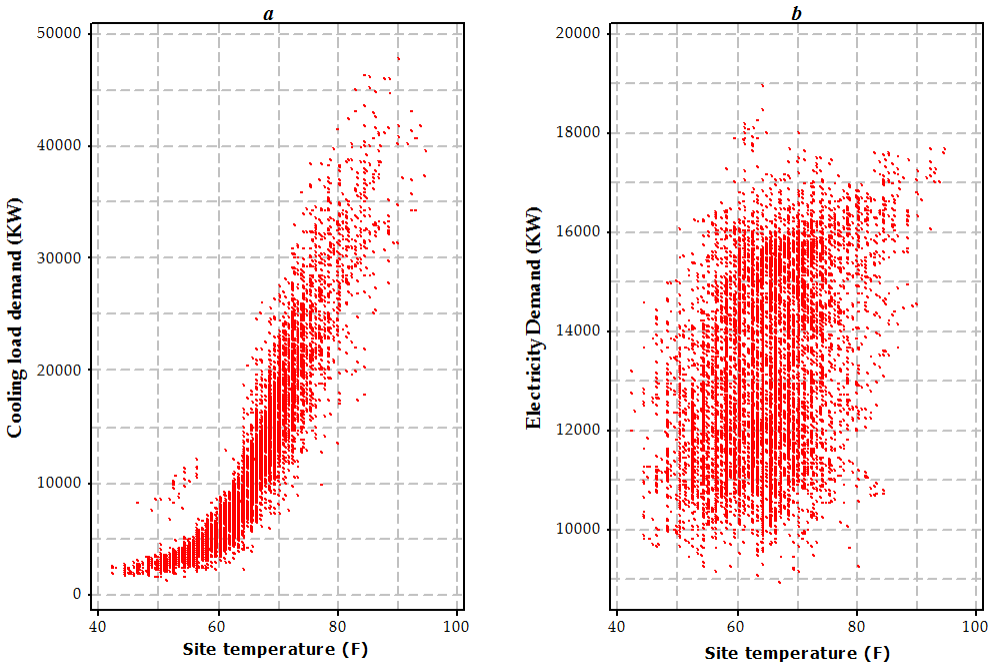

Figure 2.4: Scatter plots of Cooling and Electricity load demand vs. Site Temperature

Figure 2.4 shows scatter plots of the cooling and electricity load demands versus the ambient temperature. The cooling load values show higher correlation with ambient temperature than the electricity load demand. The estimated correlations between cooling and electricity load demands with ambient temperature are 0.905 and 0.374, respectively. This means that to find an accurate model for the electricity load demand, it is required to add more significant exogenous factors than ambient temperature.

For example, the average number of people in the campus at time t would be a potential exogenous factor for modeling the campus electricity load demand. As number of people in the campus increases, it is logical to presume that the electricity load demand increases. However, in this example, since the number of people in the campus at time t is not available we are not able to analyze its effect. As a result, those parts of variation that are related to such missing exogenous factor(s) should be explained and modeled by time series part of the proposed method.

Figure 2.5-a and Figure 2.5-b present the hourly cooling load of the campus and the residual values given by fitting a linear model of cooling versus ambient temperature.

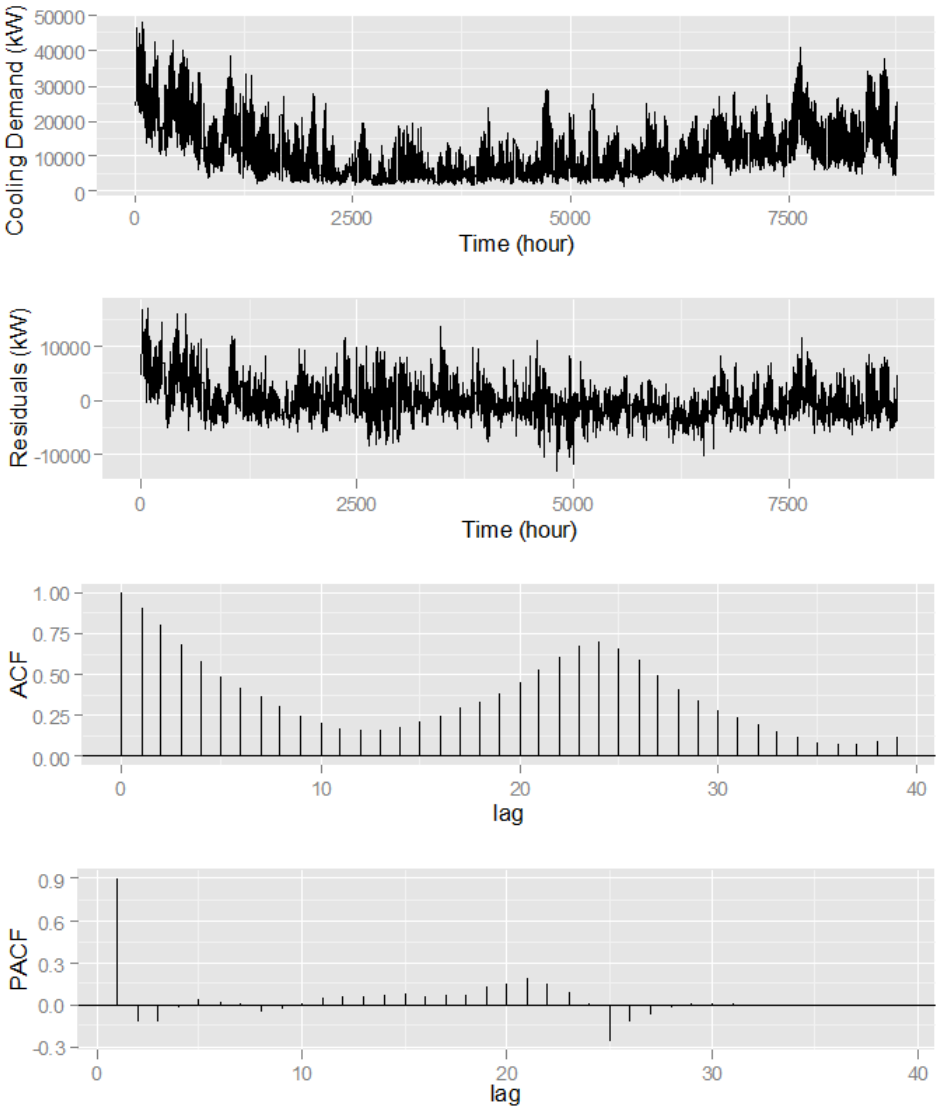

Figure 2.5: a) Time series plot for the cooling load demand, b) the residuals for a preliminary linear model, c) autocorrelation plot and d) partial autocorrelation plot for residual values

The residuals are highly autocorrelated over time in different lags (Figure 2.5-c). Furthermore, Figure 2.5-d is the partial autocorrelation function (PCAF) for residual values and can identify the extent of lags in an autocorrelation model. In this figure, PACF illustrates a strong autocorrelation structure in the first lag and the 24th lag, which accounts for seasonality in the data. Therefore, a seasonal ARMA$(1,0,0) \times (1,0,0)_{24}$ seems an appropriate candidate for the electricity load dataset.

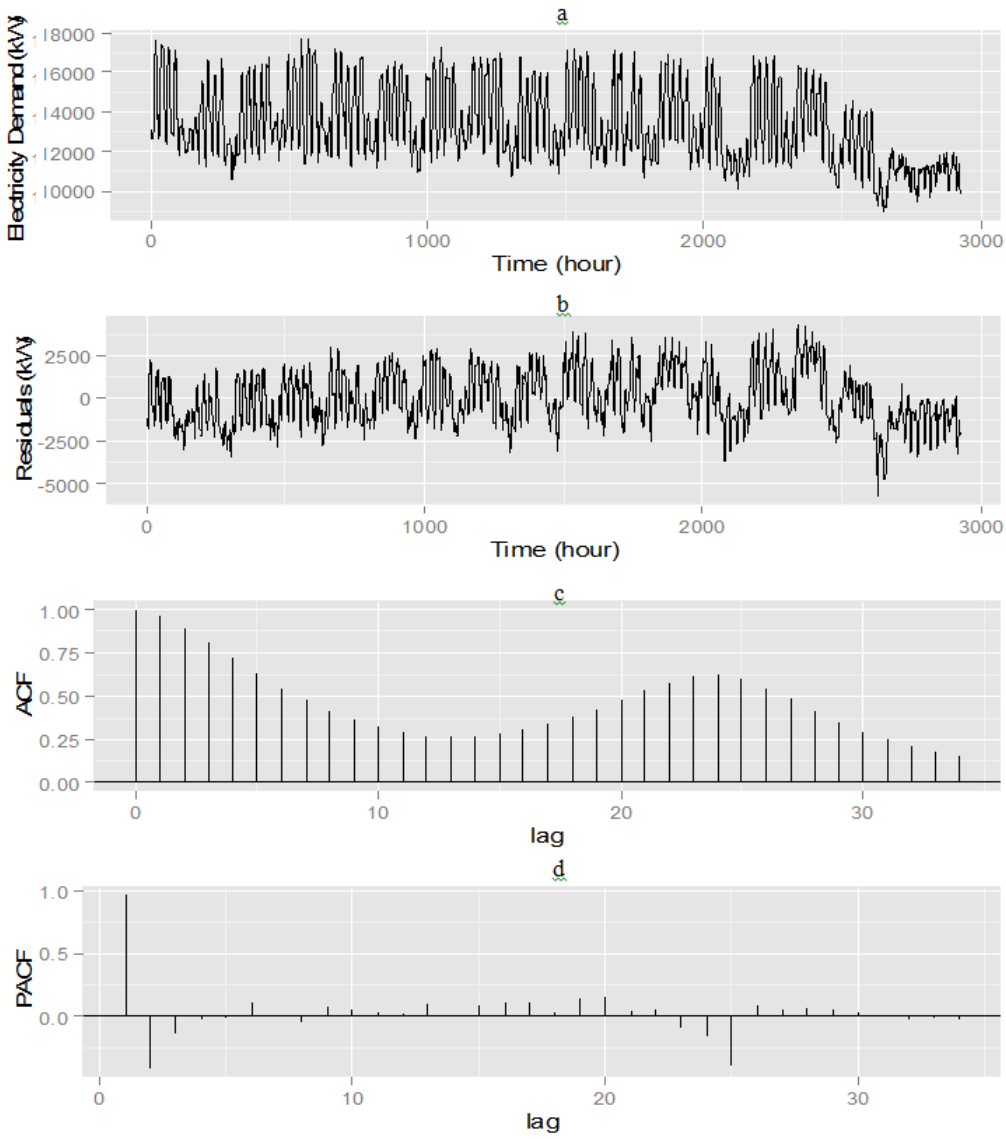

Figure 2.6: a) Time series plot for Electricity load demand, b) the residuals for a preliminary linear model, c) autocorrelation plot d) partial autocorrelation plot

Similarly, figures 2.6-a and 2.6-b are the electricity load demand and its corresponding residual values when applying a linear model to the data. Again, ACF and PACF in Figure 2.6-c and Figure 2.6-d reveal a correlated structure for the electricity load dataset. Particularly, PACF illustrates a positive autocorrelation for the first lag and a remarkable negative correlation for the 24^{th} lag. This means that a seasonal

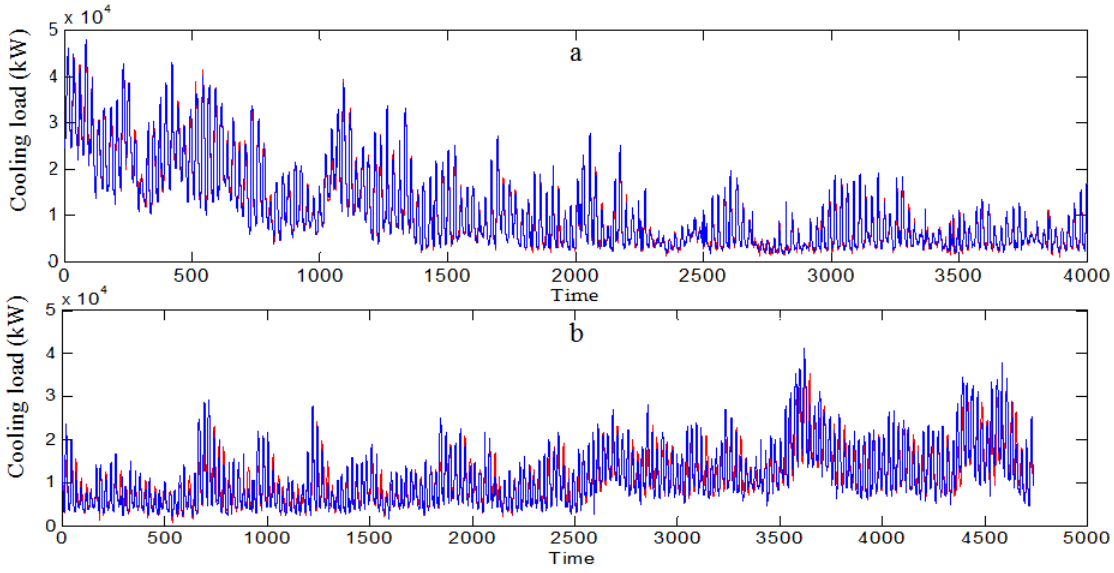

Figure 2.7: Comparison of actual and forecasted values for cooling load demand using a) training dataset (above) and b) testing dataset (below)

ARMA$(1,0,0) \times (1,0,0)_{24}$ model would be enough for the electricity load demand. Figure 2.7-a and Figure 2.7-b depict the result of forecast modeling for the cooling load demand using training and testing datasets. In Figure 2.7-a, the forecast values are very close to the corresponding actual values. This is because the training dataset is used for parameter estimation of the forecast model. Therefore, the model includes the information of actual data. Figure 2.7-b represents the performance of the model with testing dataset, which does not share any information with the estimated parameters. It is observed that the model adequately fits with the actual data.

In addition, Table 2.1 provides the estimate values of the model parameter, their standard errors as well as coefficient of determinations for both cooling and electricity load demands. For the cooling demand, coefficient of determination R^2 and adjusted coefficient of determination R^2_{adj} are 88.4% and 88.3%, respectively implying that the proposed model can explain more than 88% of the total variability within data.

Figure 2.8 and Figure 2.9 present the actual and forecast values of electricity load demand using both training and testing datasets for weekdays and weekends, respectively. As shown in Figure 2.2-b, the electricity demand patterns are significantly different in

Table 2.1: The estimates values for cooling and electricity forecast models

	Cooling		**Electricity**			
	All Data		Weekdays		Weekends	
	Estimate	Std error	Estimate	Std error	Estimate	Std error
β_0	-13441.85	1851.1	12783	458.2	9825.557	704.74
β_1	357.28	13.98	21.018	6.1137	39.168	8.809
ϕ_1	0.9059	0.016	0.8775	0.0319	1.1882	0.075
ϕ_2	0.0513	0.021	0.0018	0.0425	-0.1848	0.1162
ϕ_3	-0.083	0.02134	-0.1298	0.0423	-0.014	0.1168
ϕ_4	-0.0314	0.02138	0.0606	0.0425	-0.0594	0.1168
ϕ_5	-0.0299	0.02138	-0.1054	0.0425	-0.2021	0.1169
ϕ_6	-0.0405	0.02137	0.0073	0.0425	0.1319	0.1178
ϕ_7	0.0829	0.02138	0.1304	0.0422	0.124	0.116
ϕ_8	-0.0264	0.02142	-0.1095	0.0423	-0.1624	0.117
ϕ_9	-0.0289	0.02142	-0.0625	0.0425	0.114	0.119
ϕ_{10}	-0.0094	0.0214	0.0484	0.0425	-0.1592	0.1195
ϕ_{11}	0.0191	0.02136	0.0155	0.0426	0.1565	0.121
ϕ_{12}	0.0017	0.02135	-0.0777	0.0427	-0.0218	0.1219
ϕ_{13}	-0.0138	0.02135	0.0466	0.0427	0.139	0.1204
ϕ_{14}	-0.0112	0.02134	-0.0047	0.0427	-0.145	0.119
ϕ_{15}	0.0275	0.02134	-0.0287	0.0427	-0.1449	0.1189
ϕ_{16}	-0.0021	0.02134	0.0276	0.0426	0.0813	0.1194
ϕ_{17}	0.0012	0.02134	0.0957	0.0425	0.2598	0.1193
ϕ_{18}	-0.0074	0.02129	-0.1241	0.0424	-0.2818	0.1206
ϕ_{19}	0.0084	0.02128	0.0501	0.0426	-0.0009	0.1222
ϕ_{20}	0.0191	0.02128	0.055	0.0425	0.0622	0.1233
ϕ_{21}	0.0392	0.02128	-0.0531	0.0425	0.0664	0.1228
ϕ_{22}	0.0728	0.02124	0.0966	0.0423	0.1109	0.1241
ϕ_{23}	0.0751	0.02125	0.0439	0.0424	-0.0776	0.1239
ϕ_{24}	-0.0322	0.01576	0.0797	0.0319	-0.0285	0.0814
R^2	0.884		0.708		0.43	
R^2_{adj}	0.883		0.7		0.405	

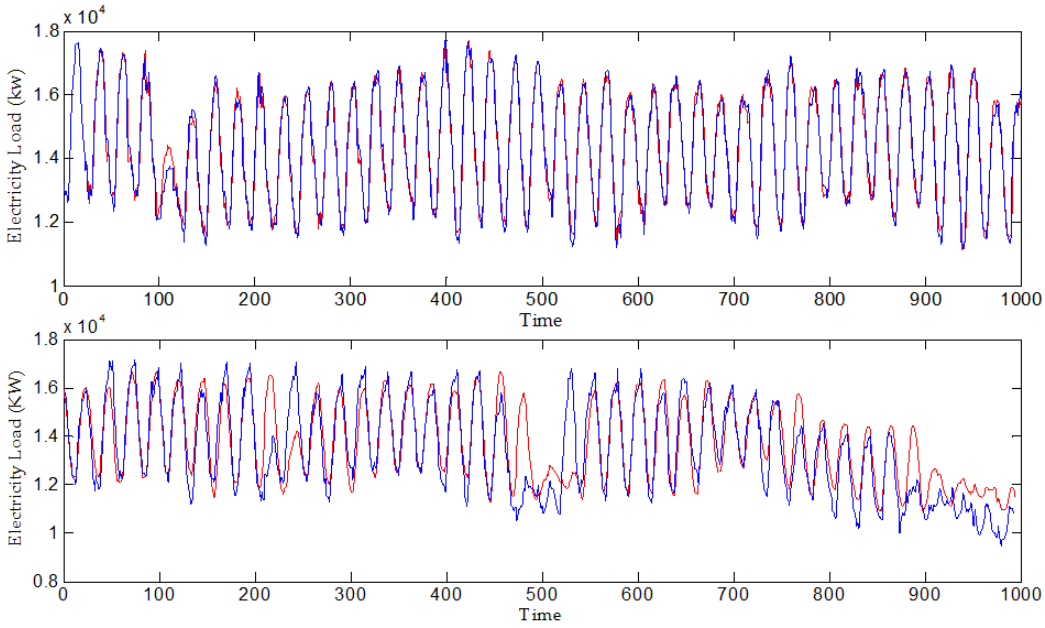

Figure 2.8: Comparison of actual and forecasted values for electricity load demand in weekdays using training dataset (above) and testing dataset (below)

weekends and weekdays, probably because of fewer numbers of people in the campus in weekends. Therefore, to improve the performance of the proposed method, we built two separate models for weekdays and weekends.

In addition, It is observed from Figure 2.8 and Figure 2.9 that the performance of the proposed model for the electricity load demand is still less than the same model proposed for the cooling load demand. This is mainly due to lack of other exogenous factors in electricity demand model. As shown in Figure 2.4, the correlation between electricity load demand and the ambient temperature is moderate. It means that the ambient temperature can only explain a relatively small portion of variation in electricity demand. This can be confirmed by observing Table 2.1. In this table, R^2 and R^2_{adj} for electricity load demand in weekdays are namely 70.8% and 70% and for electricity load demand in weekends are namely 43% and 40%. Therefore, the electricity load model should be enhanced by adding more exogenous factors e.g. occupancy into the forecast model in order to capture larger amount of variability over time.

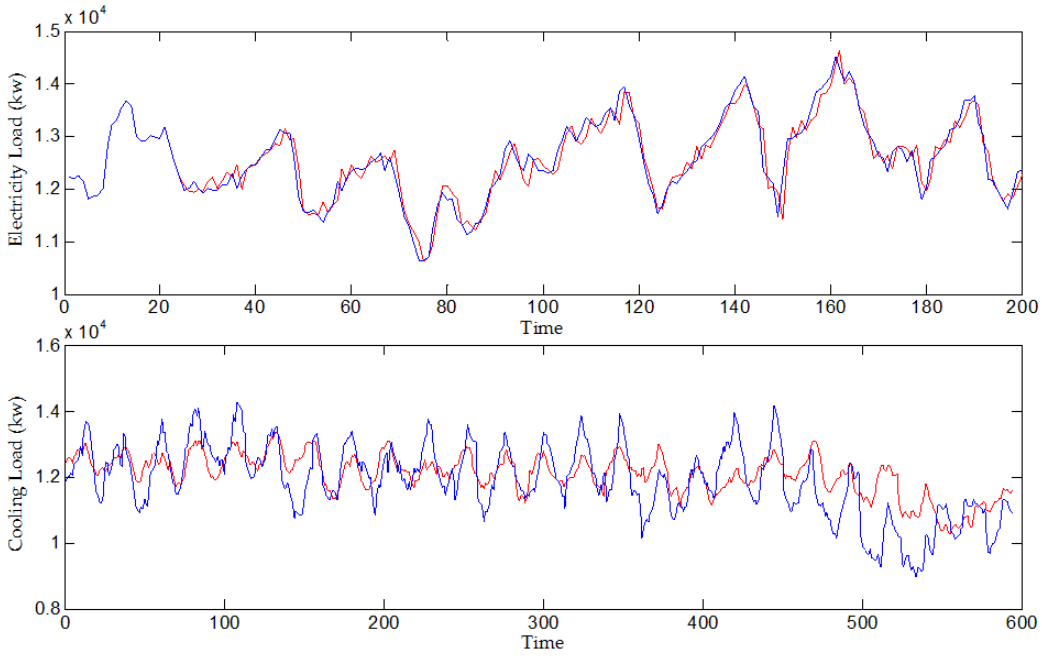

Figure 2.9: Comparison of actual and forecasted values for electricity load demand in weekends using training dataset (above) and testing dataset (below)

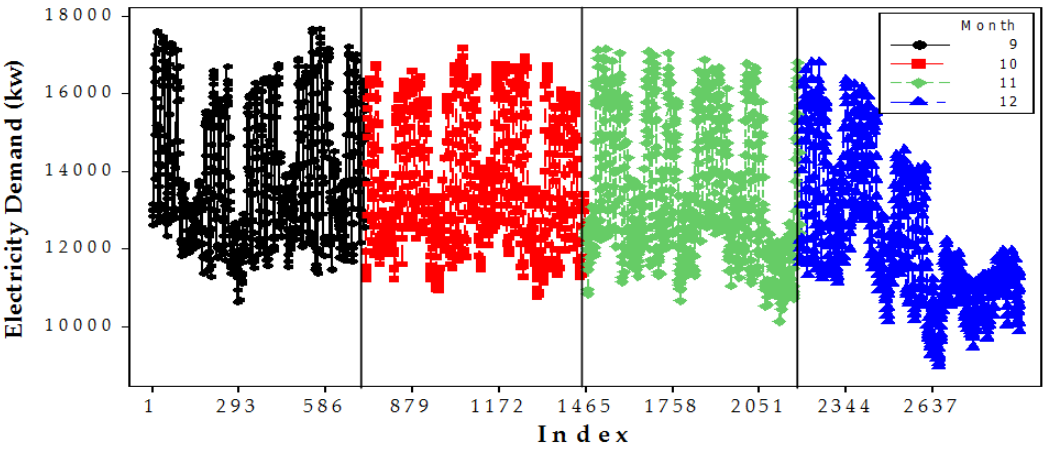

Figure 2.10: Time series plot for electricity load demand grouped by month

Another potential reason for lower performance of the electricity demand forecast model is shown in Figure 2.10. In this figure, the values of electricity load demand are plotted over time and are grouped by months. We note that the load demand in the last month follows different pattern than the other months. This is because the last month is December and the campus is probably less populated at the last days of December.

Since, we used the first two months for training and estimation and the rest of data (including December data) for the testing purposes, the model cannot fit the last part of December. A solution for this problem is to add the occupancy as another exogenous variable into the model and re-estimate the model parameters accordingly. This way, the model can differentiate between those days that more people are in campus from the days that less people are in campus including weekends. Another idea is to build a new model solely for December. In doing so, the model switch to a new model that is designed and built based on December data as soon as December begins.

2.6 Building Energy Consumption characteristics

There are many various buildings inside the campus, which obtain their electricity and cooling demands through the central CCHP plant. A logical idea is to employ the same optimal control scheme for buildings alongside with CCHP plant, which results in more savings in energy consumption. Such optimal scheme can be considered as a suboptimal control problem with different input variables than the plant input variables which leads to further saving and less operating cost over time.

In order to construct a forecast model for the building energy consumption, one should study many exogenous factors, which directly or indirectly influence building energy consumption. All factors affecting energy consumption can be categorized into two major classes: i) Controllable factors, which include operational variables such as cooling and heating air set points; ii) Uncontrollable factors, which include environmental variables e.g. weather information, uncontrollable dynamic variables e.g. occupancy or static variables e.g. building characteristics. An effective system framework provides a modeling and prediction basis in which, for a given environmental and uncontrollable dynamical variables, the building energy consumption is accurately predicted for a relatively short time horizon. Therefore, one can use Cochrane-Orcutt technique to find the relationship between building cooling and electricity consumptions with available controllable and uncontrollable variables. In this study, the actual data associated with input variables as well as cooling and electricity energy consumptions are not available.

To approximate these variables we build a simulation model using EnergyPlus that is a powerful simulation package for building energy management.

2.6.1 Results for Building Energy Consumption

We investigate the performance of the proposed model for forecasting the whole-building energy consumption. Our case study is the Advanced Power and Energy Program (APEP) building at the University of California, Irvine (UCI). APEP consists of the National Fuel Cell Research Center, the UCI Combustion Laboratory, and the Pacific Rim Consortium on Combustion, Energy, and the Environment that require many industrial equipment. This occasionally causes a remarkable industrial load alongside the building normal load consumed for lighting, cooling, heating etc. In this chapter, we only consider normal load in our analyses and parameter estimations. The building industrial load requires additional input information and different modeling approach that will be discussed later in another chapter. Since we do not have enough actual data to build the forecast model, we employ the APEP building EnergyPlus to generate the required data. In fact, our proposed forecast model is a meta-model for the APEP EnergyPlus model that provides energy information faster with less computational efforts. This is particularly important for optimization purposes, where it is required to run many various scenarios and investigate a large number of different solutions. In addition, EnergyPlus provides more weather outputs that can be used in forecasting energy consumption. In this study, using a variable selection method, we use the following variables as exogenous factors in the model: outdoor dry bulb, outdoor wet bulb, outdoor humidity ratio and Luminous Efficacy of Sky Diffuse Solar Radiation.

Table 2.2 presents the estimate values of the forecast model and their corresponding standard errors for the electricity and cooling energy consumption of the APEP building. It is observed that the proposed model can be adequately applied for both datasets. Coefficient of determination is used to evaluate both models. R2 and R2adj for the cooling energy consumption are 91.6% and 91.1% and for the building electricity are roughly 79.6% and 78.7% representing that the forecast model is capable to explain

Table 2.2: The estimates values and corresponding standard errors for APEP cooling and electricity model

	Cooling		**Electricity**	
	Estimate	Standard error	Estimate	Standard error
β_0	-534201.7	37415.11	77788.96	23887.95
β_1	80546.7	7108.92	N/A	N/A
β_2	-148695.1	16921.3	-925.45	316.35
β_3	159606617.5	17459325	N/A	N/A
β_4	-7.2	18.22	N/A	N/A
β_5	-534201.7	37415.11	N/A	N/A
β_1	0.865	0.041	0.187	0.0329
β_2	0.098	0.055	0.395	0.0334
β_3	-0.228	0.055	0.087	0.0365
β_4	-0.053	0.056	0.036	0.0365
β_5	0.085	0.056	0.01	0.0363
β_6	-0.053	0.056	-0.185	0.0362
β_7	0.012	0.056	-0.166	0.0352
β_8	0.017	0.055	-0.152	0.0355
β_9	-0.044	0.055	0.056	0.0355
β_{10}	-0.033	0.048	0.232	0.0349
β_{11}	0.049	0.041	0.133	0.0357
β_{12}	0.042	0.041	0.048	0.036
β_{13}	0.01	0.041	-0.04	0.036
β_{14}	-0.132	0.041	-0.143	0.0357
β_{15}	0.028	0.041	-0.17	0.0348
β_{16}	0.053	0.041	-0.151	0.0354
β_{17}	-0.028	0.041	0.112	0.0355
β_{18}	0.002	0.041	0.275	0.0352
β_{19}	0.037	0.041	0.065	0.0362
β_{20}	0.015	0.041	0.108	0.0362
β_{21}	0.003	0.041	-0.067	0.0364
β_{22}	0.063	0.04	-0.166	0.0364
β_{23}	0.003	0.04	-0.14	0.0332
β_{24}	0.093	0.032	0.609	0.0327
R^2	0.916		0.796	
R^2_{adj}	0.912		0.7868	

majority of variation in dataset. In addition, by adding the information of occupancy (number of people in each zone at any time), one can improve the performance of the electricity consumption model.

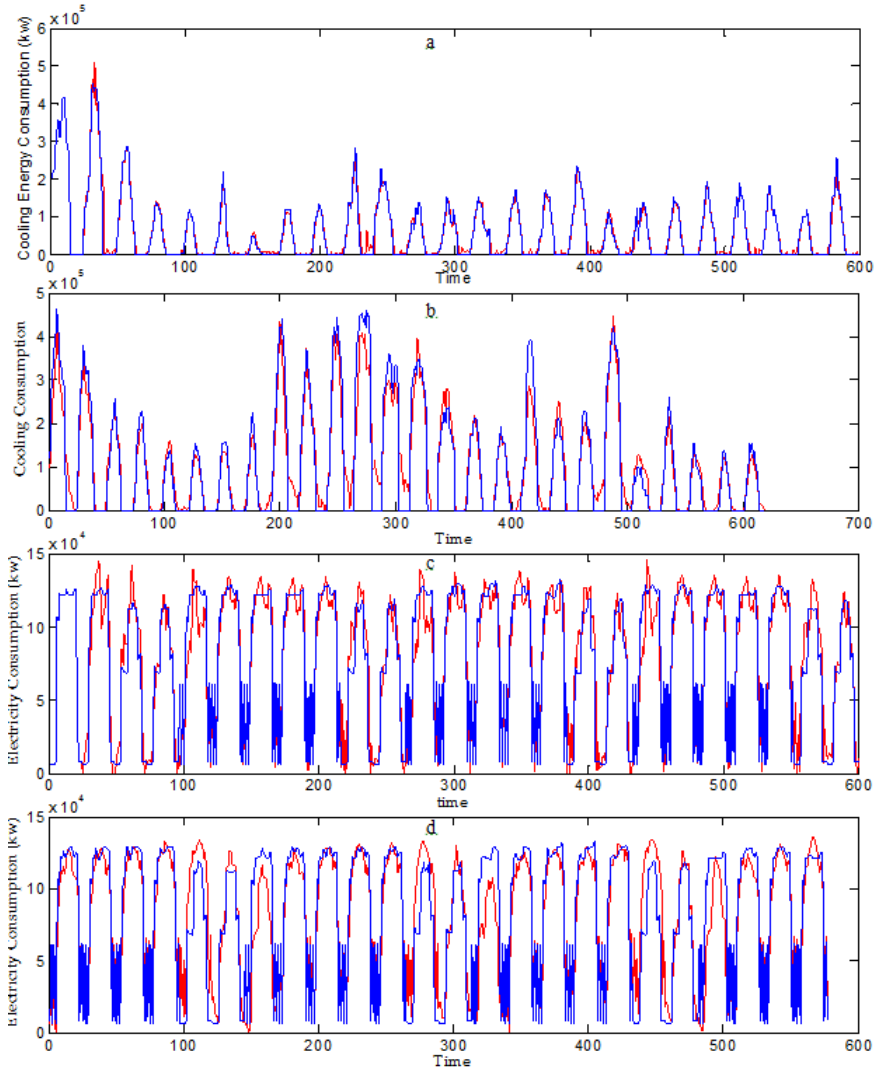

Figure 2.11: Time series plot of cooling and electricity consumptions and their forecast values for APEP building based on EnergyPlus results: cooling consumption using a) training dataset, b) testing dataset; and electricity consumption using c)) training dataset d) testing dataset.

Figure 2.11 consists of a set of time series plots associated with both cooling and electricity energy consumptions of the APEP building using both training and testing

datasets. It is observed that the forecast values are very close to the actual values for both the cooling and the electricity energy consumption.

One reason for such good performance is the structure of the building simulation model. Since datasets are output of an EnergyPlus model, the forecast model highly depends on the level of complexity considered in the building simulation model as well as the assumptions i.e. linearity applied to the model. The APEP building example shows that the proposed forecast model can accurately provide same results as EnergyPlus, but with much less computational effort. The majority of simulation optimization approaches requires running many replications to evaluate a wide range of scenarios and seek for the optimal solution [46].

By directly using EnergyPlus, it may be time consuming or even impractical to generate enough scenarios. Instead, one can employ the proposed statistical model as a meta-model and produce many scenarios in a time-efficient way. Particularly, the proposed model can be used in the initial steps of optimization, where it is required to evaluate a large number of different scenarios, while the optimization algorithm is still far from the optimal solution. In this case, a simple yet fast model can be applied to evaluate many solutions in shorter time.

Chapter 3

Optimal Control Strategy for Building Cooling/Heating Systems

3.1 Introduction

In this chapter, we introduce an approach for modeling of building cooling/heating system and present our optimal control strategy to optimize the heating/cooling energy consumption over time. In this approach, physical characterization of the building is partially captured by a collection of zonal energy balance equations with parameters estimated using a least squares estimation (LSE) technique. The data required to estimate energy balance equations are either collected from an actual building or generated by a whole-building simulation model. The zonal cooling/heating model is then fed into a forecast model to provide the look-ahead forecast values of total building energy consumption. The forecast model is similar to the model presented in Chapter 2. The combined forecast model is then used in a model predictive control (MPC) framework to manage heating and cooling set points. The formulation of the MPC algorithm includes a multi-objective mathematical programming model that minimizes total operating energy cost and daily as-used demand charges as well as total deviation from thermal comfort bounds. This work is motivated by the practical limitations of simulation-based optimization. Once the forecast model is established capturing sufficient statistical variability and physical behavior of the building, there will be no more need to run EnergyPlus in the optimization routine.

In practice, the initial training of the model parameters can be carried out using building simulation data. But, as soon as, the real building energy usage data becomes available, the forecast model updates its parameters with real data. This in turn adjusts

optimal control strategies (i.e., zonal set points) over time (e.g., on hourly basis) and ensures that internal zone tempratrues remain within prespecified limits. The practical significance of this model are two-fold: (i) The model is adaptive to real time building energy performance and directly incorporates internal temperature in its optimization, (ii) The use of EnergyPlus or similar simulation models, which are computationally too expensive for optimization, is reduced only to the initial training.

The novelty of this work is on the specific combination and application of different methods to optimize energy control of large buildings which are subject to stochastic externalities. In particular, the methodology integrates a physics-based zonal model with an advanced time series model to ensure enhanced accuracy and sensitivity of energy forecasts to incremental changes in control variables. Internal temperature measurements of different zones in the building are used in calculations. Initial training of the model parameters is carried out using highly granular building energy simulation (EnergyPlus or similar models). Unlike the current practices that run different scenarios to deal with stochastic externalities, the proposed forecasting model is adaptive and uses actual measurements to refine and update its forecast values.

3.2 Literature Review

The basic idea of MPC is to form a model that is able to represent the future behaviors of building cooling/heating dynamics and to provide optimal control actions for a specific time horizon [47-50]. Different modeling approaches can be employed for implementation of an MPC strategy. The first approach is based upon detailed physical modeling of cooling and heating dynamics. In this approach, physical characteristics of a building as well as HVAC components are extracted and fed into a series of energy balance equations. The balance equations are then used for prediction of the future evolution of cooling/heating dynamics. For instance, the authors in [50-54] model the cooling/heating dynamics using resistancecapacitance (RC) network analogy. In these works, thermal resistance and capacitor between different components of a building or a zone, such as air, inside and outside surfaces of walls, windows and ceilings as well as

heat flux due to solar radiation are represented through RC-network diagrams and heat transfer equations. The equations are then employed for prediction of cooling/heating dynamics and optimization of setpoint values. Other works [53-56] account for the effect of other dynamic variables or physical components such as occupancy, relative humidity, chilled/hot water temperature supplied or returned from building/zone, thermal storage equipment etc.

The physical MPC approach is typically too complex to solve analytically for large granular building models. Therefore, researchers often apply physical MPC models for simpler problems, e.g., a single zone or a single room [49, 51]. An alternative is to use a data-driven approach to MPC by simply fitting a metamodel to the cooling/heating data regardless of the particular physical structure of the building. A number of studies have focused on linear statistical models where input and output data have linear forms. Autoregressive with exogenous variable (ARX) and autoregressive moving average with exogenous variable (ARMAX) are two examples of this approach [57,58]. State-space modeling is another example of such an approach where model parameters are estimated over a number of specified system states [59, 60]. In other studies, researchers employ soft computing techniques, particularly artificial neural networks (ANN), to address the complexity of building energy forecast modeling and optimization [60, 61]. Artificial neural networks provide linear or nonlinear model-free structures for prediction of energy demand using different input vectors, i.e., weather conditions or wall insulation thickness [63]. These predictions can then be used for optimization of cooling/heating loads [61].

Although data-driven models are typically simple to use, their implementation is often accompanied by a number of problems that may negatively influence their performance. ARX and ARMAX models, for instance, follow linear autoregressive structures that are not necessarily able to explain full variations of load dynamics. In addition, most soft computing techniques cannot guarantee full capture of complex interactions amongst building components, dynamic variables, and cooling/heating load, especially when the

available real data is limited and the building includes a complicated multi-zone structure. To overcome such problems, a number of researchers employ a simulation-based approach to capture the dynamic behavior of buildings and thereby optimize energy use [64-66]. In this approach, first a highly granular physics-based simulation model of the building is developed. Then, by designing and running different experiments, the behavior of building energy systems is captured over time. Simulation-based optimization techniques are applied to minimize the energy used to meet cooling/heating loads. However, this is costly and time consuming particularly for larger models where simulation optimization must run over a large spectrum of possible scenarios and run in near real time. Consequently, a number of recent works combine the benefits of both simulation and data-driven approaches to provide fast and effective control solutions [57]. These approaches are similar to that developed and used herein.

3.3 Model Framework

Our proposed framework for optimal control of a building heating/cooling system is presented in Fig. 3.1. Model execution consists of two main phases: an offline phase and an online phase. The offline phase includes analysis using a set of historical data either generated by EnergyPlus, or directly gathered from building with the objective of constructing and training a heating/cooling dynamic model for the building. This heating/cooling model is then used in a building energy forecast model to calculate the 24-hour look-ahead forecast values for building energy consumption. In the online phase, both the heating/cooling model and energy forecast model are fed into an MPC scheme that is designed to provide the optimal cooling/heating set points for the next 24 hours ahead. The MPC scheme is based on a dynamic programming approach, which runs every time that it receives new actual data from the building under study. Figure 3.1 provides a schematic model for our proposed framework. It consists of four major steps as follows:

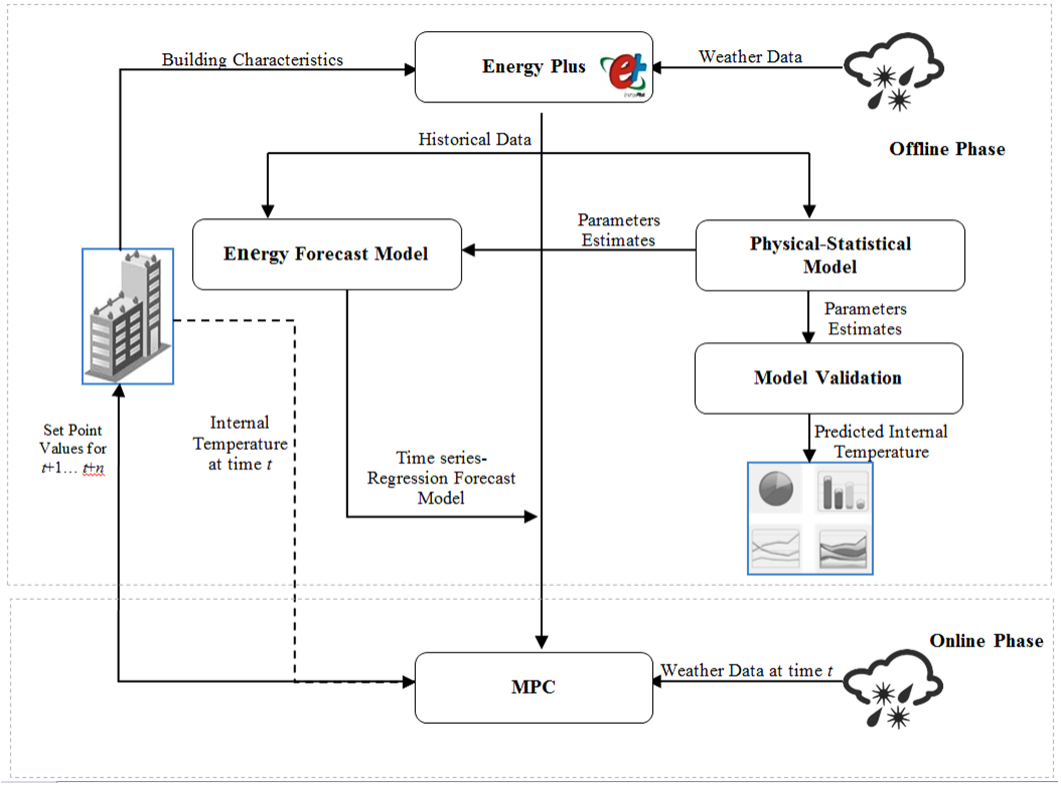

Figure 3.1: General framework of the proposed control strategy

1) *Create an EnergyPlus model for building energy management*:

For newly designed buildings this step is self-explanatory. For existing buildings, there are often not sufficient data available to capture operational variations. A valid EnergyPlus model running under a statistically proper design of experiments can provide the initial base for reducing statistical noise in the estimation of model parameters [67-69].

2) *Develop heating/cooling model and estimate its parameters*:

This is a set of heat balance equations, which provides explicit relationships between zonal internal temperatures and effective power rate. The effective power rate represents the amount of cooling/heating rate in kW that the HVAC system supplies to each building zone during any specific time period. The model is used to forecast the k-step-ahead internal temperature for each zone.

3) *Create an energy forecast model*:

This combines the model from Step 2 with a time series model, and returns 24-hour look-ahead forecast values for building total energy demand. We apply a generalized

form of Cochran-Orcutt technique to estimate the model parameters [44]. Once the total energy demands for the next 24 hours are forecasted, then one can calculate the total energy operating costs, which are then used in the next step.

4) *Develop MPC based optimal control of set points*:

We formulate a multi-objective dynamic programming code to search for optimal control set points for the next 24-hours. The total operating costs of Step 3 as well as the total penalty for exceeding the thermal comfort bounds define the objective functions, and the heat balances in Step 2 form the state constraints. In conjunction with the thermal comfort objective function, an additional set of constraints are imposed to maintain the thermal comfort between specified bounds. As shown in Figure 3.1, at time t, we find the optimal control set point values for times t+1, t+2,, t+24. Then in the next hour, we update the optimal solutions for t+2,,t+25, when we receive feedback of new information on the building (i.e., from the building energy management system or real building).

3.3.1 Heating/Cooling Model

Assume that a day is divided into a set of discrete time slots, k = 0, 1, 2 N-1. Then according to the first law of thermodynamics, the total energy exchange associated with the i^{th} thermal zone, i = 1, 2, , Z, at time step $t + k + 1$ is given by:

$$\Delta Q^{t+k+1}(i) = Q_{in}^{t+k}(i) - Q_{out}^{t+k}(i), \tag{3.1}$$

where $Q_{in}^{t+k}(i)$ and $Q_{out}^{t+k}(i)$ are the amounts of input and output energy at step t+k, and is the amount of energy gained or lost at time t+k+1 by Zone i. In this study, we assume that $\Delta Q^{t+k+1}(i)$ is a function of internal and external temperatures [49] and can be calculated as follows:

$$Q_{out}^{t+k}(i) = \phi_i(T_{in}^{t+k}(i) - T_{ext}^{t+k}(i)). \tag{3.2}$$

$T_{in}^{t+k}(i)$ and $T_{in}^{t+k}(i)$ are the internal and the external temperature of the i^{th} zone at time t+k, respectively. Assuming that the i^{th} zone is air conditioned by a heating,

ventilation, and air condition (HVAC) system with effective power rate of $\dot{R}_{ext}^{t+k}(i)$ (in kW) at time $t+k$, we can rewrite Equation (3.1) as follows:

$$\Delta Q^{t+k+1}(i) = \dot{R}^{t+k}(i) - \phi_i^k \left(T_{in}^{t+k}(i) - T_{ext}^{t+k}(i)\right) + \alpha^{t+k}, \tag{3.3}$$

where α^{t+k} is a white noise representing the additional unpredictable effects of convective internal loads, convective heat transfer from the zone surfaces, inter-zone air mixing effects and occupancy. In this study, we assume that such additional effects are negligible and are normally distributed. In addition, according to [70], the internal temperature of the i^{th} zone at time $t+k+1$ can be written as:

$$T_{in}^{t+k+1}(i) = T_{in}^{t+k}(i) + \frac{\Delta Q^{t+k+1}(i).\Delta t}{C_{air}.m_{air}}, \tag{3.4}$$

where Δt is the duration of time slot which is set one hour in this study. Furthermore, C_{air} and m_{air} are the heat capacity and the mass of air in the i^{th} zone in $\frac{J}{kg.C^o}$ and Kg, respectively. The unit of ΔQ is J and $T_{in}^{t+k}(i)$ is °C. ΔQ^{t+k+1}(i), in Equation (3.4) can be replaced by its corresponding value in Equation (3.3) and rewritten as follows:

$$T_{in}^{t+k+1}(i) = T_{in}^{t+k}(i) + \frac{\dot{R}^{t+k}(i)\Delta t}{C_{air}.m_{air}} - \frac{\phi_i^k \left(T_{in}^{t+k}(i) - T_{ext}^{t+k}(i)\right) \Delta t}{C_{air}.m_{air}} + \varepsilon^{t+k}. \tag{3.5}$$

$\varepsilon^{t+k} = \Delta t.\alpha^{t+k}/C_{air}.m_{air}$ are independently and identically distributed. C_{air} and m_{air} cannot easily and accurately be determined in practice, since the mass of air and heat capacity are different for different points at a zone. Rather, the thermal balance model presented in Equation (3.5) can be explained in terms of lost and delivered energy and the internal and external temperatures of the i^{th} zone as follows:

$$T_{in}^{t+k+1}(i) = T_{in}^{t+k}(i) + \alpha_i^k.\dot{R}^{t+k}(i) + \varphi_i^k \left(T_{in}^{t+k}(i) - T_{ext}^{t+k}(i)\right) + \varepsilon^{t+k}, \tag{3.6}$$

where α_i^k represents the amount of unit increase (decrease) in the i^{th} zone internal temperature by one unit increase (decrease)in effective energy over a time slot. Hence, the effects of C_{air} and m_{air} are hidden in α_i^k and φ_i^k , which are explicit and can be estimated using statistical techniques. For cooling seasons, it is logical to assume that $\alpha_i^k, \varphi_i^k \in \mathbb{R}^+$ and for heating seasons $\alpha_i^k, \varphi_i^k \in \mathbb{R}^-$. Equation (3.6) can be used to

forecast the i^{th} zone internal temperature at time $t+k$ given that $T_{in}^{t}(i)$ and $T_{in}^{t}(i)$ are known [70]. The forecast values are calculated by:

$$\hat{T}_{in}^{t+k+1}(i) = \hat{T}_{in}^{t+k}(i) + \hat{\alpha}_i^k.\dot{R}^{t+k}(i) + \hat{\varphi}_i^k \left(\hat{T}_{in}^{t+k}(i) - \hat{T}_{ext}^{t+k}(i)\right), \tag{3.7}$$

where $T_{in}^{t+k+1}(i)$ is the forecast of internal temperature for the i^{th} zone at time $t+k+1$, k=1,2,...,23. Assume that ν_i is the set point value of the i^{th} zone and that $[l_i\ u_i]$; where l_i and u_i are the lower and upper values for the possible set points.In optimization phase, we set $T_{in}^{t+k+1}(i) = \nu_i$ and find the corresponding $\dot{R}^{t+k}(i)$ by Equation 3.7. $\hat{\alpha}_i^k$ and $\hat{\varphi}_i^k$ are the least squared estimates for model parameters which can be given by minimizing $\mathbf{Q_i^k} = \|\mathbf{T_{in}^k} - \hat{\mathbf{T}}_{in}^{\mathbf{k}}\|$, where $\mathbf{T_{in}^k}$ are the vectors of actual and forecasted internal temperature values for the i^{th} zone and $\|\mathbf{x}\|$ is the l^2-norm of $\mathbf{x}$. $\hat{\alpha}_i^k$ and $\hat{\varphi}_i^k$ can be calculated using numerical methods (See e.g. [70]). However, we find it analytically by solving the following equation set:

$$\frac{\partial Q_i^k}{\partial \hat{\alpha}_i^k} = \sum_{t+k=1}^{n-1} \{(\dot{R}^{t+k}(i) \left(T_{in}^{t+k+1}(i) - T_{in}^{t+k}(i)\right) - \hat{\alpha}_i^k.\dot{R}^{t+k}(i)^2 - \hat{\varphi}_i^k \left(\hat{T}_{in}^{t+k+1}(i) - \hat{T}_{ext}^{t+k}(i)\right).\dot{R}^{t+k}(i)\}) \tag{3.8}$$

$$\frac{\partial Q_i^k}{\partial \hat{\varphi}_i^k} = \sum_{t+k=1}^{n-1} \{\left(T_{in}^{t+k}(i) - T_{ext}^{t+k}(i)\right) \left(T_{in}^{t+k+1}(i) - T_{in}^{t+k}(i)\right) - \hat{\alpha}_i^k \dot{R}^{t+k}(i) \left(T_{in}^{t+k}(i) - T_{ext}^{t+k}(i)\right) - \hat{\varphi}_i^k \left(\hat{T}_{in}^{t+k}(i) - \hat{T}_{ext}^{t+k}(i)\right)^2\}) \tag{3.9}$$

Let $\Delta T_i^{t+k+1} = T_{in}^{t+k+1}(i) - T_{in}^{t+k}(i)$ and $\Delta \tau_i^{t+k} = T_{in}^{t+k}(i) - T_{ext}^{t+k}(i)$ and let both above equations are set equal to zero then it can be written as follows:

$$\begin{pmatrix} \sum_{t+k=1}^{n-1} \left(\dot{R}^{t+k}(i)\right)^2 & \sum_{t+k=1}^{n-1} \Delta\tau_i^{t+k} \dot{R}^{t+k}(i) \\ \sum_{t+k=1}^{n-1} \Delta\tau_i^{t+k} \dot{R}^{t+k}(i) & \sum_{t+k=1}^{n-1} \left(\Delta\tau_i^{t+k}\right)^2 \end{pmatrix} \begin{pmatrix} \alpha_i^k \\ \varphi_i^k \end{pmatrix} = \begin{pmatrix} \sum_{t+k=1}^{n-1} \Delta T_i^{t+k+1} \dot{R}^{t+k}(i) \\ \sum_{t+k=1}^{n-1} \Delta T_i^{t+k+1} \Delta\tau_i^{t+k} \end{pmatrix} \tag{3.10}$$

Let define $\mathrm{X}_i^k = [\ \dot{R}^{t+k}(i) \quad \Delta\tau_i^{t+k}\ ]$ and $\mathbf{Y}_i^k = [\Delta T_i^{t+k+1}]$, then Equation (3.10) can be rewritten in matrix form:

$$(\mathbf{X'}_i^k\mathbf{X}_i^k)^{-1}(\mathbf{X'}_i^k\mathbf{X}_i^k)\mathbf{b}_i^k = (\mathbf{X'}_i^k\mathbf{X}_i^k)^{-1}(\mathbf{X'}_i^k\mathbf{Y}_i^k) \tag{3.11}$$

where $\mathbf{b}_i^k$ is the 21 vector of coefficients, α_i^k and φ_i^k. Equation (3.11) is given by multiplying both sides of Equation (3.10) by the inverse of $(\mathbf{X'}_i^k\mathbf{X}_i^k)$. Using Equation (3.11), α_i^k and φ_i^k i=1,2,...,Z and k=1,2,...,N, are obtained as follows:

$$\mathbf{b}_i^k = (\mathbf{X'}_i^k\mathbf{X}_i^k)^{-1}(\mathbf{X'}_i^k\mathbf{Y}_i^k) \tag{3.12}$$

α_i^k and φ_i^k can equivalently be calculated as follows:

$$\hat{\alpha}_i^k = \frac{\sum_{t+k=1}^{n-1}\Delta T_i^{t+k+1}\dot{R}^{t+k}(i)\sum_{t+k=1}^{n-1}\left(\Delta\tau_i^{t+k}\right)^2 - \sum_{t+k=1}^{n-1}\Delta T_i^{t+k+1}\Delta\tau_i^{t+k}\sum_{t+k=1}^{n-1}\Delta\tau_i^{t+k}\dot{R}^{t+k}(i)}{\sum_{t+k=1}^{n-1}\left(\dot{R}^{t+k}(i)\right)^2\sum_{t+k=1}^{n-1}\left(\Delta\tau_i^{t+k}\right)^2 - \left(\sum_{t+k=1}^{n-1}\Delta\tau_i^{t+k}\dot{R}^{t+k}(i)\right)^2} \tag{3.13}$$

$$\hat{\varphi}_i^k = \frac{\sum_{t+k=1}^{n-1}\Delta T_i^{t+k+1}\Delta\tau_i^{t+k}\sum_{t+k=1}^{n-1}\left(\dot{R}^{t+k}(i)\right)^2 - \sum_{t+k=1}^{n-1}\Delta T_i^{t+k+1}\dot{R}^{t+k}(i)\sum_{t+k=1}^{n-1}\Delta\tau_i^{t+k}\dot{R}^{t+k}(i)}{\sum_{t+k=1}^{n-1}\left(\dot{R}^{t+k}(i)\right)^2\sum_{t+k=1}^{n-1}\left(\Delta\tau_i^{t+k}\right)^2 - \left(\sum_{t+k=1}^{n-1}\Delta\tau_i^{t+k}\dot{R}^{t+k}(i)\right)^2} \tag{3.14}$$

As mentioned in the previous section, the effective power rate, $\dot{R}^{t+k}(i)$ supplied to the i^{th} zone is not often measurable directly in real world applications. We note that $\dot{R}^{t+k}(i)$ can be different from the electrical power that can be computed from Energy-Plus or metered from real devices. In fact, summing up the delivered heating/cooling to all zones,$\dot{R}^{t+k}(i)$'s will not necessarily give the total electrical energy consumption of the building. Therefore, in this article, we will use a combined statistical and Energy-Plus approach to estimate the actual energy consumed by the building. The approach will be discussed in the next section.

We estimate the building total power energy as a function of $\dot{R}^{t+k}(i)$ and $T_{ext}^{t+k}(i)$ with the latter one usually having sufficient simulated or historical data. Lets denote y^{t+k} as the total energy consumption at time t; then the relationship between aforementioned

variables can be written as $y^{t+k} = f(\mathbf{T}_{ext}^{t+k}, \mathbf{R}^{t+k}.\mathbf{J})$, where $\mathbf{R}^{t+k}$ is a $1 \times p$ vector of and $\mathbf{J}$ is a $1 \times p$ vector of ones. Next, we will present how to estimate f using a generalized form of Cochrane-Orcutt estimation technique.

3.3.2 Energy Forecast Model

The relationship between total energy consumption, $\mathbf{R}^t$ and $\mathbf{T}_{ext}^t$ can be modeled through a simple linear regression as follows:

$$y^t = \beta_0 + \beta_1 \mathbf{R}^t J + \beta_2 \mathbf{T}_{ext}^t + \varepsilon^t \tag{3.15}$$

where ε^t is he error term at time t, β_j's are linear model parameters and is response variable (total energy consumption). If the assumption of linearity were met, then ε^t would typically be assumed independent and the model parameters, β_j's , would be estimated using Least Squares Error (LSE) technique. However, the actual relationship between total power consumption at time t with effective cooling power and external temperature may follow an unknown nonlinear model. In addition, there are more variables such as occupancy and cooling fans power that can affect the total power consumption. These effects cannot be explained through the linear structure of Equation (3.15), and as a result, they emerge into the error terms. In this situation, the assumption of independency is no longer met and the ordinary LSE technique cannot be applied [44]. To avoid this problem, we employ the Cochran-Orcutt technique by rewriting Equation (3.15) as follows:

$$y^t = \beta_0 + \beta_1 \mathbf{R}^t J + \beta_2 \mathbf{T}_{ext}^t + \varepsilon^t, \varepsilon^t = \xi(\varepsilon^{t-1}, \varepsilon^{t-2}...) + e^t. \tag{3.16}$$

Similar to Chapter 2,e^t is an independent and identical white noise and ξ is a function of past error terms representing the structure of autocorrelation and y^t is response variable (total energy consumption). According to Section 2.2.1, the transformed variables can be rewritten as follows:

$$\acute{y_t} = \varphi_p(B)\Phi_P^s(B)Y_t,\ \acute{\mathbf{x}_t} = \phi_p(B)\Phi_P^s(B)\mathbf{x}_t,\ \acute{\beta_0} = \phi_p(B)\Phi_P^s(B)\beta_0. \tag{3.17}$$

where,$\varphi_p(B)$ and $\Phi_P^s(B)$ are autoregressive operators with orders of p and P that are applied to both the external temperature and the vector of zonal effective power to find the building total energy demand (See Chapter 2). Hence Equation (3.16) can be replaced by

$$y'_t = \beta'_0 + \mathbf{x'}_t\beta'_t + a_t \tag{3.18}$$

Now Equation(3.18) is an ordinal multiple linear regressions with independent error terms and can be calculated via OLS estimation method. The same algorithm discussed in Section 2.3.1 is applied to estimate the parameters. In addition, Equation(2.7) and Equation(2.8) are used to investigate the adequacy of the proposed model.

3.4 Optimal Control Strategy

In the previous sections, we introduced two models that are coupled to capture dynamic behavior of building energy consumption. In this section, we propose an optimal control strategy by developing a mathematical programming formulation that is solved dynamically over time. The cooling/heating model presented in Equation (3.6) is a dynamic model that describes how the state variables, $T_{in}^{t+k}(i)$'s, are evolved over time by starting from an initial condition $T_{in}^{0}(.)$ and by manipulating control variables, $\dot{R}^{t+k}(i)$. At time t+k-1, the actual internal temperature, $T_{in}^{t+k}(i)$ is *unknown* and is specified by replacing it with any arbitrary set point value, i.e. $T_{in}^{t+k}(i) = \nu_i \in [l_i\ u_i]$. Then $\dot{R}^{t+k-1}(i)$ can be calculated accordingly using Equation (3.7). $\dot{R}^{t+k-1}(i)$ is then fed into Equation (3.15) to calculate the corresponding building total energy use. This is repeated for the next 24 hours and for all combination of set point values between l_i and u_i and all zones to find the optimal combination of set points that minimize total energy use and total deviation from the thermal comfort.

The dynamic model requires a dynamic programming scheme to find the optimal control variables in such a way that the objective function is optimized over a specific time horizon N. In this study, we set N=24, so that the control scheme can provide the optimal control variables for any 24 look-ahead periods (hours in the current case).

At any given hour, the optimization procedure is repeated for the next 24 hours by updating the state variables $T_{in}^{t+k}(i)$'s, and external temperature values. At each time step, the optimal control scheme solves the following multi-objective problem:

$$\min_{\mathbf{R}^{t+k}} G_1(N, \mathbf{R}^{t+k}, \mathbf{T}_{ext}^{t+k}, \mathbf{T}_{in}^{t+k}) \equiv \tag{3.19}$$
$$\sum_{k=0}^{N-1} c_{t+k} y_{t+k}(\mathbf{R}^{t+k}, \mathbf{T}_{in}^{t+k}).\Delta t + \upsilon. \max_{k \in t_d} \left\{ y_{t+k}(\mathbf{R}^{t+k}, \mathbf{T}_{in}^{t+k}) \Delta t \right\}$$

$$\min_{\delta_{t+k}^u, \delta_{t+k}^l} G_2(N, \delta_{t+k}^u, \delta_{t+k}^l) \equiv p_{t+k} \sum_{k=0}^{N-1} (\delta_{t+k}^u + \delta_{t+k}^l) \tag{3.20}$$

subject to

$$T_{min}^{t+k}(i) - \delta_{t+k}^l \leq \hat{T}_{in}^{t+k}(i) \leq T_{\max}^{t+k}(i) + \delta_{t+k}^u, k = 1, 2, ..., N-1, i = 1, 2, ..., Z \tag{3.21}$$

$$\hat{T}_{in}^{t+k+1}(i) = \hat{T}_{in}^{t+k}(i) + \hat{\alpha}_i.R^{t+k}(i) + \hat{\varphi}_i(\hat{T}_{in}^{t+k}(i) - \hat{T}_{ext}^{t+k}(i)), \tag{3.22}$$
$$k = 1, 2, ..., N-1, i = 1, 2, ..., Z$$

$$T_{in}^0(i) = T_0, i = 1, 2, ..., Z \tag{3.23}$$

$\delta_{t+k}^l \geq 0, \delta_{t+k}^u \geq 0$, $\mathbf{R}^t \geq \mathbf{0}$, $k = 1, 2, ..., N-1$

where $T_{min}^{t+k}(i)$ and $T_{\max}^{t+k}(i)$ are the thermal comfort upper and lower bounds for the i^{th} zone internal temperature at time $t+k$. δ_{t+k}^l is the temperature violation below the lower bound and δ_{t+k}^u is the temperature violation above the upper bound. T_0 is the internal temperature at time 0 and Δt is the length of the time period that is set equal to one hour. The thermal comfort constraint is imposed to each single zone based on the current zone temperature. There are two objective functions: (i) $G_1(.)$ is the total cost of energy, which includes *Total Usage Cost* (cost per kWh) and *Daily As-used Demand Charges*. The latter cost is determined for each weekday in the billing period and applied to the daily peak demand during each time period. The Monthly as-used demand charges for the billing period are equal to the sum as-used daily demand charges for the time periods [71]. Here, c_{t+k} is unit price of electricity at time $t+k$ and (ii) $G_2(.)$

is the total penalty for exceeding the thermal comfort bounds. This function penalizes any deviation from the predefined comfort bounds at any given time. υ is the penalty applied on peak energy demand, is a set representing the on-peak period, and p_{t+k} is the penalty that is applied to any violation from the comfort bounds at time $t+k$. The latter parameter indicates different discomfort costs for different hours of a day.

Since $G_1(.)$ and $G_2(.)$ do not match in units and scale, it is not possible to integrate them into a single objective function by simply adding their values. Hence, we build a Multiobjective Mathematical Programming (MMP) structure using a weighted l_p metric method and discuss it in the next section.

3.4.1 Weighted Metric Method

It is typically impossible to find a single optimal solution that simultaneously optimizes all the objective functions. Pareto analysis is a preferred technique used by many. In this study, we use a classical MMP technique called weighted l_p metric method. The reason we use this method is that it requires less restrictive assumptions (See e.g. [72] and [73]). The l_p metric method scales $G_1(.)$ and $G_2(.)$ into a single objective function that is in an l_p metric form as follows:

$$G(N, \mathbf{R}^{t+k}, \mathbf{T}_{ext}^{t+k}, \mathbf{T}_{in}^{t+k}, \delta_{t+k}^{u}, \delta_{t+k}^{l}) = \tag{3.24}$$
$$\left\{ w_1 \left(\frac{G_1(N, \mathbf{R}^{t+k}, \mathbf{T}_{ext}^{t+k}, \mathbf{T}_{in}^{t+k}) - G_1^{min}}{G_1^{max} - G_1^{min}} \right)^{p} + w_2 \left(\frac{G_2(N, \delta_{t+k}^{u}, \delta_{t+k}^{l}) - G_2^{min}}{G_2^{max} - G_2^{min}} \right)^{p} \right\}^{1/p}$$

Both $G_1(.)$ and $G_2(.)$ in Equations (3.19) and (3.20) are replaced with (3.24). In this equation, w_1 and w_2 are the non-negative weights for $G_1(.)$ and $G_2(.)$, respectively, such that $w_1 + w_2 = 1$. w_1 and w_2 represent the relative importance of the objective functions and are determined by the decision maker. $p \in [1, \infty)$ indicates the type of metric we use in our problem. For example, p=1 is equivalent to solving the weighted sum of deviations from ideal values, whereas, p=2 means minimizing the weighted Euclidean distance of any point in the objective space from its ideal point. It is proven that if there exist bounded solutions for G1 and $G_1(.)$ and $G_2(.)$, then for any combinations of w_i's and $p(> 1)$ values, there is one or more Pareto solutions [72-74]. A Pareto solution

has the property that, for any point in the Pareto set, there does not exist another point that results in better performance for both objectives simultaneously [74].

$G_j^{\min}$ and $G_j^{\max}$ are the minimum and maximum possible values of the j^{th} objective function. It is easy to find the minimum and maximum possible values for the second objective function. The minimum penalty for exceeding the thermal comfort bounds is 0, when the internal temperature is within thermal comfort $\left(T_{min}^{t+k}(i) \leq \hat{T}_{in}^{t+k}(i) \leq T_{\max}^{t+k}(i)\right)$ or equivalently $\delta_{t+k}^{l} = \delta_{t+k}^{u} = 0$. The maximum penalty for exceeding thermal comfort, $G_2^{\max}$, can be calculated by multiplying the maximum penalty, p_{t+k}'s and the maximum deviation form thermal comfort as follows:

$$G_2^{\max} = \max_{1 \leq k \leq N} \{p_{t+k}\} \times \max_{1 \leq k \leq N} \left\{\delta_{t+k}^{l}, \delta_{t+k}^{u}, k = 1, 2, .., N\right\} \tag{3.25}$$

Similarly, the minimum value of the first objective function, $G_1^{\min}$, is set equal to zero. This is because the first objective function is the total energy consumption cost, and when there is no consumption, the cost is zero. $G_1^{\max}$ can be found using EnergyPlus by calculating the maximum energy consumed by HVAC. That is,

$$G_1^{\max}(t+k) \equiv \max_{1 \leq k \leq N} \{c_{t+k}\} y_{t+k}(R^{\max}, \hat{T}_{ext}^{\max}(i))\Delta t + \upsilon . \max_{k \in t_d} \left\{y_{t+k}(\mathbf{R}^{t+k}, \mathbf{T}_{in}^{t+k})\Delta t, \right\} \tag{3.26}$$

$k = 1, 2, ..., N$

where $R^{\max}$ is the maximum load that can be generated by HVAC at any time and $T_{ext}^{\max}(i))$ is the highest external temperature. Note that Equation (3.26) calculates the maximum cost for the maximum energy consumed by HVAC in the highest daily temperature. This gives an upper limit for total energy consumption cost at any time. Both components of Equation (3.24) are normalized between 0 and 1 and as a result the metric function $G(N, \mathbf{R}^{t+k}, \mathbf{T}_{ext}^{t+k}, \mathbf{T}_{in}^{t+k}, \delta_{t+k}^{u}, \delta_{t+k}^{l})$ varies between 0 and 1. One disadvantage of the weighted metric method compared to those methods that normalize objective functions is that its performance highly depends on the values of $G_j^{\min}$ and $G_j^{\max}$. For example, in this study, calculating the maximum HVAC capacity and the highest external temperature may result in extremely large value of $G_1^{\max}$. In this

case, the first component of Equation (3.24) is much smaller than the second component (thermal comfort). This means that the thermal comfort can always influence the result of optimization.

To tackle this problem, it is required to modify $G_1^{\max}$ value by using domain specific knowledge or historical information on the building. In addition, a potential alternative for the weighted metric method would be using desirability functions, which further depend on the Decision Maker preferences. These will be discussed in the next chapter.

3.4.2 Dynamic Programing Model

The proposed MMP Equations (19-24) can be rewritten as follows:

$$\min_{\mathbf{R}^{t+k}} G(N, \mathbf{R}^{t+k}, \mathbf{T}_{ext}^{t+k}, \mathbf{T}_{in}^{t+k}, \delta_{t+k}^{u}, \delta_{t+k}^{l}) \tag{3.27}$$

subject to

$$T_{min}^{t+k}(i) - \delta_{t+k}^{l} \leq \hat{T}_{in}^{t+k}(i) \leq T_{\max}^{t+k}(i) + \delta_{t+k}^{u}, k = 1, 2, ..., N-1, i = 1, 2, ..., Z \tag{3.28}$$

$$\hat{T}_{in}^{t+k+1}(i) = \hat{T}_{in}^{t+k}(i) + \hat{\alpha}_i.R^{t+k}(i) + \hat{\varphi}_i(\hat{T}_{in}^{t+k}(i) - \hat{T}_{ext}^{t+k}(i)), \tag{3.29}$$

$k = 1, 2, ..., N-1, i = 1, 2, ..., Z$

$$T_{in}^{0}(i) = T_0, i = 1, 2, ..., Z \tag{3.30}$$

$\delta_{t+k}^{l} \geq 0, \delta_{t+k}^{u} \geq 0$, $\mathbf{R}^t \geq \mathbf{0}$, $k = 1, 2, ..., N-1$

The model is now an ordinary mathematical programing with single objective function and can be solved using Dynamic Programming algorithm. At time t, the model is solved and the optimal control values for the next 24-hour are obtained. Then, in the next hour, once some new data from zones internal temperature are received, we update all state variables and solve the model with updated parameters. This process is repeated every hour and once we receive new information about state variables.

3.5 Numerical Example

In this section, we evaluate the performance of our proposed control strategy through an illustrative building. We follow our proposed framework presented in Section 3.3 and Figure 3.1. The example uses a large office model, which represents a commercial reference-building developed by the he U.S. Department of Energy (Further details can be found in [75]). In Offline phase, we select twelve main zones of the building and run the simulation using 2009 Phoenix weather data. We collect one-month hourly data (July 2009) and extract 744 hourly basis simulated output data on the following variables: zonal internal temperatures, building external temperature, zonal cooling power rate values as well as the building total energy consumption. Similarly, we mimic Online Phase (see Figure 3.1), by using one-month simulation data for August 2009. In this phase, at each hour, the simulation model is run one time, the model parameters and optimization model are repeated, and optimal set point values are updated. The outputs are as follows: the total energy consumption cost including usage cost, demand charge and thermal discomfort penalty are calculated in a daily and the set of optimal set point values for each zone at time $t + l$ to time $t+k$.

3.5.1 The Heating/Cooling Model Results

As shown in Figure 3.1, in Offline Phase, we construct two models used for forecasting internal temperature (the heating/cooling model) as well as building total energy consumption (the energy forecast model). In this section, we will investigate the performance of both models. The estimated parameters of the proposed cooling/heating model are presented in Table 3.1. In this chapter, we assume that $\hat{\alpha}_i^k$ and $\hat{\varphi}_i^k$ are fixed over time or equivalently $\hat{\alpha}_i^k = \hat{\alpha}_i =$ and $\hat{\varphi}_i^k = \hat{\varphi}_i$ for $k = 1, 2, ..., 24$. It implies that during simulation the overall weather pattern does not change significantly. This assumption may work for a short time, however, for a long-term optimal control strategy; one should estimate the parameters adaptively. This assumption will be relaxed in Chapter 4.

Table 3.1: The least square error (LSE) estimates for cooling/heating model parameters

Zone											
1	2	3	4	5	6	7	8	9	10	11	12
-0.38	-0.18	-0.32	-0.28	-0.37	-0.16	-0.3	-0.27	-0.38	-0.14	-0.32	-0.28
-0.26	-0.1	-0.22	-0.19	-0.25	-0.09	-0.21	-0.18	-0.26	-0.09	-0.22	-0.19

As shown in Table 3.1, α's are all (< 0) showing negative correlations between the next hour internal temperature and zonal effective power rate. This is because the simulated dataset is run in a summer month and the effective power is used for cooling of the building. Similarly, φ's (< 0) show negative correlation between current internal temperature and external temperature. Figure 3.2 displays a radar chart for the correlations between the actual internal temperature values and their corresponding k-step-ahead forecast values for each zone. In this figure, the i^{th} radius represents the ith zone and the k^{th} irregular polygon represents the correlation between the k-step-ahead forecasted internal temperature and its corresponding actual temperature. It shows that the correlations between actual internal temperature values and its 1-step-ahead forecast values (k=1) vary between 0.75 and 0.85. This also shows that the proposed cooling/heating model can appropriately provide the one-step-ahead forecast for the zonal internal temperature. Furthermore, it is observed that the performance of the proposed heating/cooling model decreases as the lag increases. For instance, the correlation between the actual and forecasted internal temperature for the third lag (k=3) varies around 0.5, which is expected.

[H] This also can be seen in Figure 3.3. In this figure, we plot the first zones actual and forecasted internal temperature values for the first and fifth lags. The one-step-ahead forecast values are approximately close to the actual data while the 5-step-ahead forecast values are relatively far from the actual internal temperature. As previously discussed, this is mainly because we assume that $\hat{\alpha}_i^k = \hat{\alpha}_i =$ and $\hat{\varphi}_i^k = \hat{\varphi}_i$ for $k = 1, 2, ..., 24$. It means that the structure of balance equations does not change as time passes. The performance of the proposed forecast values will be increased by applying a time-dependent parameter estimation method in the next chapter.

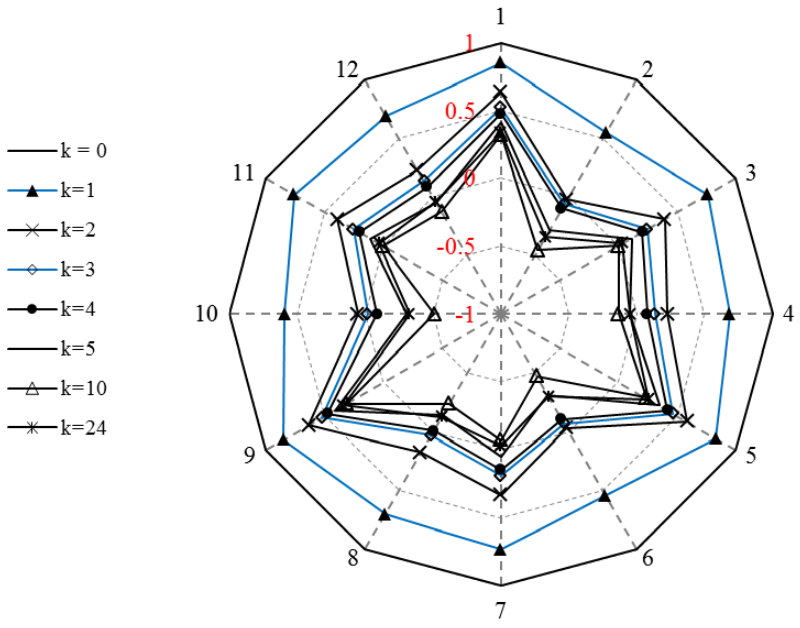

Figure 3.2: Correlation values between actual internal temperature and its corresponding k-step-ahead forecasted values

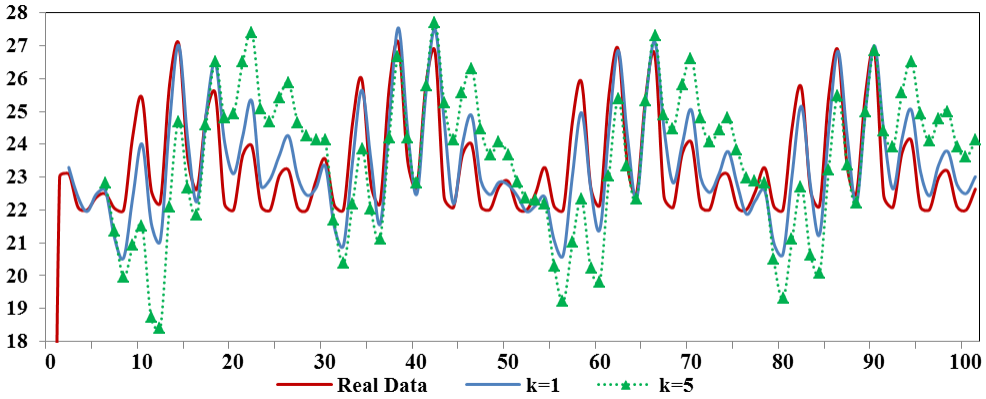

Figure 3.3: Comparison of simulated and forecasted values for the first zone internal temperature

3.5.2 The Energy Forecast Model Results

According to the proposed framework shown in Figure 3.1, the energy forecast model is employed the cooling power rate data and external temperature values to forecast total energy consumption. In this section, we evaluate the performance of the energy

forecast model using simulated data. Again, to construct the energy forecast model we use the 2009 July data, which is generated by EnergyPlus in Offline Phase. Table 3.2 represents the estimated parameters of the proposed energy consumption model as well as performance measure values. The correlation values for all lags are greater than 0.95. The coefficient of determination R^2 and the adjusted coefficient of determination R^2_{adj} for the 24th lag are 95.9% and 95.7%, respectively. This indicates that the proposed model can provide high quality 24-hour-step-ahead forecast values for total energy demand, which are very close to the actual energy demand.

Table 3.2: The estimates values for energy consumption forecast model

	Parameters								
	β_1	β_2	ϕ_1	ϕ_2	ϕ_3	ϕ_4	ϕ_5	ϕ_6	ϕ_7
Estimates	4.3528	0.4808	0.078	-0.012	0.014	0.019	-0.028	0.002	-0.002
Std. Error	0.3922	0.1015	0.0238	0.0243	0.0242	0.0239	0.024	0.0241	0.024
Hour	-	-	1	2	3	4	5	6	7
R^2	-	-	96.37	96	96.03	96.01	95.95	96.018	96.02
R^2_{adj}	-	-	96.18	95.8	95.83	95.8	95.74	95.81	95.81
	Parameters								
	ϕ_8	ϕ_9	ϕ_{10}	ϕ_{11}	ϕ_{12}	ϕ_{13}	ϕ_{14}	ϕ_{15}	ϕ_{16}
Estimates	-0.006	-0.003	-0.012	0.005	-0.027	0.026	-0.018	0.016	0.004
Std. Error	0.0237	0.0239	0.0241	0.0241	0.0241	0.0242	0.0242	0.0241	0.024
Hour	8	9	10	11	12	13	14	15	16
R^2	96.02	96.02	96.02	96.03	96.02	96.04	96.02	96.02	96.01
R^2_{adj}	95.81	95.81	95.81	95.82	95.81	95.83	95.81	95.8	95.8
	Parameters								
	ϕ_{17}	ϕ_{18}	ϕ_{19}	ϕ_{20}	ϕ_{21}	ϕ_{22}	ϕ_{23}	ϕ_{24}	
Estimates	-0.009	-0.004	0.003	0.002	-0.022	-0.026	0.007	0.936	-
Std. Error	0.0239	0.0237	0.0237	0.0238	0.0238	0.0237	0.0239	0.0239	-
Hour	17	18	19	20	21	22	23	24	-
R^2	96.01	96	95.99	96	95.99	95.98	95.96	95.97	-
R^2_{adj}	95.8	95.79	95.78	95.78	95.78	95.76	95.75	95.75	-

Figure 3.4 presents a comparison between the actual and forecasted total energy consumption for the 24^{th} lag. The forecast model can capture the majority of the variations. Thus, the proposed forecast model is deemed a reasonable replacement for the simulation, particularly well-suited for optimization purposes.

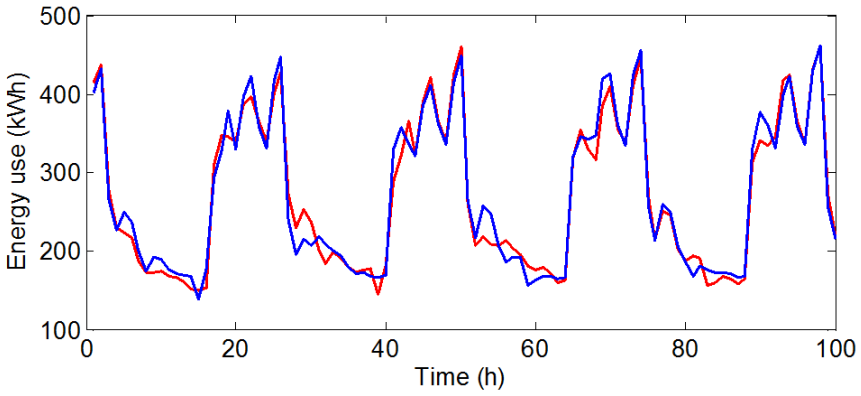

Figure 3.4: Comparison of simulated and forecasted values for the building total energy consumption

3.5.3 The Optimization Model Results

In this section, we investigate the performance of the proposed optimal control strategy for the above illustrative model. Table 3.3 presents the input parameters of the proposed mathematical model (Equations 3.19-3.25). Note that $\hat{p}_{t+k}$, the thermal discomfort penalty, is a normalized multiplier, defined by the decision maker, to weigh the importance of keeping the internal temperature within the thermal comfort at time $t+k$. In this study, $\hat{p}_{t+k}$ is normalized based on the number of people working in each zone such that the total thermal discomfort penalty over 24 hours is equal to 1.0. Also,

Table 3.3: The cost coefficients and thermal discomfort penalty values

	k											
	1	2	3	4	5	6	7	8	9	10	11	12
c_{t+k}	0.11	0.11	0.11	0.11	0.11	0.11	0.11	0.11	0.11	0.11	0.11	0.21
$\hat{p}_{t+k}$	0	0	0	0	0	0	0.009	0.037	0.093	0.093	0.093	0.093
	k											
	13	14	15	16	17	18	19	20	21	22	23	24
c_{t+k}	0.25	0.35	0.45	0.35	0.35	0.35	0.25	0.25	0.25	0.11	0.11	0.11
$\hat{p}_{t+k}$	0.093	0.093	0.093	0.093	0.074	0.037	0.037	0.019	0.019	0.019	0.009	0

it is assumed that the internal temperature values can vary between 62F and 76F with an increment rate of 0.5 units. However, $T_{min}^{t+k}(i)$ and $T_{\max}^{t+k}(i)$ in Equation (3.28) are fixed and set equal to 68 and 72, respectively. Therefore, any internal temperature value less than 68 or greater than 72 is penalized by applying thermal discomfort cost.

Besides, w_1 and w_2, the importance factors associated with objective functions $G_1(.)$ and $G_2(.)$ are set equal to 0.7 and 0.3 indicating that the energy consumption cost is relatively more important than thermal discomfort penalty. Without loss of generality, we assume p =1 which turns the problem into a weighted sum of normalized deviations. Figure 3.5 illustrates the effect of the proposed weighted metric method in combining both objective functions. The figure plots the minimum cost-to-go values (minimum total cost from step 1 to step k) in dynamic programming. The x-axis shows the feasible set point values ranging between 62 °F to 78 °F and the y-axis shows the minimum values of the combined function, $G(.)$, over the reduced horizon from t+1 to t+k when $k < N$. For the first six hours, as set point values increase, the minimum cost-to-go value decreases. This is because we set the thermal discomfort penalty equal to zero for the first six hours (see Table 3.3). This implies that for the first six hours, the only active objective function is $G_1(.)$. In this case, higher temperature values result in lower demands without increasing the thermal discomfort objective function.

Figure 3.6 presents values of optimal set point, energy demand, and operating costs versus time for a period of 72 hours. Figure 3.6.a for instance, depicts the optimal set point values and their corresponding values of internal temperature that is an average value over all building zones. It is worth noting that in an ideal HVAC system, the optimal set points and internal temperature are same values. However, in real world, many unknown or uncontrollable factors can significantly cause the actual internal temperature to be deviated from the set point values. This is particularly obvious when the proposed control scheme select a very low set point at time t after a higher set point value at time t-1(e.g. see t=11 in Figure 3.6.a). In this situation, HVAC system cannot reach the optimal set point value in such a short time frame. In fact, this is one reason that the model is updated when new information from internal temperature is received.

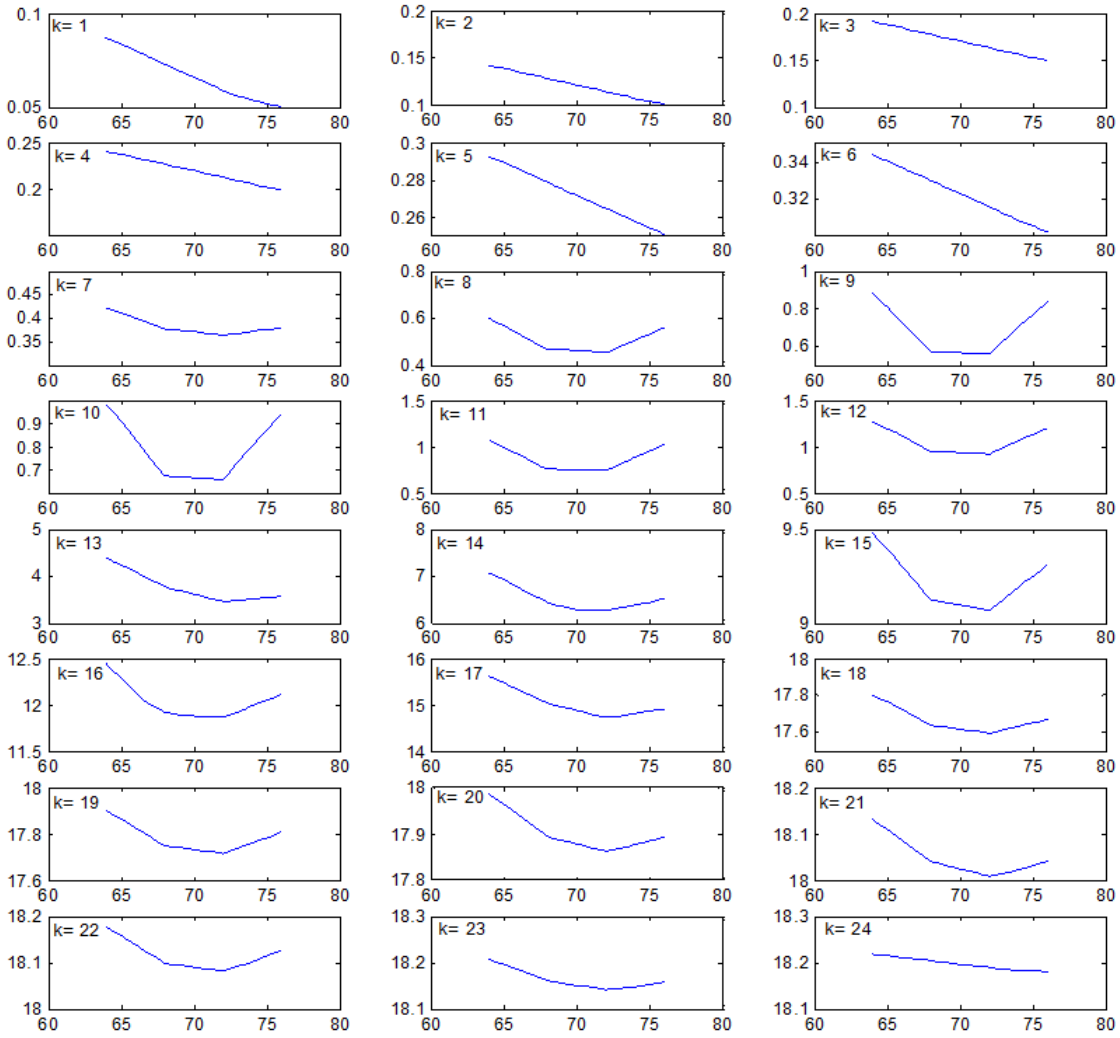

Figure 3.5: The minimum cost-to-go profile over different internal temperatures for $k = 1, 2, ..., 24$. For each subplot x-axis is the feasible set point values °F) and y-axis is the sum of the minimum values of the combined function, $G(.)$, over the reduced horizon from $t+1$ to $t+k$ for $k < 24$.

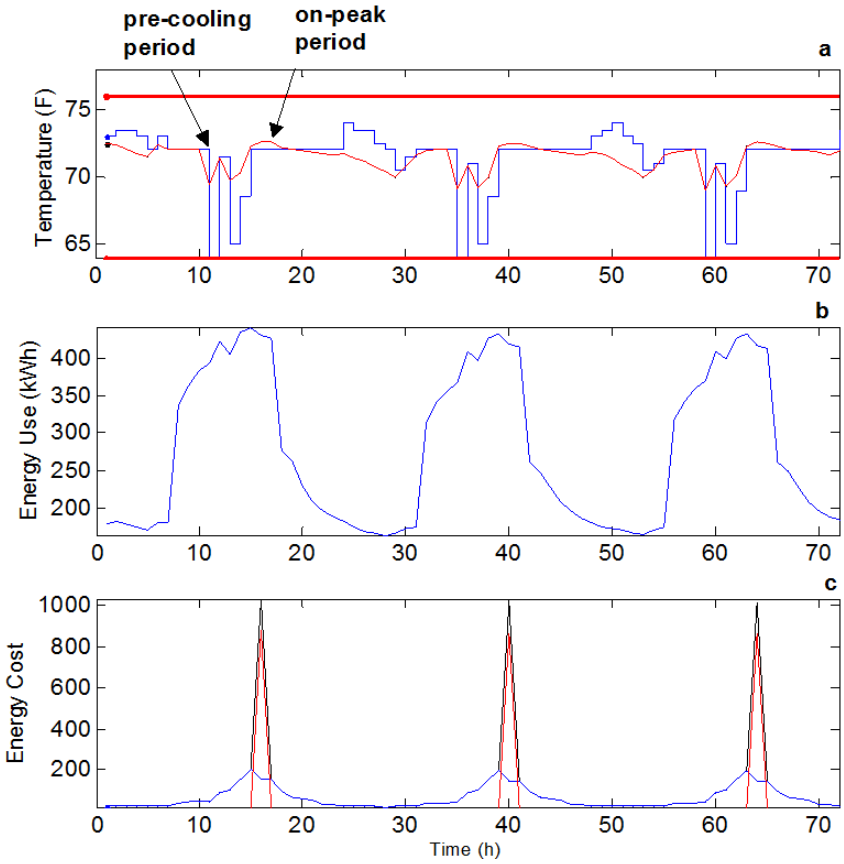

Figure 3.6: The results of the proposed control strategy: a) The optimal set point values and average internal temperature, b) Optimum energy consumption profile over time c) Optimum total operating cost profile including variable cost and demand charge cost.

Figure 3.6.b illustrates that total building energy demand oscillates according to the zone effective power and set point values. Figure 3.6.c includes separate profiles for total use cost per kWh, the daily as-used demand charge cost and total energy cost. Note that in this example, it is assumed that the daily as-used demand charge is applied once in a day to the maximum energy consumed in peak hours between 1:00 p.m. and 6:00 p.m. Therefore, the pre-cooling time is immediately before 1:00 p.m. and is applied to lower the maximum energy demand after 1:00 and as a result reduce the daily as-used demand charge cost.

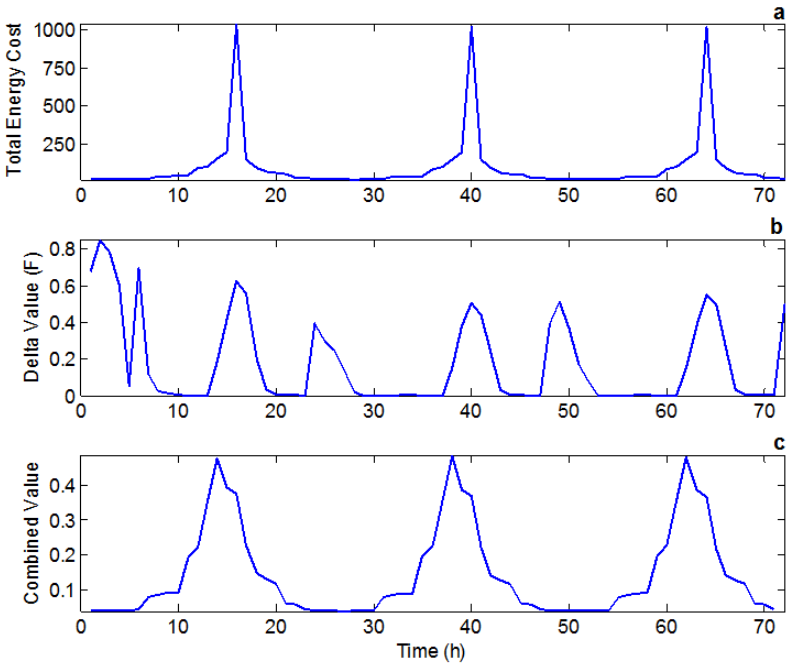

Figure 3.7: The results of the proposed control scheme: a) Total Energy Consumption, b) the temperature violations below or above the thermal comfort bounds, c) Combined weighted metric values.

Figure 3.7 presents further details about how the two different objective functions are combined to shape the single measure that is optimized. Figure 3.7.a is the total energy cost including energy costs and daily as-used demand charges. Figure 3.7.b depicts the temperature violation from the thermal comfort bounds over time. As shown in this figure, the maximum and minimum values for each of these functions are different. Although the violation from thermal comfort is slightly higher in off-peak periods, when less people are in the building, there are still large violations in on-peak periods. This is because, in on-peak periods, the energy demand is very high and the proposed model attempts to reduce the costs by allowing some violations above or below the thermal comfort bounds. A normalized version of this figure is presented in Figure 3.8. These plots present the normalized profiles associated with total energy cost, $G_1(.)$, as well as the total thermal comfort violation penalty $G_2(.)$. The maximum values of these two

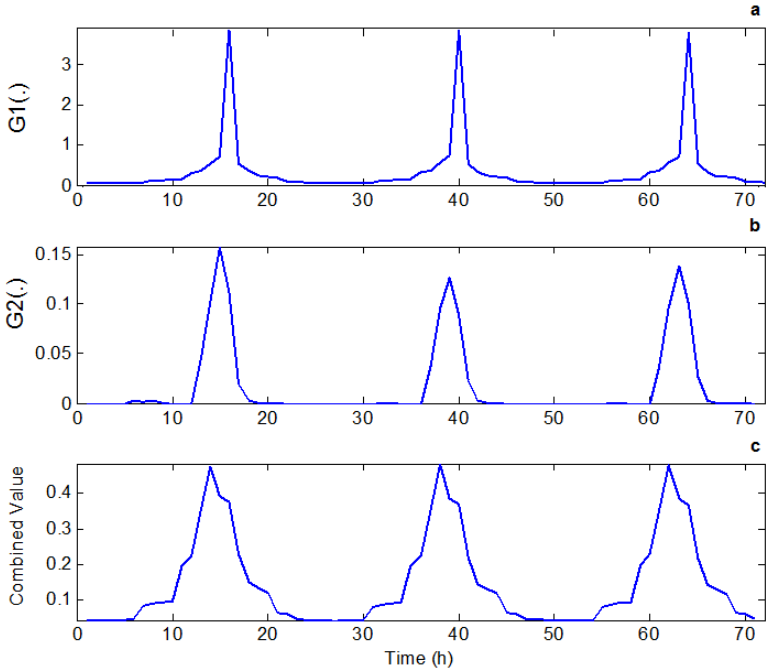

Figure 3.8: a) The normalized energy cost profile, b) the normalized thermal discomfort penalty profile, c) the normalized combined metric profile

functions are slightly different. The maximum values of $G_1(.)$ are in peak hours while the maximum values of $G_2(.)$ occur immediately before peak hours. This configuration leads to the minimum combined metric profile that is $G_1(.)$.

We also compare our proposed control scheme with a number of simple alternative control schemes as shown in Figure 3.9. These configurations are set to cover different scenarios and provide good insights about the proposed control scheme. The Constant Controller 1 and the *Highest Value* control schemes have fixed set point values that do not change during the 24 hour period shown. The *Highest Value* controller is set equal to be76 °F and as a result, returns the lowest total energy cost but the maximum thermal discomfort cost for this particular day that requires cooling. The dynamic controllers vary over time using different patterns. For example, *Dynamic Controller 2* allows HVAC to provide more cooling before peak hours and then during peak hours it increases the set point values. We use different controllers to understand the characteristics of the proposed control scheme.

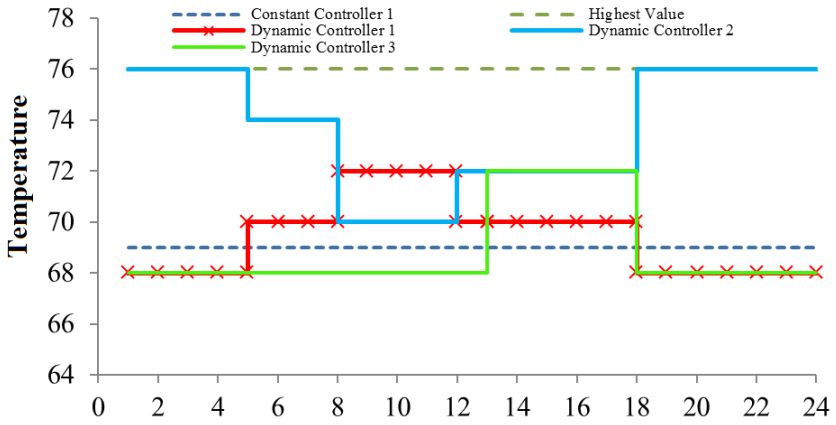

Figure 3.9: Alternative Control Schemes

Table 3.4 depicts the results of running different control schemes for the Medium Office Model. It shows that the proposed scheme is superior to other alternatives in total combined metric value, $G(.)$, that is the combined objective function for this problem. It means that the proposed control scheme is able to find the best compromise between energy consumption costs and thermal comfort. The energy consumption cost is minimal for the *Highest Value* controller. This is obvious, because it provides the minimum possible cooling load and keeps the internal temperature around 76 °F. However, the normalized thermal discomfort penalty $G_2(.)$, for such controller is 0.81 that is significantly greater than the other controllers. Such an extreme controller provides internal temperature values are often beyond the upper thermal comfort bound and are impractical in real world. Note that the maximum thermal discomfort penalty, $G_2(.)$, is one implying that the internal temperature would never go below the maximum thermal discomfort value.

On the other hand, the normalized energy consumption cost, $G_1(.)$ for the constant controller (Set point = 69 Fahrenheit) is 0.27, which is the highest energy cost among the alternatives. The minimum normalized energy consumption cost is associated with the proposed control scheme as well as the Highest Value Controller and is equal to

Table 3.4: Comparison between the Proposed Control Strategy and Other Control Schemes

	Control Schemes			
	Proposed Controller	Constant Controller1	Constant Controller2	Highest Value
Daily Energy Cost	2450.12	2639.72	2508.73	2312.6
Daily Usage Cost	1462.29	1613.27	1517.32	1399.2
Daily Demand Charge	987.83	1026.45	991.41	913.37
Normalized Cost, G_1	0.2	0.27	0.26	0.25
Violation from Comfort,	0.06	0.02	0.02	0.81
Normalized Discomfort, G_2	0.01	0	0	0.22
Combined Metric, G	0.08	0.11	0.11	0.17
	Control Schemes			
	Dynamic Controller1	Constant Controller2	Constant Controller3	
Daily Energy Cost	2622.52	2410.23	2658.9	
Daily Usage Cost	1598.66	1457.31	1624.27	
Daily Demand Charge	1023.86	952.92	1034.63	
Normalized Cost, G1(.)	0.24	0.2	0.24	
Violation from Comfort,	0.02	0.45	0.02	
Normalized Discomfort, G2(.)	0	0.08	0	
Combined Metric Value, G(.)	0.1	0.11	0.1	

0.20. This implies that the proposed control scheme offers the set point values with minimum cost and maintains the thermal comfort in an appropriate level, thus $G(.)$ is minimized.

Although the energy consumption costs for control schemes are clearly different, their normalized values of energy cost $G_1(.)$ are very close to each other (from 0.20 to 0.26). This is because the maximum value of energy consumption cost, $G_1^{max}(.)$ is very large. If is large, then the first component of Equation (3.24) (the normalized energy cost) becomes very small. To tackle this problem, one can propose better choices for $G_1^{max}(.)$ or apply other multi-objective techniques to combine the two objective functions. Further details will be discussed in the next chapter. Table 3.4 reveals that the proposed framework can adequately be employed to minimize building energy-use costs and at the same time keep the internal temperature in an acceptable thermal comfort bounds. The example presented in this section provides a clear insight about the performance of the proposed model. The results and analyses can be summarized as: (i) The proposed

heating/cooling model can appropriately forecast the next hour internal temperature, but needs more extensions for other lags; (ii) The energy forecast model works quite well for total energy consumption; (iii) the proposed control scheme provides the set point values which minimize both total energy consumption cost and thermal discomfort penalty at the same time. Although the proposed framework can be used to control the energy consumption costs of building complexes, further extensions and potential improvement can be done to improve the performance of the proposed framework and to address the real world challenges. We will discuss some of these improvements in the next chapter.

Chapter 4

Extensions of Optimal Control Strategy for Building Cooling/Heating Systems

4.1 Introduction

In Chapter 3, a physics-based statistical model was developed to capture the variability of energy dynamics within each zone. The model assumed that the effective power rate and the internal and external temperatures did not significantly change over a short period of time. Therefore, the model parameters were set to be fixed for the hours of a day. This assumption is relaxed in this chapter by including time-dependent variables and using a more generalized statistical model.

In addition, although the optimal control strategy presented in Chapter 3 can directly be used to reduce total building energy cost, several extensions and potential improvements can still be done to improve its performance. In this chapter, the of the proposed dynamic programming is revised to highlight the role of the daily as-used demand charge in calculating total building energy cost.

4.2 The Extended Cooling/Heating Model

The cooling/heating model presented in the previous chapter is a physics-based data driven model and is written as follows:

$$T_{in}^{t+k+1}(i) = T_{in}^{t+k}(i) + \alpha_i^k.\dot{R}^{t+k}(i) + \varphi_i^k \left(T_{in}^{t+k}(i) - T_{ext}^{t+k}(i)\right) + \varepsilon^{t+k}, \qquad (4.1)$$

where α_i^k represents the amount of unit increase (decrease) in the i^{th} zone internal temperature by one unit increase (decrease) in effective power rate at time $t+k$ (for

$k = 1, 2, ..., 24$). φ_i^k represents the amount of unit increase (decrease) in the zone internal temperature by one unit increase (decrease) in the difference between inside and outside temperature. In the previous chapter we assume that α_i^k and φ_i^k are fixed for different hours of a day or equivalently $\alpha_i^k = \alpha_i$ and $\varphi_i^k = \varphi_i$ for $k = 1, 2, ..., 24$. This assumption would be reasonable if the ambient temperature has a stationary pattern over time or in other words, if the weather does not radically change during the day.

In addition, in the previous chapter, the time interval between two samples is set to be one hour. Therefore, any dynamic change less than an hour is completely or partially lost in the proposed model. Also, there is less control on zones set point values during the process of optimization. In the extended model, the time interval is set to be 15 minutes, so that short-term variability can be captured. Furthermore, shorter time intervals provide smother models that can appropriately fit with the lower-order models (e.g. Linear models). On the other hand, smaller time interval can decrease the computational efficiency of the optimization algorithm.

There are two approaches to extend the cooling/heating model presented in Equation (4.1): The first approach is to directly estimate all α_i^k and φ_i^k parameters and obtain their values using the same method presented in Chapter 3 (equations 3.13 and 3.14). To do this for the i^{th} zone, 24 values of α_i^k and φ_i^k should be obtained using historical data. Therefore, for a building with N zones,$24N$ values of α_i^k and $24N$ values of φ_i^k must be estimated. For 15-minute time interval, number of estimated values will be $96N$. This needs a large sample size of historical data for parameter estimating the parameters.

The second approach is to pool all data together and define a set of time-based indicator variables representing the dynamics of system over time. In this approach, a set of indicator variables (time variables) are defined to represent different time parameters (month, day, hour, etc.). These variables assigns a unique set of binary values for each specific time and date that is able to differentiate between hours of day, days of week, weekdays or weekends, month etc. To do so, we define $z_{t+k,p}^q$ as the q^{th} indicator variable representing the p^{th} time component at time $t+k$. $\mathbf{z}_{t+k}$ can be represented in

a vector form as $[z^q_{t+k,p}]$.

For example, assume that two components are selected for representing time and date as follows: hours of a day and days of a week (p=2)). Then 23 variables can be used to show 24 *hours of a day* and 6 variables can be used to show *7 days of a week*. In this case, z_{t+k} is a vector with 23+6 = 29 components. It is worth noting that for any p-level time variable, p-1 binary variables are required. For example, 6 indicator variables can represent 7 days of a week as follows: Sunday [100000], Monday [010000], Tuesday [001000], Wednesday [000100], Thursday [000010], Friday [000001] and Saturday [000000]. Using the same way, 23 indicator variables are required to show 24 hours of a day. The main reason to use p-1 variables to show a p-level time variable is that it prevents any linear dependency in further matrix calculation [44].

Another advantage of the above model is that, the indicator variables can appropriately capture the effects of any latent factors that are effective in zonal cooling/heating system or zone internal temperature. There are many factors that significantly affect cooling/heating system, but are not directly observe or measured. For example, occupancy of a zone may affect the heat transfer balances and internal temperature of a particular zone. However, such information cannot be easily collected especially in many public buildings. The idea is that occupancy, as a latent variable, changes over time and as a result, the time-dependent indicator variables can capture their effect indirectly. Many other factors such as equipment, interconnectivity between zones, break time, lunch time, etc. that i) are either unknown or cannot be measured or controlled and ii) change over time can be potentially modeled using indicator variables.

With the above indicator variables, cooling/heating dynamics can be modeled using three quantities: i) The difference between the zone internal temperature at time t, and $t+1$; ii) the difference between zone internal temperature and outside temperature at time t, and iii) a vector of time-dependent indicator variables. In Chapter 3, the first two items are used to build a physical model for the zone internal temperature and the sensible cooling/heating power (Equation 3.7). Here, a more general model is used as

shown in Equation 4.2;

$$\dot{R}^{t+k}(i) = \Phi^i\left(T_{in}^{t+k+1}(i) - T_{in}^{t+k}(i)\right) + \Pi^i\left(T_{in}^{t+k}(i) - T_{ext}^{t+k}(i)\right) + \Theta\left(z_{t+k}\right) + a_{t+k} \quad (4.2)$$

where $\dot{R}^{t+k}(i)$ is sensible cooling/heating rate generated by HVAC system and supplied to the i^{th} zone at time t+k, $T_{in}^{t+k+1}(i)$ and $T_{in}^{t+k}(i)$ are the internal temperature of the i^{th} zone at time t+k+1 and t+k, respectively, $T_{ext}^{t+k}(i)$ is the external temperature at time t. $\Phi^i(.)$,$\Pi^i(.)$ and $\Theta(.)$ are arbitrary functions that can be computed from historical or simulated data. a_{t+k}'s are random noises of the i^{th} zone that are identically and independently distributed over time. For linear $\Phi^i(.)$,$\Pi^i(.)$ and $\Theta(.)$ we have:

$$\dot{R}^{t+k}(i) = \beta_0^i + \beta_1^i\left(T_{in}^{t+k+1}(i) - T_{in}^{t+k}(i)\right) + \beta_2^i\left(T_{in}^{t+k}(i) - T_{ext}^{t+k}(i)\right) + \theta^i z_{t+k} + a_{t+k}(i), \quad (4.3)$$

where, β_1^i and β_2^i are parameters that represent the effect of changes in internal and external temperature for the i^{th} zone, respectively. θ^i are the vector of parameters for indicator variables. The above linear approximation seems to fit well energy data obtained from EnergyPlus simulations.

Equation (4.3) can be written in a matrix form by reshaping the independent variables and responses by their own matrix forms:

$$\mathrm{B}^i = \begin{bmatrix} \beta_0^i & \beta_1^i & \beta_2^i & \theta^i \end{bmatrix}_{p\times 1}$$
$$\mathbf{R}^i = \left[R^{t+k}(i)\right]_{N\times 1}$$
$$\mathbf{a}^i = \left[a_{t+k}(i)\right]_{N\times 1}$$
$$\mathrm{B}^i = \begin{bmatrix} \mathbf{e} & T_{in}^{t+k+1}(i) - T_{in}^{t+k}(i) & T_{in}^{t+k}(i) - T_{ext}^{t+k}(i) & z_{t+k} \end{bmatrix}_{N\times p}$$

when $t + k = 1, ..., N$. Equation (4.4) can then be rewritten as follows:

$$\mathbf{R}^i = \mathrm{B}^i\mathbf{X}^i + \mathbf{a}^i \quad (4.4)$$

B^i is a $p \times 1$ vector of parameters and is calculated using the least square error method for statistical linear model. Unlike the model presented in Chapter 3, in Equation 4.3, there is no pre-determined physics-based model. Therefore, the parameters can be freely estimated to minimize the sum of square errors between actual cooling/heating

loads and their predictions. This implies that Equation 4.3 is able to outperform the physics-based model presented in Chapter 3, when there are physical characteristics that are not appeared in the model.

The predicted cooling/heating values can be obtained instantly and fed into another forecast model to estimate the total energy supplied to the HVAC system. In other words, by knowing the external temperature and the current internal temperature for each zone, the heating/cooling model (Equation 4.3) estimates the *cooling/heating loads* required to reach a specific set point in the next hours. Then the second model (Equation 3.15) is employed to calculate the total energy needed by HVAC system to generate the required cooling/heating loads. For the second model, in Chapter 2, we present a regression-time series model that is the direct generalization of the Cochrane-Orcutt estimation technique. According to Figure 3.3 and Table 3.2, this forecast model performs well and does not need to be improved for this chapter. We also do some minor revisions in the optimization model presented in Section 3.5 and discuss it in the next section.

4.3 Mathematical Modeling for Optimal Control Strategy

In Chapter 3, we proposed a mathematical dynamic programing for minimizing total building energy-related costs and at the same time minimizing the deviations from thermal comforts. The proposed model includes two objective functions as follows:

$$\min_{\mathbf{R}^{t+k}} G_1(N, \mathbf{R}^{t+k}, \mathbf{T}_{ext}^{t+k}, \mathbf{T}_{in}^{t+k}) \equiv \tag{4.5}$$
$$\sum_{k=0}^{N-1} c_{t+k} y_{t+k}(\mathbf{R}^{t+k}, \mathbf{T}_{in}^{t+k}).\Delta t + \upsilon. \max_{k \in t_d} \left\{ y_{t+k}(\mathbf{R}^{t+k}, \mathbf{T}_{in}^{t+k}) \Delta t \right\}$$

$$\min_{\delta_{t+k}^u, \delta_{t+k}^l} G_2(N, \delta_{t+k}^u, \delta_{t+k}^l) \equiv p_{t+k} \sum_{k=0}^{N-1} (\delta_{t+k}^u + \delta_{t+k}^l) \tag{4.6}$$

where $\mathbf{R}^{t+k}$,$\mathbf{T}_{ext}^{t+k}$ and $\mathbf{T}_{in}^{t+k}$ are the vectors of heating/cooling load, external temperature and zone internal temperature given from cooling/heating model (Equation (4.3)). c_{t+k} and υ are cost of each unit of energy per kWh and cost of daily as-used

demand charge. $y_{t+k}(\mathbf{R}^{t+k}, \mathbf{T}_{in}^{t+k})$ is energy used at time $t+k$ in order to generate $\mathbf{R}^{t+k}$, the vector of cooling/heating load values for all zones. p_{t+k} is the penalty that is applied to any violation from the comfort bounds at time $t+k$; δ_{t+k}^{u} and δ_{t+k}^{l} are the total violation from thermal comfort at time $t+k$.

Since there are two objective functions in the proposed control strategy, weighted metric method is proposed to solve the optimization problem. The weighted metric method minimizes a weighted combination of all objective functions from their minimum values:

$$G(N, \mathbf{R}^{t+k}, \mathbf{T}_{ext}^{t+k}, \mathbf{T}_{in}^{t+k}, \delta_{t+k}^{u}, \delta_{t+k}^{l}) = \tag{4.7}$$
$$\left\{ w_1 \left(\frac{G_1(N, \mathbf{R}^{t+k}, \mathbf{T}_{ext}^{t+k}, \mathbf{T}_{in}^{t+k}) - G_1^{min}}{G_1^{max} - G_1^{min}} \right)^{p} + w_2 \left(\frac{G_2(N, \delta_{t+k}^{u}, \delta_{t+k}^{l}) - G_2^{min}}{G_2^{max} - G_2^{min}} \right)^{p} \right\}^{1/p}$$

As mentioned in Chapter 3, G_i^{min} and G_i^{max} $i = 1,2$ are the maximum and minimum values for the i^{th} objective function used for normalizing the combined function of $G(.)$. If there are m objective functions, then G_i^{min} would be found by solving m single mathematical programming. However, in this study, since we solve a real time dynamic programming, it is not possible to obtain the optimal solutions of individual mathematical problems. The reason is that in dynamic programing any optimal solution at any stage depends on the previous stages and one should find the optimal solutions for all combinations which is practically impossible. In previous chapter, we set $G_i^{min} = 0$, which is justifiable. It means that when no equipment is functioning in the building, then the total cost of energy is zero. Furthermore, to find G_1^{max}, we first calculate, the maximum energy required to reach the lowest possible set points, when the internal and external temperature values are maximum. This means that it is expected that G_1^{max} becomes very large and at as a result, the denominator of Equation 4.7 becomes very small. In other words, comparing to the second objective function, the first part of Equation 4.7, which is related to the first objective function becomes very small and does not significantly contribute in the combined objective function.

One practical way to tackle this problem is to choose moderate values for G_1^{max}. For example, one can set G_1^{max} equal to the maximum energy use during the last month.

The second approach is to use utility function instead of metric function and choose

G_i^{min} and G_i^{max} based on the highest and lowest preferences of the decision maker. Utility function varies between 0 to 1. It returns zero for $G_1(N, \mathbf{R}^{t+k}, \mathbf{T}_{ext}^{t+k}, \mathbf{T}_{in}^{t+k}) < G_i^{min}$ and returns one for $G_1(N, \mathbf{R}^{t+k}, \mathbf{T}_{ext}^{t+k}, \mathbf{T}_{in}^{t+k}) > G_i^{max}$. The only problem of this approach is to find a way to create an appropriate functional form for utility, which fits the decision makers preferences.

In this Chapter, we still use Weighted Metric Method, to combine both objective functions. However, instead of Equations (3.25) and (3.24), we sample the past and current energy consumption of a specific period and calculate G_i^{max} based on the records. The value is then added by a constant to prevent any objective function value greater than one.

4.4 Structure of the Proposed Dynamic Programing Model

Our proposed optimal control strategy is explicitly represented in equations 3.27 through 3.30. At time t, the state variables $\mathbf{T}_{in}^t = \left[T_{in}^t(1), ..., T_{in}^t(Z)\right]$ and $\mathbf{T}_{ext}^t = [T_{ext}^t(1), ..., T_{ext}^t(Z)]$ are known and $\mathbf{R}^{t+k} = \left[R^{t+k}(i)\right]$ $i = 1, 2, ..., Z; k = 1, 2, ..., N$, is the i^{th}, zones cooling/heating loads required to reach to a specific set point at time *t+k*. In fact, the optimal control strategy searches for a set of set point values, which minimize total energy consumption as well as deviation from thermal comfort over 24 hours a day. Therefore, $\mathbf{T}_{in}^{*t+1}, \mathbf{T}_{in}^{*t+2}, ..., \mathbf{T}_{in}^{*t+N}$ are the optimal set point values associated with $\mathbf{R}^{*t+1}, \mathbf{R}^{*t+2}, ..., \mathbf{R}^{*t+N}$ for time *t+1* through *t+N*. The *principle of optimality* can be met by using Bellmans dynamic programming algorithm to find the optimal set point values [47, 76]. It states that for $\mathbf{T}_{in}^{*t+1}, \mathbf{T}_{in}^{*t+2}, ..., \mathbf{T}_{in}^{*t+N}$ to be optimal, the set point values starting from any intermediate set point $\mathbf{T}_{\mathbf{in}}^{*t\,+\,j}, j = \mathbf{1}, \mathbf{2}, ..., N$ should be optimal. To do this, let us define $J_{0\to j}^1(.)$ and $J_{0\to j}^2(.)$ as the cost over the reduced horizon from 0 to j for the first and second part of Equation (4.5):

$$J_{0\to j}^1(\mathbf{R}^t ... \mathbf{R}^{t+j}, \mathbf{T}_{ext}^t ... \mathbf{T}_{ext}^{t+j}, \mathbf{T}_{in}^t) = \sum_{k=0}^{j-1} c_{t+k} y_{t+k}(\mathbf{R}^{t+k}, \mathbf{T}_{in}^{t+k}).\Delta t$$

$$J^2_{0\to j}(\mathbf{R}^t...\mathbf{R}^{t+j}, \mathbf{T}^t_{ext}...\mathbf{T}^{t+j}_{ext}, \mathbf{T}^t_{in}) = \upsilon. \max_{k\in\{t_d\}\cap\{0,...,j-1\}} \left\{ y_{t+k}(\mathbf{R}^{t+k}, \mathbf{T}^{t+k}_{in})\Delta t \right\} \quad (4.8)$$

These are also called *cost-to-go* functions. Now the *optimal cost-to-go* is defined as follows:

$$\mathbf{J}^*_{0\to j+1}(\mathbf{R}^t, ..., \mathbf{R}^{t+j}, \mathbf{T}^t_{ext}...\mathbf{T}^{t+j}_{ext}, \mathbf{T}^t_{in}) =$$

$$\min_{\mathbf{R}^{t+j+1}} c_{t+k} y_{t+j+1}(\mathbf{R}^{t+j+1}, \mathbf{T}^{t+j+1}_{in})\Delta t + J^{*1}_{1\to j}(\mathbf{R}^t...\mathbf{R}^{t+j}, \mathbf{T}^t_{ext}...\mathbf{T}^{t+j}_{ext}, \mathbf{T}^t_{in})$$

$$\upsilon. \max_{\mathbf{R}^{t+j+1}} \left\{ y_{t+j+1}(\mathbf{R}^{t+j+1}, \mathbf{T}^{t+j+1}_{in})\Delta t, J^{*2}_{1\to j}(\mathbf{R}^t...\mathbf{R}^{t+j}, \mathbf{T}^t_{ext}...\mathbf{T}^{t+j}_{ext}, \mathbf{T}^t_{in}) \right\}, \quad (4.9)$$

where $J^{*1}_{0\to j}(\mathbf{R}^t...\mathbf{R}^{t+j}, \mathbf{T}^t_{ext}...\mathbf{T}^{t+j}_{ext}, \mathbf{T}^t_{in})$, and $J^{*2}_{0\to j}(\mathbf{R}^t...\mathbf{R}^{t+j}, \mathbf{T}^t_{ext}...\mathbf{T}^{t+j}_{ext}, \mathbf{T}^t_{in})$ are the first and second parts of optimal cost to go at time *t+j* that is $\mathbf{J}^*_{0\to j}(\mathbf{R}^t, ..., \mathbf{R}^{t+j}, \mathbf{T}^t_{ext}, \mathbf{T}^t_{in})$. The principle of optimality states that the optimal cost-to-go from time 1 to time *j+1*, $\mathbf{J}^*_{0\to j+1}(\mathbf{R}^t, ..., \mathbf{R}^{t+j}, \mathbf{T}^t_{ext}, \mathbf{T}^t_{in})$, can be calculated by minimizing two components of Equation (4.9). In other words, at any time $J^{*1}_{0\to j}(.)$, $J^{*2}_{0\to j}(.)$ and $\mathbf{J}^*_{0\to j}(.)$ are calculated and the results are updated using Equation (4.9) until $j = N$. Similarly, the optimal cost-to-go for the second objective function (Equation 4.6) is calculated as follows:

$$\begin{aligned}\mathbf{I}^*_{0\to j+1}(\mathbf{R}^t, ..., \mathbf{R}^{t+j}, \mathbf{T}^t_{ext}...\mathbf{T}^{t+j}_{ext}, \mathbf{T}^t_{in}) = \min_{\mathbf{R}^{t+j+1}} p_{t+j+1} y_{t+j+1}(\delta^u_{t+k} + \delta^l_{t+k}) \\ + \mathbf{I}^*_{0\to j}(\mathbf{R}^t, ..., \mathbf{R}^{t+j}, {}^t_{ext} ...\mathbf{T}^{t+j}_{ext}, \mathbf{T}^t_{in})\end{aligned} \quad (4.10)$$

In equations (4.9) and (4.10) the decision variable for stage *j+1* is $\mathbf{R}^{*t+j+1}$ that is given by the set point value at time *t+j+1* for all zones. Also,$\mathbf{R}^{*t+1}, ..., \mathbf{R}^{*t+j}$ have already been selected optimally and calculated within $J^{*1}_{0\to j}(\mathbf{R}^t...\mathbf{R}^{t+j}, \mathbf{T}^t_{ext}...\mathbf{T}^{t+j}_{ext}, \mathbf{T}^t_{in})$ and $J^{*2}_{0\to j}(\mathbf{R}^t...\mathbf{R}^{t+j}, \mathbf{T}^t_{ext}...\mathbf{T}^{t+j}_{ext}, \mathbf{T}^t_{in})$.

Assume that there are m different candidate set points (say $s_1, ...s_m$), at time *t+j+1*, and that $\mathbf{J}^*_{0\to j+1}(\mathbf{R}^t, ..., \mathbf{R}^{t+j+1}, \mathbf{T}^t_{ext}, \mathbf{T}^t_{in})$ is a m-vector showing the optimal cost-to-go at step *j+1*, given that $= \mathbf{T}^{t+j}_{in} = s_i$ where *i*=1,2,, *m'*. In other words, $\mathbf{J}^*_{0\to j+1}(.)$ is the lowest value of a table in which there are *m'* rows, each corresponded to a specific set point in previous time of *t+j*; and m columns, each corresponded to a specific set point at current time of *t+j+1*. Therefore, to calculate $\mathbf{J}^*_{0\to j+1}(\mathbf{R}^t, ..., \mathbf{R}^{t+j+1}, \mathbf{T}^t_{ext}, \mathbf{T}^t_{in})$,

we need to have a set of tables for $\mathbf{J}^*_{0\to k}(\mathbf{R}^t, ..., \mathbf{R}^{t+j+1}, \mathbf{T}^t_{ext}, \mathbf{T}^t_{in})k = 1, 2, ..., j$. For example, suppose that at stage j+1, we are searching for $\mathbf{T}^{*t+j+1}_{in}$ that minimizes $\mathbf{J}^*_{0\to j+1}(\mathbf{R}^t, ..., \mathbf{R}^{t+j+1}, \mathbf{T}^t_{ext}, \mathbf{T}^t_{in})$ given that the optimal set point value at time j is $= \mathbf{T}^{*t+j+1}_{in} = s^*_i$. In fact, $= \mathbf{T}^{*t+j+1}_{in} = s^*_i$ has already been given by minimizing $\mathbf{J}^*_{0\to j}(\mathbf{R}^t, ..., \mathbf{R}^{t+j+1}, \mathbf{T}^t_{ext}, \mathbf{T}^t_{in})$ for a given value of set point at stage j-1 –say for example, $\mathbf{T}^{*t+j-1}_{in} = s'^*_i$ that minimizes $\mathbf{J}^*_{0\to j-1}(\mathbf{R}^t, ..., \mathbf{R}^{t+j+1}, \mathbf{T}^t_{ext}, \mathbf{T}^t_{in})$.

Therefore, at time t+j+1, when we are checking a specific set point (say $= \mathbf{T}^{t+j+1}_{in} = s_1$), the cost-to-go function at time t+j+1 is related to previous *optimal* cost-to-go functions that are minimized over time to reach to s1 at time t+j+1. Again for any other value of set point at time *t+j+1* (say $= \mathbf{T}^{t+j+1}_{in} = s_2$), there is *another* set of previous *optimal* cost-to-go values that are minimized over time to reach to s_2 at time t+j+1. For calculating the second part of Equation 4.9, we draw all optimal cost-to-go values and their corresponding set points. This method results in real optimal cost-to-go for daily as-used demand charge.

4.5 Numerical Example and Comparisons

In this section, the performance of the modified optimal control strategy is evaluated using a numerical example. We use the same simulation model presented in Chapter 3, which is the Large Office model developed by U.S. Department of Energy [75]. In addition, we follow our proposed framework presented in Section 3.3 and Figure 3.1. We select the same zones and run the simulation using 2011 Phoenix weather data. The training dataset includes one-month data (from 2011/07/1 through 2011/07/31) followed by a one-month testing dataset (from 2011/08/1 through 2011/09/01). The data are sampled every 15-minute. Therefore, total sample size is 5952 that is 31×(2 months) ×4(every 15 minutes) ×24 (hours a day).

4.5.1 Results of The Extended Cooling/Heating Model

Table 4.1 depicts the estimated parameters of our proposed cooling/heating model presented in Equation (4.3). The i^{th} column of Table 4.1 corresponds to $\mathrm{B}^i = [\ \beta_0^i \quad \beta_1^i \quad \beta_2^i \quad \theta^i\ ]_{p\times 1}$, the i^{th} vector of Equation (4.4). The estimated values of β_1^i and β_2^i are all negative. This is because these two parameters are coefficients of $T_{in}^{t+k+1}(i) - T_{in}^{t+k}(i)$ and $T_{in}^{t+k+1}(i) - T_{ext}^{t+k}(i)$ in Equation (4.3). In summer time, to lower the temperature at time $t+k+1$, more cooling power must be supplied. In this situation should be negative and a negative value of β_1^i can guarantee that the cooling load will be greater than zero ($R^{t+k}(i) > 0$).

With the same intuition, in summer time, the warmer external temperature needs more

Table 4.1: The estimated values of the extended cooling/heating model

	Zone											
β_j^i	1	2	3	4	5	6	7	8	9	10	11	12
0	4.02	2.88	4.39	2.65	3.97	3	4.31	2.76	4.02	3.16	4.39	2.65
1	-2.53	-1.67	-2.58	-1.62	-2.53	-1.68	-2.59	-1.65	-2.53	-1.72	-2.58	-1.62
2	-0.28	-0.2	-0.25	-0.27	-0.27	-0.18	-0.24	-0.24	-0.28	-0.18	-0.25	-0.27
3	-1.28	-0.08	-0.97	-0.21	-1.23	-0.04	-0.91	-0.7	-1.28	-0.09	-0.97	-0.21
4	-0.39	-0.1	-0.45	-0.28	-0.26	-0.04	-0.31	-0.3	-0.39	-0.16	-0.45	-0.28
5	-1.33	-0.15	-1.07	-0.36	-1.21	-0.07	-0.94	-0.74	-1.33	-0.25	-1.07	-0.36
6	-0.83	-0.2	-0.91	-0.43	-0.59	-0.09	-0.67	-0.59	-0.83	-0.33	-0.91	-0.43
7	-1.43	-0.26	-1.2	-0.52	-1.25	-0.14	-1.01	-0.81	-1.43	-0.43	-1.2	-0.52
8	-0.66	0.54	-1.13	-0.57	-0.32	0.69	-0.84	-0.74	-0.66	0.47	-1.13	-0.57
9	-0.45	3.11	-1.21	-0.72	-0.2	3.27	-0.96	-0.85	-0.45	3.68	-1.21	-0.72
10	3.01	8.69	1.42	0.47	3.46	8.98	1.9	0.77	3.01	10.03	1.42	0.47
11	0.89	7.83	0.86	0.49	1.09	7.84	1.13	0.35	0.89	9.75	0.86	0.49
12	4.09	11.5	4.03	0.82	4.37	11.43	4.47	1.9	4.09	13.63	4.03	0.82
13	1.13	7	2.27	0.6	1.25	6.62	2.46	0.44	1.13	8.87	2.27	0.6
14	4.83	7.97	7.16	1.32	4.93	7.56	7.37	2.34	4.83	9.36	7.16	1.32
15	1.12	3.29	3.34	0.68	1.15	2.93	3.4	0.46	1.12	4.18	3.34	0.68
16	5.06	5.44	8.04	3.61	4.99	4.97	7.95	4.54	5.06	6.23	8.04	3.61
17	1.14	2.7	2.9	4.77	1.07	2.44	2.75	4.81	1.14	3.56	2.9	4.77
18	4.98	4.73	6.82	11.01	4.8	4.37	6.52	10.22	4.98	5.53	6.82	11.01
19	0.85	2.03	1.74	8.46	0.7	1.83	1.51	8.8	0.85	2.82	1.74	8.46
20	3.16	2.16	3.25	9.16	2.89	1.82	2.81	8.06	3.16	2.67	3.25	9.16
21	0.04	0.75	0.07	3.42	-0.13	0.57	-0.18	2.84	0.04	1.16	0.07	3.42
22	2.13	1.13	2.07	2.95	1.82	0.84	1.66	2.48	2.13	1.18	2.07	2.95
23	-1.08	0.2	-0.65	0.51	-1.23	0.1	-0.81	-0.38	-1.08	0.37	-0.65	0.51
24	0.79	0.38	0.83	0.78	0.6	0.24	0.62	0.67	0.79	0.29	0.83	0.78
25	-1.21	0.04	-0.84	0.05	-1.25	0.02	-0.88	-0.61	-1.21	0.1	-0.84	0.05
26	0.01	-0.15	0.03	0.12	0.01	-0.14	0.02	0.09	0.01	-0.15	0.03	0.12

power to cool down the building, therefore a negative coefficient for $T_{in}^{t+k}(i) - T_{ext}^{t+k}(i)$ seems logical. It is also worth noting that, the model needs to be estimated again in wintertime, and the parameters should be updated.

We evaluate the performance of the extended cooling/heating model using coefficient of determination, R^2 and adjusted coefficient of determination, R^2_{adj} (See equations 2.7 and 2.8). As discussed in Chapter 2, these measures quantify the amount of total variability within all data that is explained using the model. A model with coefficient of determination of one shows an ideal model that can explain all the variations within the data. Table 4.3 presents R^2 and R^2_{adj} for both training and testing datasets. These measures are provided with and without using the time-dependent indicator variables discussed in Section 4.2.Therefore, R^2 and R^2_{adj} for testing dataset indicate the performance of the extended heating/cooling model for any future occasions.

It is observed that the extended cooling/heating model can appropriately explain total variations within the simulated data. The model is able to explain more than 90% of all variations for most zones when the time indicator variables are added to the model. However, R^2 and R^2_{adj} for the model without indicator variables vary for different zones.

Table 4.2: Coefficient of determinations and adjusted coefficient of determinations for the extended cooling/heating model; Tr: Training dataset, Ts: Testing dataset

Zone	1	2	3	4	5	6	7	8	9	10	11	12
R^2(Tr)	0.975	0.863	0.982	0.935	0.974	0.866	0.982	0.938	0.975	0.858	0.982	0.935
R^2_{adj}(Tr)	0.975	0.862	0.982	0.934	0.973	0.864	0.982	0.937	0.975	0.857	0.982	0.934
R^2(Te)	0.95	0.877	0.925	0.91	0.953	0.881	0.93	0.916	0.95	0.876	0.925	0.91
R^2_{adj}(Te)	0.949	0.876	0.924	0.909	0.952	0.88	0.93	0.916	0.949	0.875	0.924	0.909
Zone	1	3	4	5	6	7	8	9	10	11	12	12
R^2(Tr)	0.808	0.209	0.748	0.574	0.784	0.195	0.72	0.547	0.808	0.153	0.748	0.574
R^2_{adj}(Tr)	0.808	0.208	0.748	0.574	0.784	0.195	0.72	0.546	0.808	0.152	0.748	0.574
R^2(Te)	0.774	0.164	0.501	0.428	0.752	0.158	0.491	0.413	0.774	0.123	0.501	0.428
R^2_{adj}(Te)	0.774	0.163	0.501	0.428	0.752	0.158	0.491	0.412	0.774	0.123	0.501	0.428

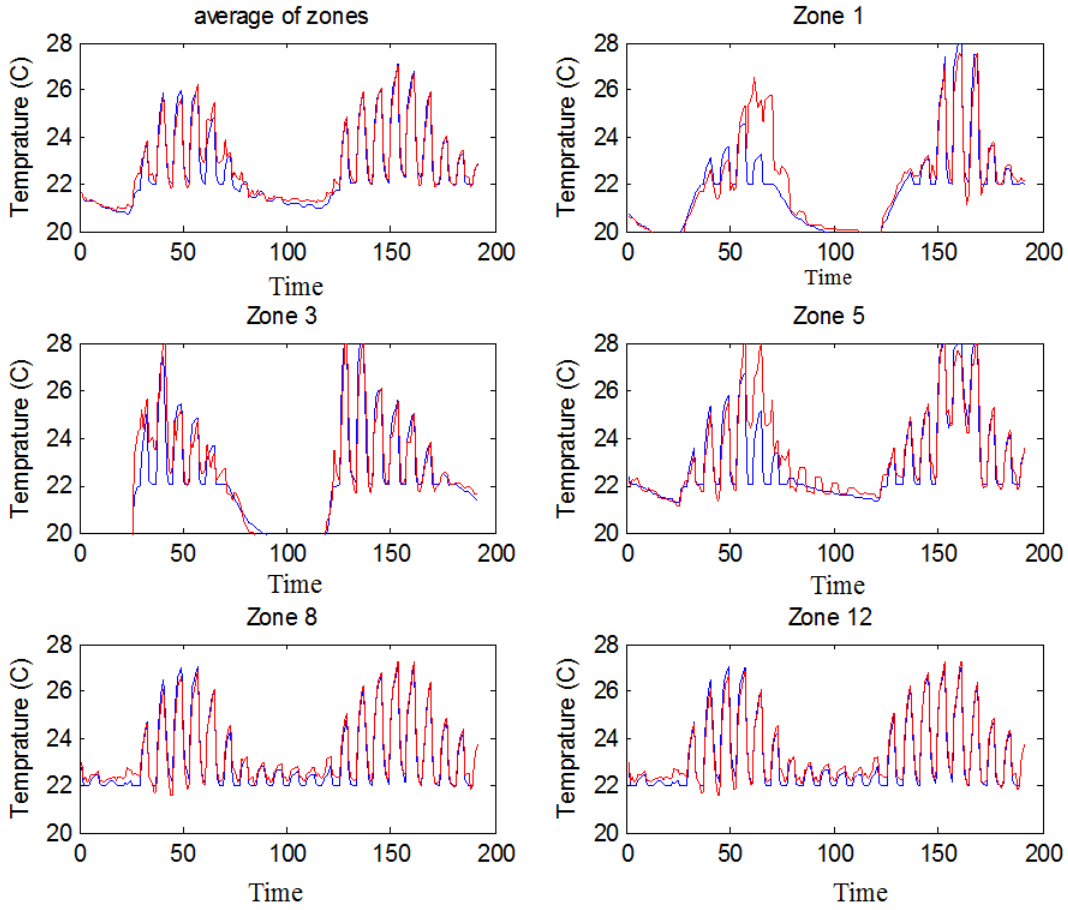

Figure 4.1: The simulated and predicted internal temperature for a selected number of zones and average of all zones (Time unit = 15 minutes)

These measures range between 0.156 to 0.808, which show that the time variables significantly contribute in zonal cooling and heating models. The main reason for the importance of time variables was discussed in Section 4.2. Many latent factors directly or indirectly affect the heat balance transfer of a zone. Occupancy, interconnectivity of heat between different zones, equipment, the structure of walls, windows, doors, chairs, desks, etc., are only a small number of such factors. A perfect model should directly consider the effects of all these factors. However, many of these factors are not measurable, or not easy to calculate. The time indicator variables are replaced by all those

unknown or immeasurable variables that dynamically change with time. Time indicator variables can model a portion of total variability that is caused by any systematic time patterns. They do not provide any information about the nature of the factors. Instead, the indicator variables tell us about those systematic patterns that are hidden in the data. It is worth mentioning that only the factors that are totally known and controllable can be considered for optimization purposes.

Figure 4.1 illustrates a sample data from the predicted and simulated internal temperature for a number of zones also for the average of all zones. In order to generate data using EnergyPlus; we intentionally keep changing set point values between 22 °C and 28 °C every 30 minutes. In doing so, the internal temperature values, and other heating/cooling variables change accordingly. Therefore, more variability can be potentially captured using the proposed model. This is the main reason that data oscillates between 22 °C and 28 °C during daytime in Figure 4.1.

4.5.2 Results of the Extended Cooling/Heating Model

The performance of the proposed optimal control strategy is investigated in this section. We use the same parameters presented in Table 3.3 to run this model. Again, the differences between the models presented in Chapters 3 and 4 are as follows: i) this model employs an extended cooling/heating model that is able to predict the required loads and the zone internal temperature more accurately; ii) the optimization model is repeated every 15 minutes, so that the optimal control strategy can manipulate the set point variables in shorter time; iii) this model employs an improved method to effectively consider the impact of demand charge in optimal control strategy. In this example, the parameters of Equation (4.7) are set as follows: $w1 = w2 = 0.5$ and $p = 2$.

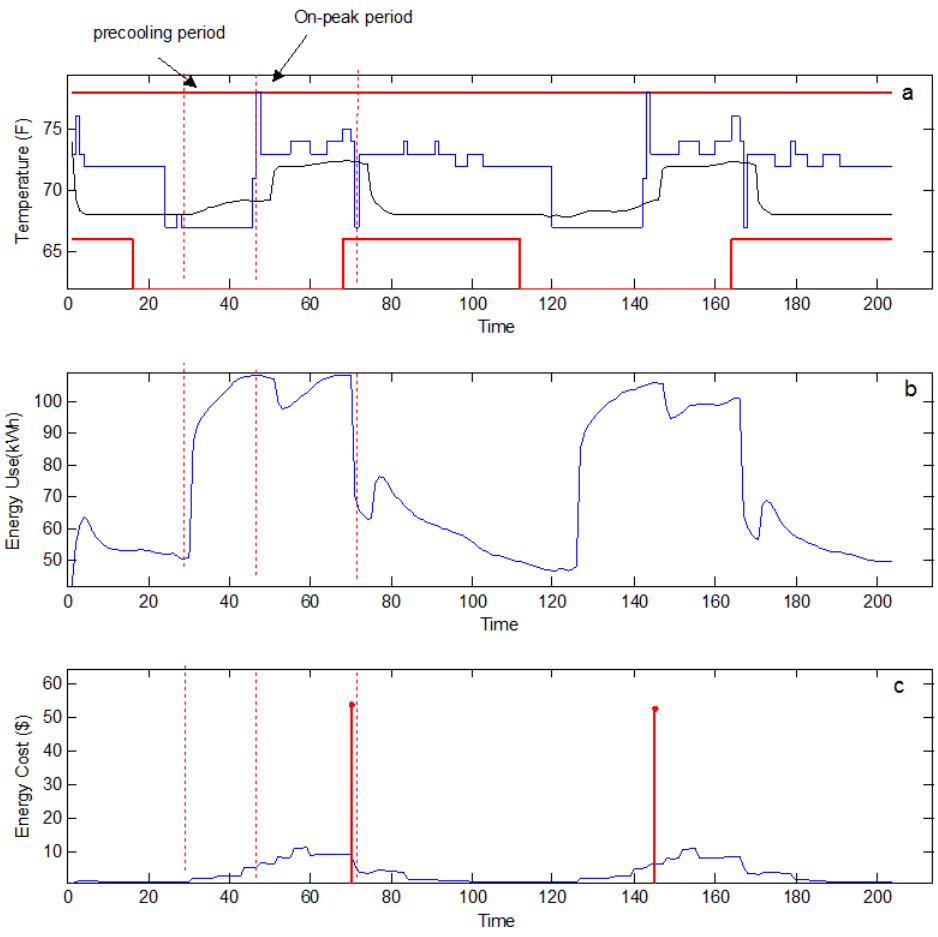

Figure 4.2: The results of the proposed control strategy: a) The optimal set point values and average internal temperature, b) Optimum energy consumption profile over time c) Optimum total operating cost profile including variable cost and demand charge cost

Figure 4.2 illustrates the results of the proposed control strategy over a range of approximately two days. Figure 4.3.a presents the optimal set point value, the average internal temperature, as well as the lower and upper control limits. The on-peak period starts from the 48th time slot (12:00 p.m.) and ends at the 72^{nd} time slot (6:00 p.m.). It is observed from Figure 4.3.a that during the precooling period, the optimal control strategy keeps the temperature lower so that more cooling air can be saved for the on-peak period. The unit cost of energy ($/kWh) before 12:00 p.m. (before peak hours) is set to be lower, so that the overall cost of energy is less expensive during precooling

time. In addition, there is no daily as-used demand charge applied before or after peak hours. It is also shown that during the precooling period, the set point never goes below 68 °F. The reason might probably be related to the second objective function, thermal comfort. Although, the set point value can get the values smaller than 68 °F during the precooling time, the thermal comfort objective function is active and does not allow the set point to reach lower values. According to Table 3.3, from 9:00 a.m. to 4:00 p.m. the penalty for deviation from thermal comfort has its highest value. Therefore, it does not allow the set point to be very small. This example shows how two objective functions work together and compromise over time. Figure 4.2.b presents the total energy use (kWh) for the optimal control strategy. Note that the energy-use sharply increases during precooling time in order to provide enough cooling power. Then in the first hours of the on-peak period, the energy-use slightly decreases, probably because it uses the remaining cooling power generated in precooling time. The highest energy use occurs in the last hour of on-peak period (70th time slot 5:30 p.m.).

Figures 4.3.a and 4.3.b presents the total energy cost and the average deviations from thermal comfort. It can be shown from Figure 4.3.a that most deviations from thermal comfort occur during peak hours that seems reasonable. During these hours, unit cost of energy ($/kWh) is a higher and demand charge is available. Therefore, the proposed optimal control model allows some deviations from the thermal comfort bound, in order to significantly decrease the total cost of energy. Figure 4.3.b depicts the combined normalized objective function. It shows that the maximum combined function occurs during peak hours when there are both higher variable costs as well as higher deviation from thermal comfort. After 4:00 p.m. (time slot 64), although, it is still in on-peak period, the combined normalized objective function decreases. This is probably because of the less penalty value for deviation from thermal comfort after 4:00 p.m.

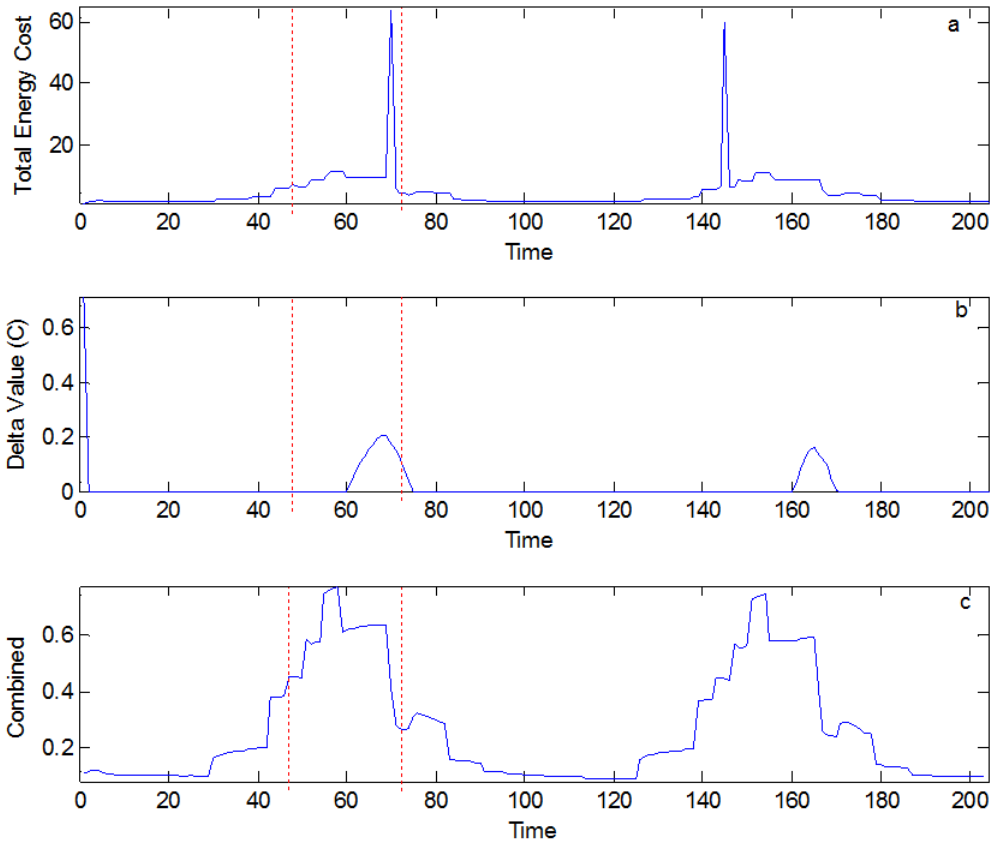

Figure 4.3: The results of the proposed control scheme: a) Total Energy Consumption, b) the temperature violations below or above the thermal comfort bounds, c) Combined weighted metric values (Time unit = 15 minutes).

Figure 4.4 presents $G_1(.)$, the normalized values of the first objective function, $G_2(.)$ the normalized values of the second objective function and combined normalized objective function. The highest values of $G_1(.)$ and $G_2(.)$ are both within the on-peak period, but not exactly at the same time. In addition, in Figure 4.4.a, $G_1(.)$ values are sometimes greater than one. The reason is the new modification that is added in this chapter. G_1^{max} in Equation (4.7) is calculated using the method presented in this chapter. G_1^{max} is calculated by obtaining the maximum energy consumption for the optimal control set points from time 0 to j which does not necessarily include the demand charge cost.

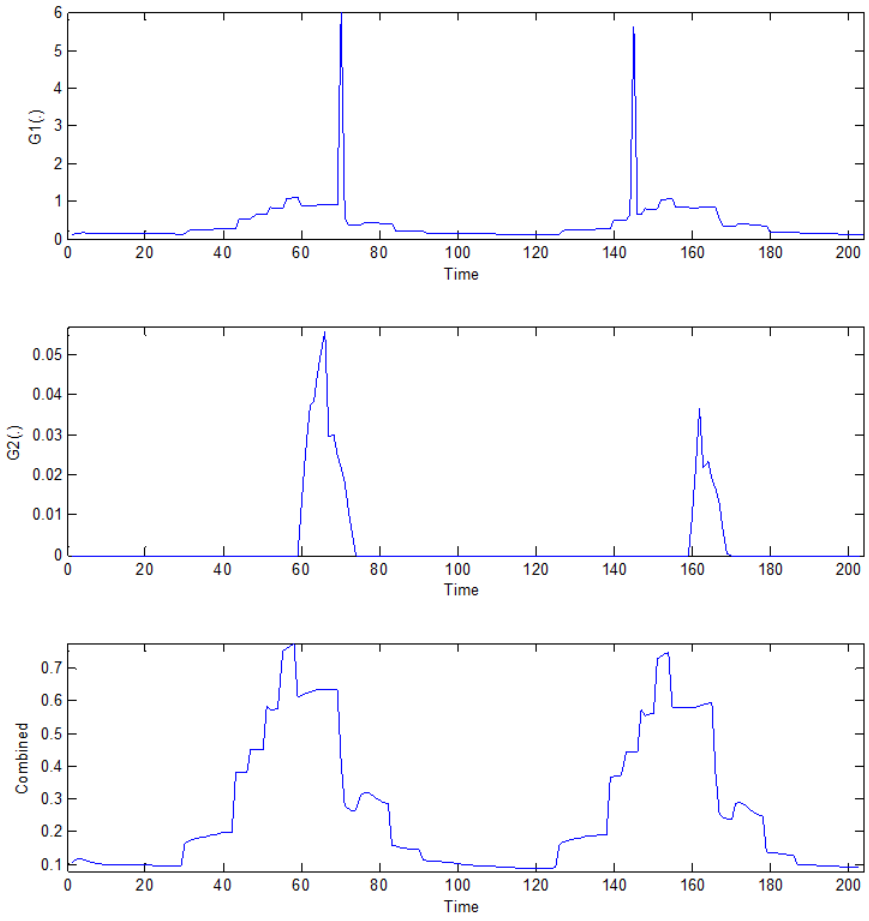

Figure 4.4: the normalized energy consumption cost profile, b) the normalized thermal discomfort penalty profile, c) the normalized combined metric profile (Time unit = 15 minutes).

We also compare the proposed control strategy with various configurations appeared in Figure 3.9. A number of configurations are fixed over time and do not change during the 24 hours. They provide an insight about upper and lower energy consumptions as well as upper and lower penalties for deviations from thermal comfort. Other dynamic controls are logical controllers that try to minimize either total energy related cost or thermal comfort. For example, Dynamic Control 1 in Figure 3.9 picks larger set point values around on-peak hours and smaller values in off-peak hours when there is smaller cost energy per unit. All other parameters, simulation runs, environmental variables

are fixed.

Table 4.3: Comparison between the Extended Control Strategy and Other Control Schemes

	Control Schemes					
	Proposed Controller	Constant Controller1	Highest Value	Dynamic Controller 1	Dynamic Controller2	Dynamic Controller3
Daily Energy Cost	418.35	451.38	401.20	436.04	428.49	438.61
Daily Usage Cost	367.38	389.35	351.39	383.13	374.22	385.10
Daily Demand Charge	50.97	55.33	49.81	52.91	54.26	53.51
Normalized Energy Cost, G1(.)	0.40	0.59	0.38	0.41	0.41	0.42
Violation from comfort	0.20	0.02	1.07	0.02	0.34	0.02
Normalized comfort, G2(.)	0.03	0.00	0.23	0.00	0.02	0.00
Combined Metric Value, G(.)	0.25	0.37	0.30	0.27	0.28	0.29

It is observed from Table 4.3 that the proposed control strategy provides lowest energy consumption cost after the *Highest Value* controller, which selects a constant set point value of 76 °F. The table also includes the average daily demand charge for which our proposed control performs as good as the *Highest Value* controller. From the thermal comfort viewpoint, the proposed control strategy outperforms Dynamic Controller 2, and Highest value. The proposed method is however, larger than Constant Controller 1, which has a constant set point value of 69 °F, as well as Dynamic Controller 3. The performance of the proposed strategy is very close to Dynamic Controller 1 as well as Dynamic Controller 2. Note that the proposed controller has the lowest value of the total combined metric. It implies that the proposed control strategy can provide optimal set point values with lower energy cost than other dynamic controllers can, and at the same does not significantly violates from the thermal comfort bounds.

4.6 Conclusions

The following results can be concluded from this chapter: The proposed control strategy presented in this chapter is a direct extension of the method explained in Chapter 3. It can accurately predict the required cooling/heating load and internal temperature. The model performs well for any lags within a day. In addition, the proposed control strategy can be implemented for any actual or simulated building in order to minimize total energy consumption while minimizing any deviation from a pre-specific thermal

comfort.

Currently, at each time, the proposed control strategy provides the same optimal set point value for all zones. It means that at any time it seeks for a unique set point value that minimizes the total cost of energy as well as penalty for deviation from thermal comfort. Once, it finds the optimal value, the proposed control strategy sets all setpoint values equal to the optimal value. Then it updates the results over time as soon as new information is available. This method is particularly effective when there are relatively large numbers of zones with the same functionality in a building, such as offices, university buildings, etc. One potential extension is to propose a control strategy, which seeks for different set point values for different zones. This can be considered as a large-scale optimization model as the algorithm needs to search in a much bigger feasible region. For example, for a building with 25 zones, and 10 set point candidates, the total combinations of set points and zones would be 10^{25} for each time step. Therefore, if the time step is set to be one hour, 24×10^{25} combinations are potentially available. It means that the algorithm should search for optimal solutions among 24×10^{25} possible solutions in every single hour (or 15 minutes). In this situation, many other solvers including exhaustive search and evolutionary algorithms do not effectively work.

To overcome this problem, one idea is to decrease the search spaces. An effective method would merge similar zones into a bigger zone and reduce the dimension of the problem. To do this, a zone selection approach is required to classify similar zones. This can be done by either using the engineering knowledge of building or using computational algorithms that compare all combinations and provide the best classes of zones based on a number of features. The second idea is to develop an optimal control strategy that can fit with large-scale dynamic problems. Dynamic programing is typically considered as an efficient algorithm to search for optimal solution. For many cases, the algorithm process time is polynomial in the number of states (number of zones) as well as number of actions (number of available set point values) [77]. However, it is not yet practical

for very large problems. Approximating methods can also be chosen to solve large-scale dynamic programming (See for example, feature-based methods in [78], parallel computing methods [79], and other numerical methods [80]). This is a potential topic for future researches.

Chapter 5

Predictive Analytics Approach to Modeling Building Industrial Load

5.1 Introduction

In previous chapters, several models were proposed for forecasting and optimization of energy use in residential or office buildings. Industrial sector also significantly contributes in total energy use and accounts for about 50% of the worlds total energy conversion [81,82]. In addition, from 41% energy used in the U.S. buildings, 19% are delivered to non-residential buildings, which accounts for 3.6% of total world energy consumptions combined. However, more attention seems to be directed toward residential or office buildings by researchers. One main reason would be the complex nature of non-residential buildings. The main source(s) for energy usage in different non-residential buildings are often different from one industry to another. Another reason would be the characteristics of industrial loads in non-residential buildings that are often extremely large, non-stationary with random fluctuation over time. This is different with the energy usage data in residential buildings that are often function of occupancy and temperature. Overall load in non-residential buildings typically consists of two components: i) the baseline load, which is the normal load due to daily activities, cooling, heating, and lighting and is often function of temperature and occupancy; 2) the industrial load, which is mainly due to the operation of equipment and machinery and is often larger than the baseline load. In this chapter, a data-driven risk analysis approach is proposed to evaluate and control of demand response actions, such as load shedding and load shifting strategies in non-residential buildings. The proposed methodology consists of two major steps: In the first step, it employs a set of predictive

analytics tools to capture and predict the patterns of industrial load profiles. These tools can also estimate the probability of the day-ahead load pattern. Once the pattern(s) of industrial loads is determined, a risk analysis method is used to evaluate the worst-case, best-case, and most-likely estimations of energy cost. Any demand response programs can be analyzed for worst-case, best-case, and most-likely scenarios and the best program can be selected accordingly.

Unlike, the load forecasting methods discussed in Chapters 2 and 3, the predictive analytics methods do not provide online hourly forecast values for the building energy-use. Instead, they identify the hidden patterns of industrial load data and use them to calculate the risk of energy scenarios. In addition, unlike Chapter 3, the proposed method does not provide an optimal control strategy to minimize total cost of energy in an hourly-basis. But, it calculates the risk of different demand response programs, so that the users can select the program(s) with minimum risk.

5.2 Background Study

There has been little attention paid to modeling and control of industrial loads in non-residential buildings. Westphal and Lamberts employ a simplified weather data to model and analyze the thermal loads of non-residential building using average, maximum and minimum of monthly energy data. However, in their study, the building peak electric load is not extremely large. In addition, weather data is not always a good representative for energy-use patterns in the buildings with industrial load. Coughlin et al. investigate the impacts of building characteristics as well as weather data for estimation of baseline load profiles in non-residential buildings [84]. Their method is particularly useful to measure the load impacts from certain types of load-reduction programs. Again, in their case studies, they do not report the effect of extremely large industrial loads.

In addition, to avoid the complexity of industrial loads in non-residential buildings, a number of researchers integrate the energy-use data into a longer horizon and propose long-term forecasting models (See e.g. [85-88]).

Furthermore, the correlation between power consumption and the operations of the manufacturing systems has also been investigated by several researchers [89]. Energy-aware scheduling (EAS) is a popular approach to deal with modeling and optimization of energy dynamics in manufacturing systems. The EAS approach proposes a set of mathematical models to optimally schedule manufacturing operations by considering energy-related parameters such as cost of energy, carbon footprint, etc. The energy-related parameters can be presented as a constraint or objective function in EAS approach [90-93]. The only drawback of EAS models is that the traditional scheduling problems are often complex problems. They are mathematical programing models that determine the optimal schedule of manufacturing machinery and equipment to minimize total manufacturing costs. EAS problems add further decision variables and/or constraints into the traditional scheduling problems, which even make it more complex. Our proposed methodology is different with the above researches in different aspects. First, it is proposed for buildings with extremely large loads over time. In addition, it does not provide the optimal solution e.g. the optimal demand response program. Instead, it evaluates the risk of different demand response programs and selects the program that lowest risk and best predicted performance.

5.3 Problem Statement

In this chapter, the proposed data-driven risk-based approach is explained through an example. Although the magnitude and forms of industrial load profiles may vary from one building to another based upon the operations and functionalities of the building; the proposed framework is generic and can be applied with minor changes. Again, since industrial load patterns have much larger variance compared to the baseline load patterns, the models presented in the previous chapters do not work well to predict and control energy consumption. Figure 5.1 shows the total building power loads (kW) for three non-residential buildings in Colorado. It is observed that power consumption values for Building II are extremely large–greater than 850 kW in some cases. This obviously shows that there are extremely large industrial loads in this building, which

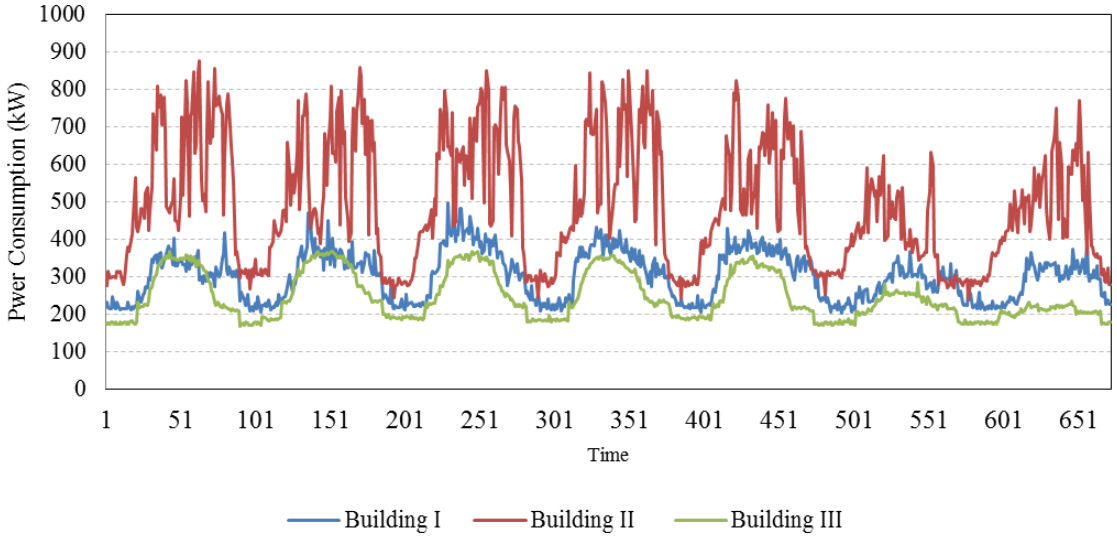

Figure 5.1: Total power consumption for three non-residential buildings (Time unit = 15 minutes)

affect the building baseline loads.

Building I and Building III are non-residential building as well; however, they are not affected by large industrial loads. These buildings can be analyzed using the approaches discussed in the previous chapters. In this chapter, we apply our proposed framework to Building II. Figure 5.2 presents the daily load profiles of Building II. It has 208 daily profiles collected every 15 minutes from the building. Each profile includes 96 load samples so the overall sample size is 19968 (24 (hours) $\times$ 4 (15 minutes) $\times$ 208 (days) =19968). The average daily profile and 2-sigma upper and lower limits are also presented. It is observed from Figure 5.2 that the total variability of daily load profiles is very large. In other words, patterns of daily load are significantly different from one day to another. Since, the variance of the load profile data is very large, it is reasonable to use a clustering method and classify the load profiles into groups with smaller variance. This is beneficial for the risk analysis purposes, when the decision maker can calculate the probability of each class for the day ahead. In the next section, we will describe the proposed framework.

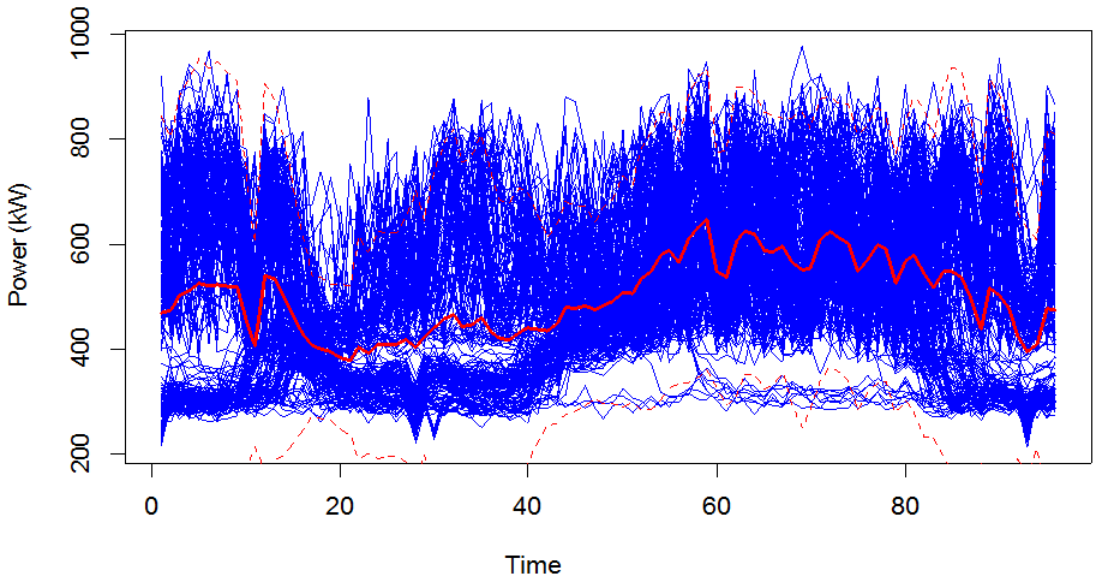

Figure 5.2: Daily Load Profile Data for Power Consumption of Building II (Time unit = 15 minutes)

5.4 The Proposed Data-Driven Risk-based Framework

Figure 5.3 illustrates a general framework for the proposed data-driven risk-based methodology. First, a sample of historical load profiles, weather, and time data are required to create and validate the statistical models. Then a preliminary data analysis is applied to capture the general characteristics of load profile data. A clustering method is also required to assign load profiles to a particular number of groups with lower variability. The clustering method is followed by a classification model that is built to determine the appropriate group of any future load profile. The classification model assigns a probability to each group, which determines the chance of having a load profile from a particular group in the day ahead. Once the probabilities of the day-ahead industrial load are obtained, the risk of industrial load profile is calculated using the expected cost of energy. A cost-based risk analysis can be applied to investigate the effect of demand response programs. It investigates how any particular demand response program can decrease risk of the day-ahead industrial load.

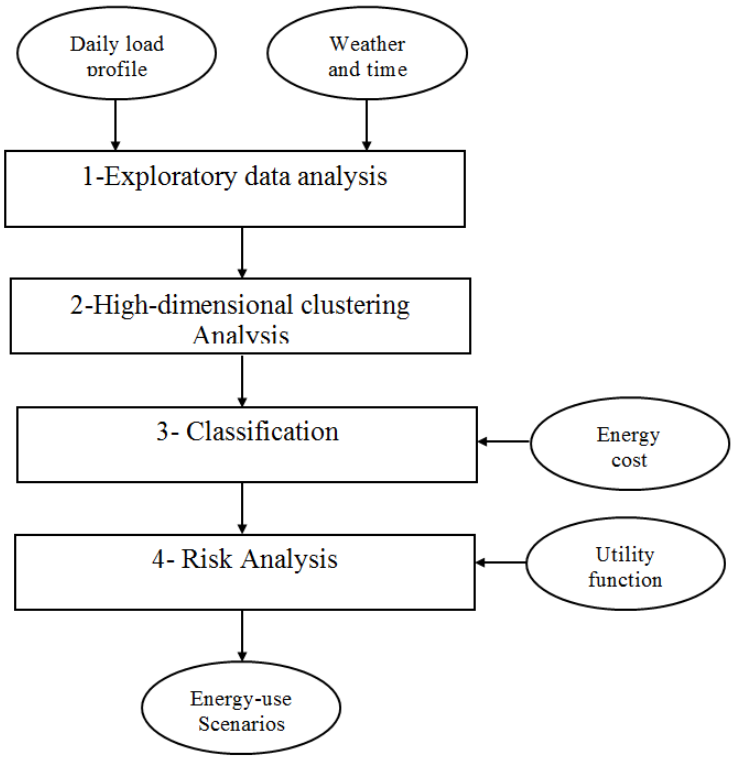

Figure 5.3: The proposed data-driven risk-based framework for industrial load profiles

The first three steps of the proposed data-driven risk-based approach is often referred to as Predictive Analytics. Predictive analytics is a variety of statistical and machine learning techniques that analyze historical data to make prediction or inference about future events [94, 95]. In this study, the predictive analytics (steps 1-3) is applied to obtain the probabilities of load profile groups in the day ahead. In this next subsection, technical details of the predictive analytics are explained.

5.4.1 Exploratory Data Analysis

Exploratory data analysis (EDA) was first introduced by John Tukeythe famous American statistician as an approach to explore historical data [96, 97]. It is typically defined as a set of quantitative and graphical tools that are employed to summarize the main characteristics of data, and to select appropriate statistical models. A number of researchers use EDA in the area of energy, particularly when there are enough data

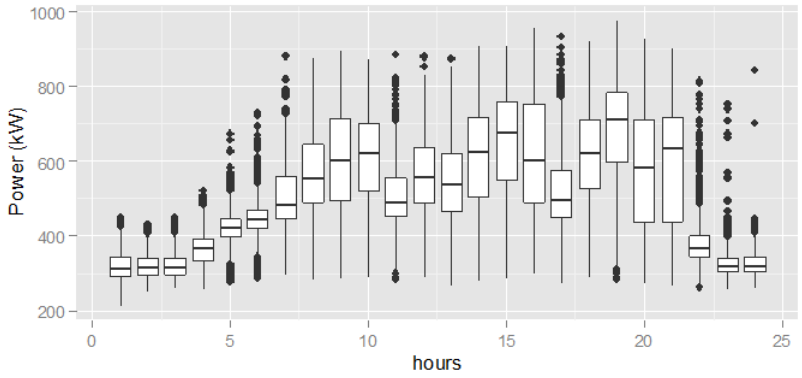

Figure 5.4: Box Plot for industrial load profile categorized by hours of a day

available [98-100]. In this section, we employ EDA to understand the behavior of industrial load profiles in Building II. Figure 5.4 shows a boxplot drawn from the daily load profile data of Building II. It is observed that the largest consumptions (peak loads) occur in the following hours: 8:00 a.m. to 10:00 a.m., 1:00 p.m. to 3:00 p.m. as well as 7:00 p.m. This is significantly different with a typical building where peak hours are usually between 12:00 p.m. to 4:00 p.m.

In addition, there are many outliers in 5:00 a.m., 6:00 a.m., 10:00 p.m. and 11:00 p.m. The large number of outliers shows that in some hours the load distribution is heavy-tailed with many extreme load values. This could be a major source of load variation within load data. In Figure 5.5, the load profiles are categorized by weekdays. It is observed that the load profile cannot be distinguished based on the weekdays. There is not any specific pattern that is different with overall load profile. Again, this result is different with residential buildings and many non-residential buildings, particularly office buildings. It is interesting to note that weekdays load profiles is approximately similar to the weekends load profiles.

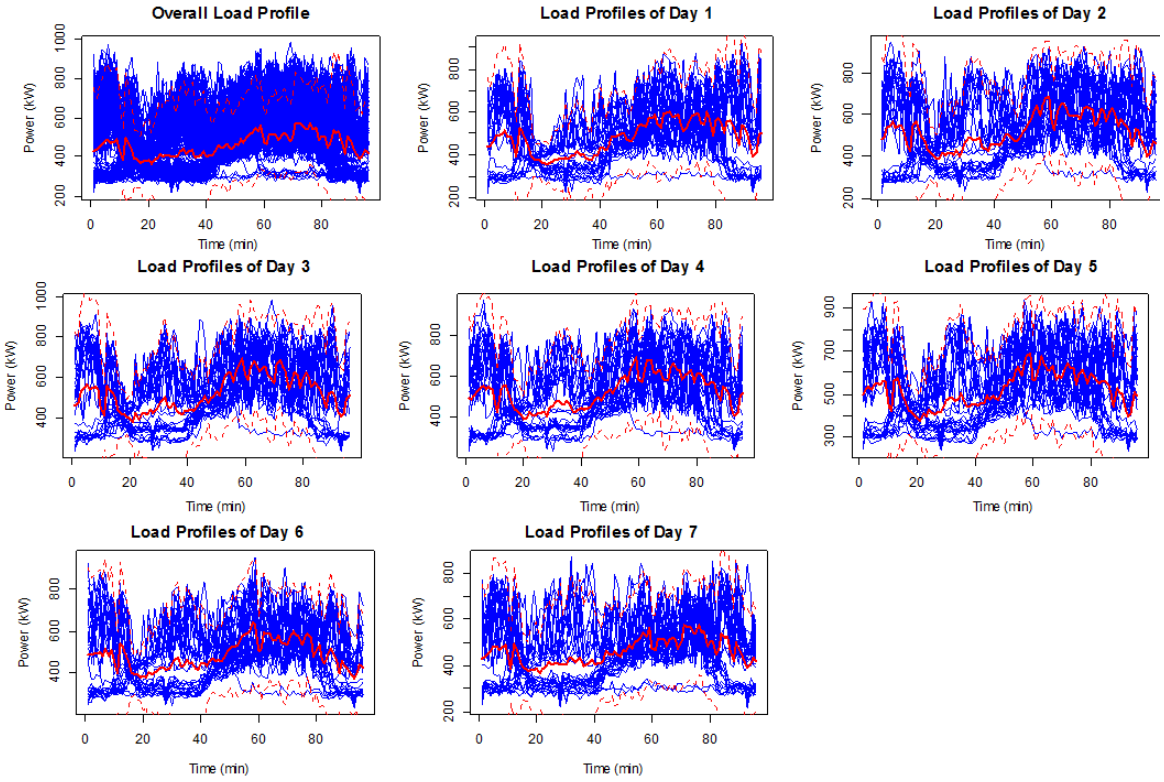

Figure 5.5: Industrial load profiles categorized by days of a week

Figure 5.6 presents load profile data categorized by months. Unlike weekdays, the patterns of load profiles are different for different months. Particularly, Months 2, 3 and 4 are different with Months 5 and 6. In addition, Months 5 and 6 are slightly different from Months 7, 8 and 9. This figure shows that the activities in this building can potentially change in a monthly basis. Therefore, a set of variables should be added to the model, which represent the month that the load profile is collected.

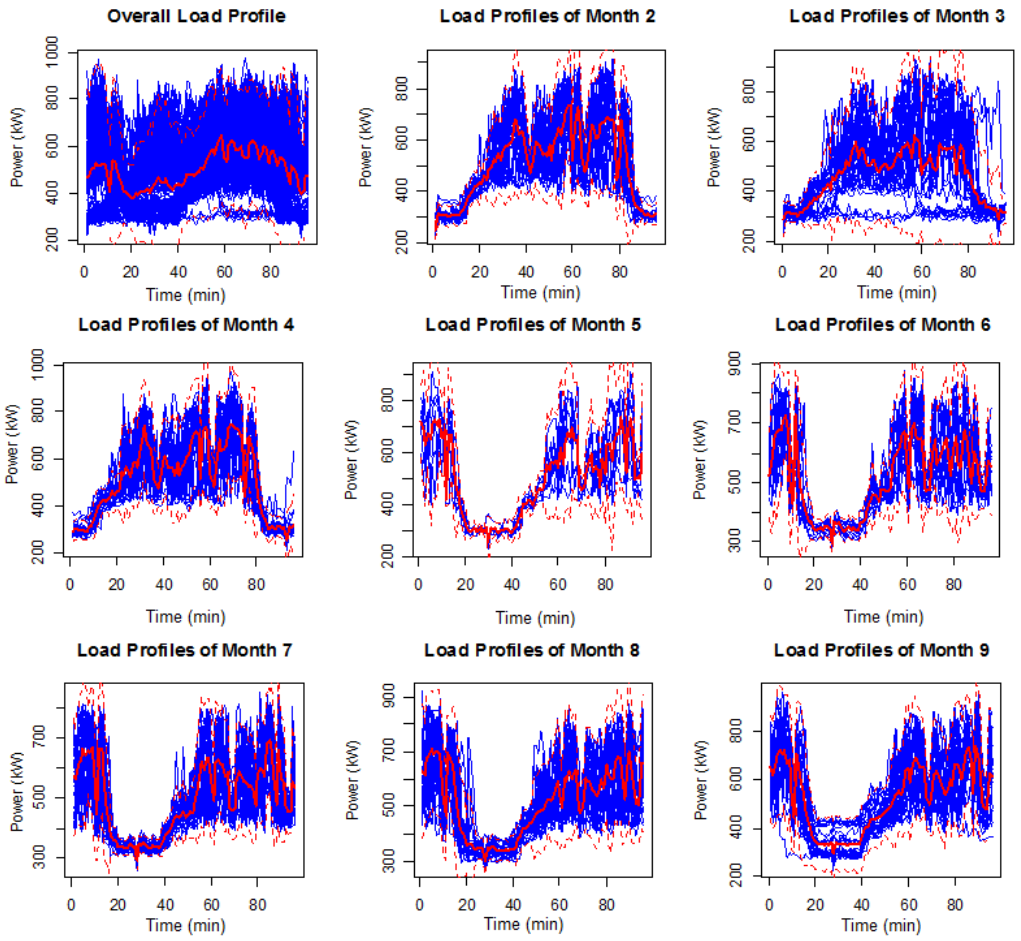

Figure 5.6: Industrial load profiles categorized by months

Figure 5.7 demonstrates a visual summary of load profile data based on month, weekdays, and weekends. Figure 5.7.a presents the variation of power consumption values by months. Variation is larger in the first third months. The load profile data for weekdays and weekends are illustrated in Figure 5.6.b. From clustering viewpoint, it seems ineffective to classify load profiles based on days of a week.

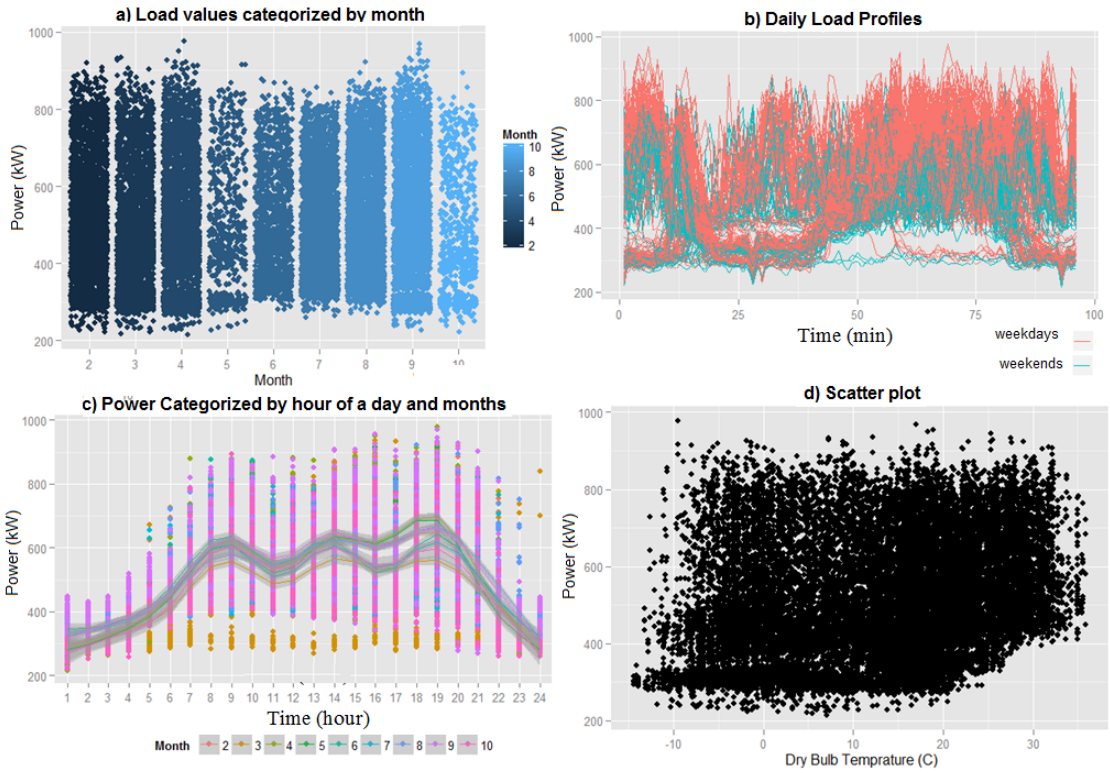

Figure 5.7: visual summary of load profile data: a) Load profile data categorized by month, b) load profile data for weekends and weekdays, c) The average of load profile data categorized by month and d) the scatter plot between power consumption (kW)

In addition, Figure 5.7.c plots the power consumption values with different colors for different months. This figure also includes the average load profile for each month. The overall monthly patterns and average load profiles are slightly different with each other suggesting that data can be separated by month. Again, note that the maximum power consumption in this building occurs between 9:00 am, 2:00 p.m., 6:00 p.m., and 7:00 p.m. These hours are very close to breakfast, lunch, and dinner times, respectively. Therefore, it can be guessed that Building II might be a restaurant or some activities that occur during eating hours. It is also observed that since the load profiles for this building are extremely large, the building probably serves food for a large crowd of people. Finally, Figure 5.7.d depicts a scatter plot between temperature (°C) and power (kW). It reveals a small correlation between power consumed in Building II and

the ambient temperature. Therefore, the power consumptions in Building II is only slightly related to the building cooling/heating systems. In overall, based on the above analysis, months of the year is an important factor that should be an input for the classification model.

5.4.2 High-Dimensional Clustering Analysis

In this section, a clustering analysis technique is employed to allocate load profile data into smaller number of homogenous groups. As mentioned before, in this study, each sample is a daily load profile, which consists of a vector of power consumptions collected every 15 minutes. Therefore, there are 208 vectors of daily profile data and each profile consists of 96 load values. In other words, the total sample size is 208; each sample is a vector of 96 observations. As a result, the dimension of load profile vectors is relatively large compared to the sample size. In this situation, the ordinary clustering methods do not perform well. Instead, we employ a high-dimensional clustering analysis that can be applied to data with high dimensions from a number of dozens to many thousands. In general, there are two approaches for data clustering problems [101]: i) model-based clustering methods, which aim to partition data into groups that presumably follow the same distributions; ii) nonparametric clustering methods, which define similarity metrics (distances); and partition data with the highest similarity into the same groups. In this study, we use a model-based approach.

To do this, let us assume that the vector of load profile data is denoted by $\mathbf{y}$ and we have a dataset of size n $\{\mathbf{y}_1, ..., \mathbf{y}_n\}$, where $\mathbf{y}_i \in \mathbb{R}^p$. In addition, assume that $\mathbf{y}_i$s come from K different populations each with a multivariate distribution, $\phi(y; \mu_k, \Sigma_k)$. The mixed distribution of $\mathbf{x}_i$s can be shown as:

$$f(\mathbf{y}, \theta) = \sum_{k=1}^{K} \pi_k \phi_k \left(\mathbf{y}; \mu_k, \Sigma_k\right) \tag{5.1}$$

where π_k is the mixture proportion of the k^{th} class and ϕ_k is a multivariate density function, presumably Gaussian density function parameterized by a vector mean of μ_k and variance matrix of Σ_k for the k^{th} component. The problem is that in many cases,

the dimension of data, p is very large even in some cases bigger than the sample size, n– curse of dimensionality. This causes some mathematical problems (e.g. ill-conditioned covariance matrix) and unexpected behaviors in clustering methods [101]. Most model-based high-dimensional clustering methods typically propose methods to project the p-dimensional problem into a smaller subset of $p' < p$ (See [102] and [103] to review model-based high-dimensional clustering methods). In this research, we investigate a well-known clustering model which is referred to as High-Dimensional Data Clustering HDDC algorithm. The algorithm is available in CRAN server and can be downloaded and used in R. It assumes that in high-dimensional spaces, data accommodate in different subspaces with lower dimensionality. In the HDDC algorithm, a constraint is imposed to Gaussian mixture models through the covariance matrix Σ_k as follows:

$$\Sigma_k = Q_k \Lambda_k Q_k' \tag{5.2}$$

where Q_k is the orthogonal matrix with eigenvectors of Σ_k as column andΛ_k is a diagonal matrix which contains the eigenvalues of Σ_k and can be presented as $\Lambda_k = diag(a_{k1}, ..., a_{k,dk}, b_k..., b_k)$ [103,104].a_{ki}s parameterize the within-variance of subspace and b_ks account for variance of the noise. The algorithm offers to select any combinations of model $[a_{ki}, b_k, Q_k, d_k]$ to reduce the spaces and use the classical Gaussian mixture model with a full-rank covariance matrix [105].

By applying the HDDC algorithm, the load profiles can be classified into three groups that are shown in Figure 5.8. This figure presents the load profiles allocated to each group together with their average, upper and lower load profiles. Before applying the clustering method, there are no pre-determined classes for the load profile dataset, therefore, it is not possible to evaluate the performance of the HDDC algorithm. However, in order to have an insight about the results, Figure 5.8 illustrates that the clustering algorithm successfully allocates same load profiles into the same class. It is observed from Figures 5.8.a and 5.8.b that all load profiles within same class follow the same patterns, while the patterns of different classes are completely different. Finally, HDDC algorithm allocates the remaining profiles that do not follow the patterns of the first

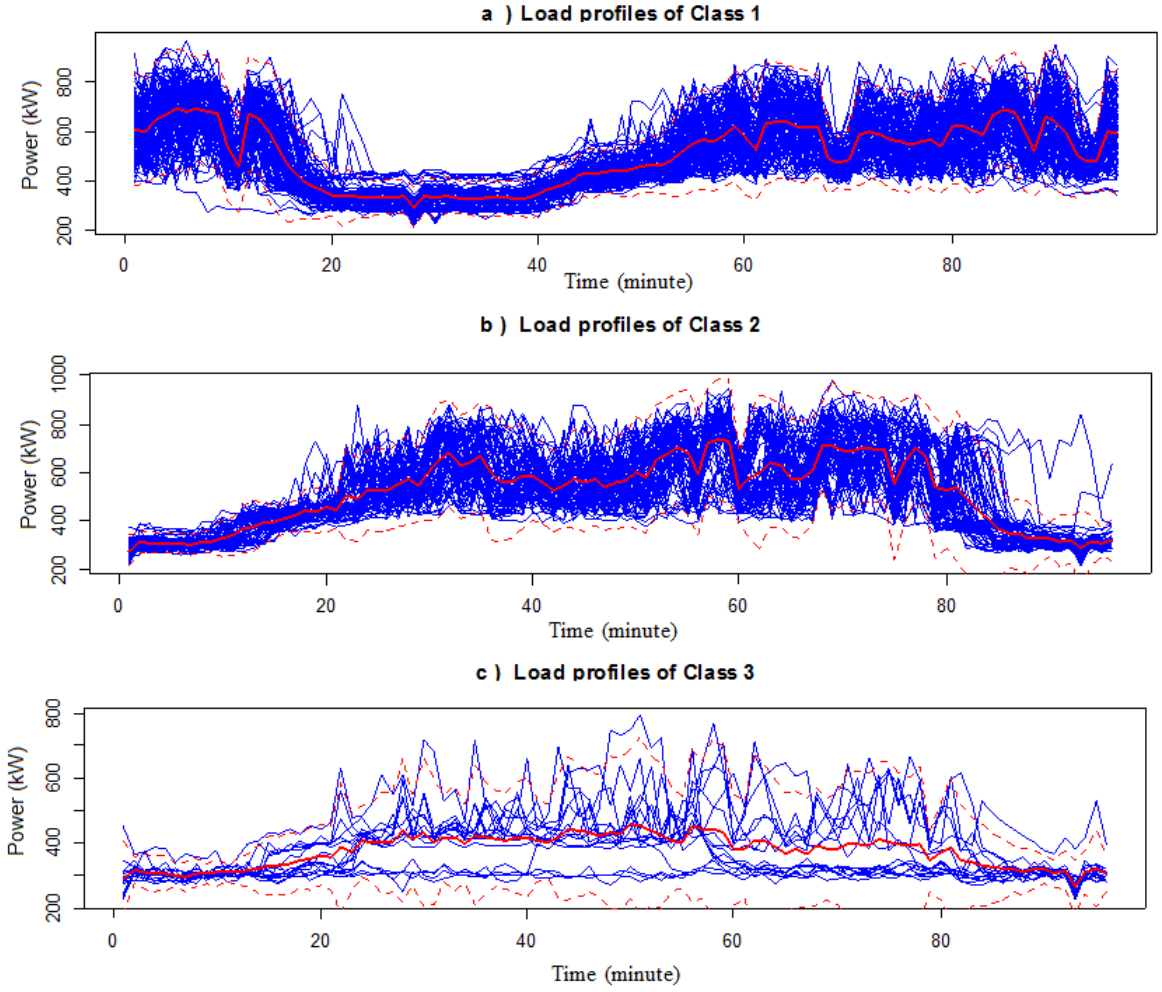

Figure 5.8: Load profiles categorized by classes given through the high-dimensional cluster analysis method.

or second classes, into a third class. Comparing to other classes, the third class has much more variability. This shows that the algorithm compromises between selecting minimum number of classes and minimum variability within each class.

5.4.3 Classification

Once the classes are obtained, it is useful to develop a model that can predict the appropriate class of any future load profile. Classification technique is typically used to

find the probability that the day ahead profile belongs to a particular class given that a set of input variable such as weather and time variables. The classification method calculates the correlation between a particular set of input variables with available classes, and then tries to guess the best class that fit data.

To do classification, a wide range of methods and techniques are available. In this section, we employ a Multinomial Logistic Regression model to identify to which of classes a new load profile belongs. A training dataset is randomly selected to train the model and the rest of data is used to evaluate the performance of the models.

Multinomial logistic regression

Assume that $z_t = 1, 2, 3$ showing the class that the t^{th} load profile belongs to; and that $\pi_{it} = Pr(z_t = i)$ is the probability that the t^{th} load profile data belongs to the i^{th} class, then a multinomial logistic model can be shown as follows:

$$\log \frac{p_r(z_t = i|X_t)}{p_r(z_t = 3|X_t)} = \log \frac{\pi_{it}}{\pi_{3t}} = \beta_i X_t; i = 1, 2, ..., c-1 \tag{5.3}$$

Where X_t is the vector of input variables, including temperature and time variable. As mentioned in Chapter 4, time variables are indicator variables defined to differentiate between different months of a year, day of a month, hours of a day, etc. As clearly shown in figures 5.5 and 5.6, months and weekdays are time indicator variables in this study and together with the ambient temperature create the vector of X_t . c is number of classes, which is 3 in this study. Multinomial distribution is a special form of generalized exponential family, which can be used to obtain the Maximum Likelihood Estimation (MLE) of βi values. To do this, βi should be found to maximize the following function [106]:

$$\begin{aligned} lik(\beta_i) &= \prod_{t=1}^{n} p_r(z_t = i|X_t) \cong \prod_{t=1}^{n} \pi_{1t}^{z_{1t}}.\pi_{2t}^{z_2 t}.\pi_{2t}^{1-z_{1t}-z_{2t}} \\ &\cong \prod_{t=1}^{n} \exp\left(\beta_1 X_t\right)^{z_{1t}}.\exp\left(\beta_2 X_t\right)^{z_{2t}}.\left(\frac{1}{1+\exp\left(\beta_1 X_t\right)^{z_{1t}}+\exp\left(\beta_2 X_t\right)^{z_{2t}}}\right)^3 \end{aligned} \tag{5.4}$$

By taking log, Equation 5.4 can be written as follows:

$$\log\left(lik(\beta_i)\right) = \sum_{t=1}^{n} z_{1t}\beta_1 X_t + z_{2t}\beta_2 X_t - 3\log(1 + \exp(\beta_1 X_t) + \exp(\beta_2 X_t)) \tag{5.5}$$

then βi can be found by finding the derivation of $\log(lik(\beta_i))$ with respect to each element of βi and by setting the result equal to zero [107].

$$\begin{aligned} &\frac{\partial \log(lik(\beta_i))}{\partial \beta_i} \cong \sum_{t=1}^{n} [z_{it}\beta_1 X_t - \left(\frac{1}{1+\exp(\beta_1 X_t)^{z_{1t}}+\exp(\beta_2 X_t)^{z_{2t}}}\right)\times \\ &\frac{\partial}{\partial \beta_i} 3\log(1+\exp(\beta_1 X_t)+\exp(\beta_2 X_t) \end{aligned} \tag{5.6}$$

By simultaneously solving the above equations, the MLE estimated values of βi can be obtained. Since these equations are often difficult to solve analytically, researchers typically employ numerical method. For example, package *nnet* in R, obtains the MLE estimated values of βi via neural networks [108]. Once βi values are estimated,$\pi_{it} = Pr(z_t = i)$ can be found as follows:

$$\begin{aligned} &\hat{\pi}_{it} = \frac{\exp(\beta_i X_t)^{z_{1t}}}{1+\exp(\beta_1 X_t)^{z_{1t}}+\exp(\beta_2 X_t)^{z_{2t}}}, i = 1,2 \\ &\hat{\pi}_{3t} = 1-\hat{\pi}_{1t}-\hat{\pi}_{2t} = \frac{1}{1+\exp(\beta_1 X_t)^{z_{1t}}+\exp(\beta_2 X_t)^{z_{2t}}} \end{aligned} \tag{5.7}$$

$\hat{\pi}_{it}$s estimates can then be used to determine the class of each observation. In the simplest case, the t^{th} observation is assigned to the k^{th} class, if $\hat{\pi}_{kt} = \max\{\hat{\pi}_{it}; i = 1,2,3\}$. To evaluate the performance of the proposed method, we divided the load profiles data into the training and testing datasets. Sample size for both subsets is 104 and the training and testing samples are drawn randomly. We also tried Support Vector Machine another classification method, in order to compare with the MLR method presented in this chapter. Table 5.1 summarizes the results of classification methods. Rows and columns present the actual class and predicted class of profiles. It is observed that both methods are able to correctly predict Class 1 and Class 2. This rate is 100% for Class 1, for both training and testing datasets. MLR method is also able to identify Class 2 with the accuracy rate of more than 94%. The overall accuracy rates for multinomial logistic regression (MLR) method are 92.31% and 87.5% for the training and testing datasets, respectively. The corresponding accuracy rates for support vector machine (SVM) are 99.04% and 86.54%, respectively. Both classifiers are not able to accurately determine the load profiles in the third class. This is mainly because the sample size of Class 3 is very small, so that the algorithms cannot be perfectly trained. Another reason would be the variance of load profiles in Class 3. It can be seen from

Table 5.1: The accuracy of the proposed classification methods: multinomial logistic regression (MLR) and support vector machine (SVM). Rows: Real classes, Columns: Predicted classes

			Predicted classes			
			1	2	3	frequency
		1	100.00%	0.00%	0.00%	60
	MLR (Training)	2	0.00%	94.30%	5.70%	35
		3	0.00%	66.70%	33.30%	9
			1	2	3	frequency
	SVM	1	100.00%	0.00%	0.00%	60
	(Training)	2	0.00%	100.00%	0.00%	35
		3	0.00%	11.10%	88.90%	9
			1	2	3	
Real classes		1	100.00%	0.00%	0.00%	58
	MLR (Testing)	2	0.00%	80.00%	20.00%	40
		3	0.00%	83.30%	16.70%	6
			1	2	3	
		1	100.00%	0.00%	0.00%	58
	SVM (Testing)	2	0.00%	77.50%	22.50%	40
		3	16.70%	66.70%	16.70%	6

Figure 5.8 that the variance of load profiles of Class 3 are large without a particular distinguishable pattern. To improve the results one should merge Class 3 with another class, or more effectively, should collect more samples.

5.5 Risk Analysis

Thus far, we have proposed a methodology i) to create load profiles; ii) to propose a method to classify the load profiles into classes with lower within-variability and iii) to build a classifier to predict the actual classes of the future load profiles. In this section, we propose a cost-based risk approach to calculate risk of energy decisions in non-residential buildings. Equation (5.7) estimates $\hat{\pi}_{it}$, the probability that the next load profile belongs to the i^{th} class, given that the input variables (weather and time) is equal to a specific vector of $X_t = x_t$. At time t, $\hat{\pi}_{it}$'s are calculated for all classes. If μ_i^k and ω_i^k are the average and standard deviation of load profiles in the i^{th} class at the k^{th} hours of a day ($k = 1, 2, ..., 24$), then the most likely, lower, and upper values

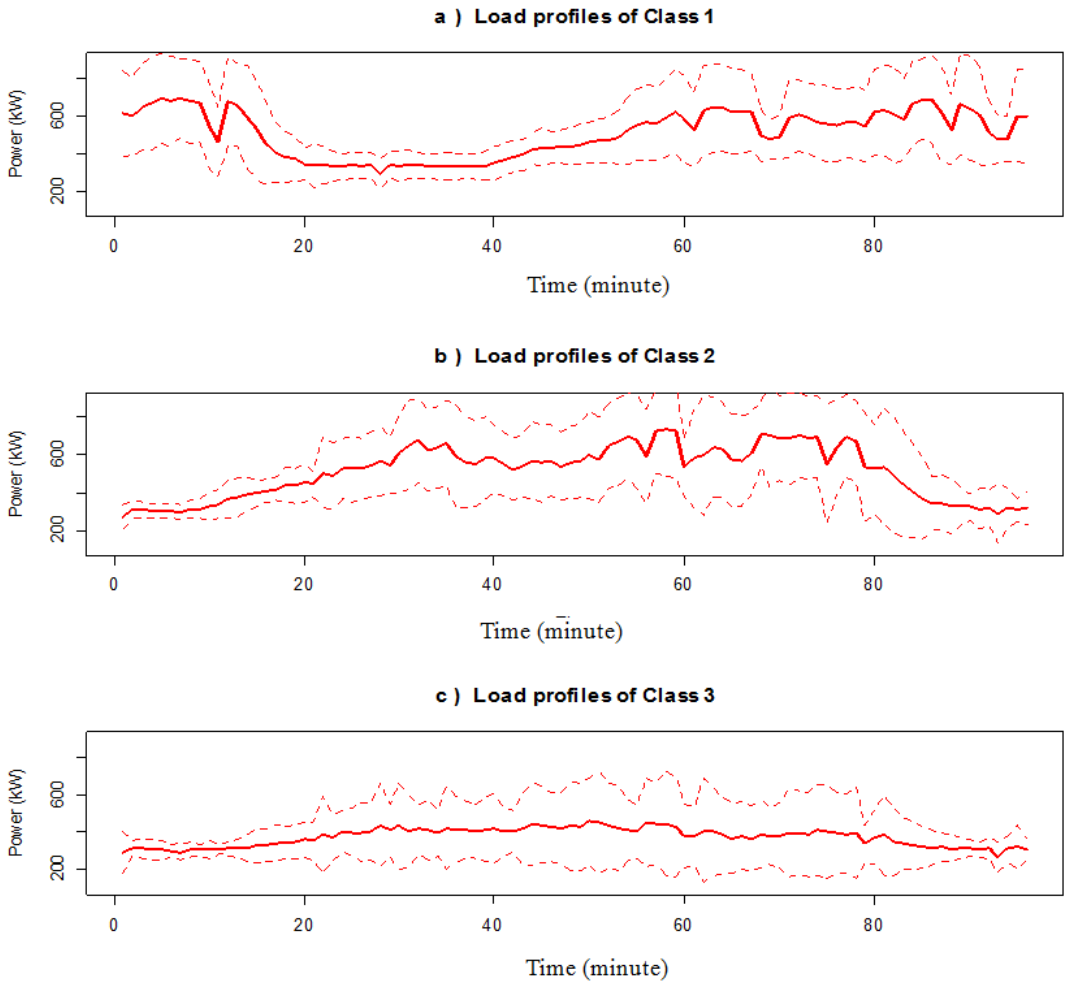

Figure 5.9: The upper, lower, and most likely estimates of load profiles for each class

of load profiles are $\hat{\mu}_i^k$,$\hat{\mu}_i^k - m\hat{w}_i^k$, $\hat{\mu}_i^k + m\hat{w}_i^k$; where m is a multiplier that adjusts the upper and lower values and $\hat{\mu}_i^k$ and $\hat{w}_i^k$ can be obtained as follows:

$$\hat{\mu}_i^k = \frac{\sum_{j=1}^{n_i} y_i^k(j)}{n_i}, w_i^k = \sqrt{\frac{\sum_{j=1}^{n_i} \left(y_i^k(j) - \hat{\mu}_i^k\right)}{n_i}} \tag{5.8}$$

$y_i^k(j)$ is the j^{th} power consumption value associated with k^{th} hour at the i^{th} class. Figure 5.9 presents $\hat{\mu}_i^k$, $\hat{\mu}_i^k - m\hat{w}_i^k$, $\hat{\mu}_i^k + m\hat{w}_i^k$ for the i^{th} class. As mentioned before, the proposed classification method provides the estimation of the probability of the i^{th} class for any given input value. Therefore, the total risk of energy-use can be calculated based on the cost of energy. To do so, assume that c_k is the unit cost of energy per

kWh at time k, and is the cost of daily as-used demand charge. The most likely, lower (worst-case) and upper limits (best-case) of total energy cost can be calculated as follows:

$$TC_i^t = \sum_{k=1}^{N} c_k.\hat{\mu}_i^k.\Delta t + \upsilon.\max_{k\in t_d}\left\{\hat{\mu}_i^k\right\} \tag{5.9}$$

$$TCL_i^t = \sum_{k=1}^{N} c_k.(\hat{\mu}_i^k - m\hat{w}_i^k).\Delta t - \upsilon.\max_{k\in t_d}\left\{\hat{\mu}_i^k - m\hat{w}_i^k\right\} \tag{5.10}$$

$$TCU_i^t = \sum_{k=1}^{N} c_k.(\hat{\mu}_i^k - m\hat{w}_i^k).\Delta t + \upsilon.\max_{k\in t_d}\left\{\hat{\mu}_i^k - m\hat{w}_i^k\right\} \tag{5.11}$$

TC_i^t, TCL_i^t and TCL_i^t are most likely, worst-case, and best-case estimations of the energy cost for the i^{th} class and the t^{th} load profile. Then cost-based risk can be calculated by combining these values for all classes:

$$CR^t \equiv \sum_{k=1}^{c} \hat{\pi}_{i,t} TC_i^t \tag{5.12}$$

$$CRL^t \equiv \sum_{k=1}^{c} \hat{\pi}_{i,t} TCL_i^t \tag{5.13}$$

$$CRU^t \equiv \sum_{k=1}^{c} \hat{\pi}_{i,t} TCU_i^t \tag{5.14}$$

where c is the number of classes and $\hat{\pi}_{i,t}$ is the probability that the t^{th} load profile belongs to the i^{th} class. CR^t, CRL^t and CRU^t are realistic, optimistic and pessimistic cost-based risk values for the t^{th} profile (at day t). In this section, an example is presented to show how the proposed risk model works. Cost of energy per kWh and demand charge cost per unit are similar to Table 3.3. Table 5.2 presents an example of a particular load profile for which the realistic, optimistic and pessimistic risk values are calculated. The first row presents the estimated probability that the load profile belongs to the i^{th} class. The lower, upper and most likely cost of energy presented in other rows. They provides an insight about the lower and upper energy cost that the decision maker expects to see during the day ahead. To evaluate the accuracy of these values, we compare the estimated load daily energy cost using Equation 5.10 and their corresponding actual costs. To do so,$\hat{\pi}_{i,t}$ values are first calculated using the proposed

Table 5.2: Cost-based risk values for a sample load profile

	Class			
i	1	2	3	Total
$\hat{\pi}_{i,t}$	23.50%	71.00%	5.50%	
CR^t	\$324.03	\$289.15	\$199.97	\$292.45
CRL^t	\$248.13	\$214.87	\$155.03	\$219.39
CRU^t	\$400.08	\$363.97	\$246.97	\$366.02

classification technique. Then the estimated cost of energy for each load profile is calculated and compared with the actual cost of energy using the actual profile values in the testing dataset.

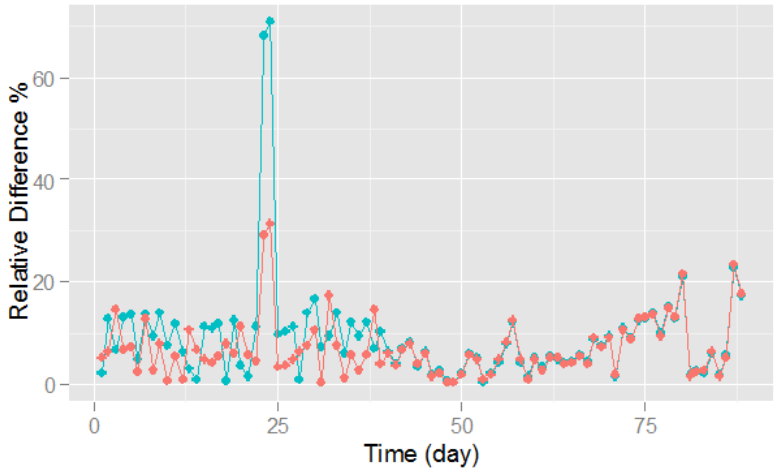

Figure 5.10: The Relative differences between the actual and estimated cost of energy for proposed method (red line) and the average load profile (blue line)

Figure 5.10 shows the relative differences between the actual and estimated cost of energy using the proposed cost-based risk method (red line) as well as total average of load profiles. It shows that the proposed cost-based risk method is often deviated from the actual cost values less than 10% and is superior to the total average load profile. This shows that the cost-based risk method proposed in this chapter is able to provide accurate information about the actual cost of energy.

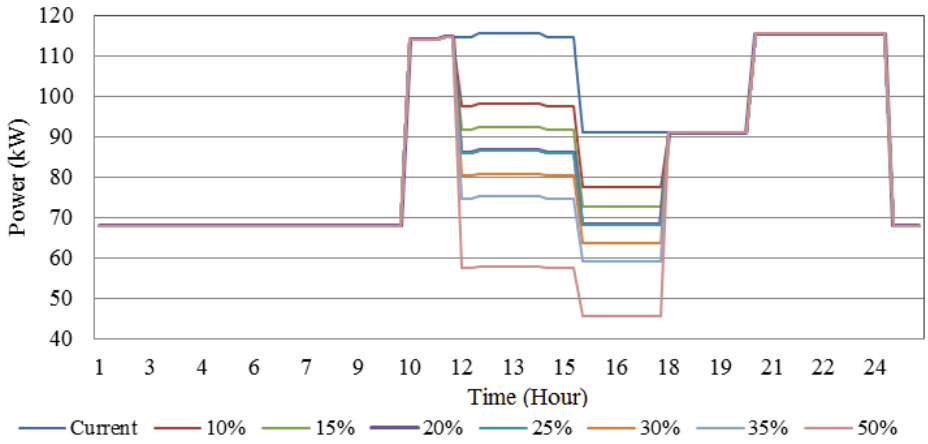

Figure 5.11: Lighting schedule scenarios for the building under study including schedules with k% reduction in total lighting power in peak hours (k=0, 10%, 15%,20%, 25%, 30%, 35%,50%)

Another application of the proposed cost-based risk model is in demand response management. Industrial loads in nonresidential buildings are stochastic and often uncontrollable. In addition, the magnitude of industrial loads is usually much larger than baseline loads. However, since the baseline load is typically controllable, it can still decrease total building power consumption. For example, in a large non-residential building complex, when majority of people are in the dining hall, the heating/cooling or lighting in other buildings (or floors) can be significantly lowered to save a portion of energy and as a result, cost of energy. For example, Figure 5.11 presents a few simple demand response scenarios for reducing the lighting powers in peak hours. In each scenario, a portion of scheduled lighting load is reduced in peak hours in order to lower the total load profile. For each scenario, the most-likely, the best-case and worst-case estimated cost of energy are calculated and their corresponding risk values are evaluated.

Table 5.3 presents the percentage of reduction in risk values for different lighting scenarios presented in Figure 5.11. It is observed that the total cost-based risk values can be reduced by up to 4% by reducing 50% of lighting power in peak hours. This is a small saving compared to the total cost of energy; however, it is directly saved from the

baseline load, which is much smaller than an industrial load. In addition, since daily as-used demand charge is based upon the highest energy consumption over peak hours, even a small portion of saving can have an acceptable impact in total energy costs. Heating/cooling loads can also be minimized to lower consumption in peak hours when there is an industrial load.

Table 5.3: percentage reduction in risk value for different lighting scenarios

	Lighting schedule scenarios							
	0%	10%	15%	20%	25%	30%	35%	50%
Class 1	200.67	199	198.33	197.5	196.67	195.83	194.33	192.67
	0.00%	**0.80%**	**1.20%**	**1.60%**	**2.00%**	**2.40%**	**3.20%**	**4.00%**
Class 2	270.33	268.33	267.33	266.33	265.5	264.67	263.5	262.5
	0.00%	**0.60%**	**1.00%**	**1.30%**	**1.60%**	**1.90%**	**2.50%**	**3.00%**
Class 3	433.75	430.75	429	427.5	426	425	423.75	422.5
	0.00%	**0.70%**	**1.10%**	**1.40%**	**1.80%**	**2.00%**	**2.30%**	**2.60%**
Expected Cost	262.9	261	260	259	258.2	257.3	256.1	254.9
	0.00%	**0.70%**	**1.10%**	**1.40%**	**1.80%**	**2.10%**	**2.50%**	**2.90%**

It is worth noting that, reducing lighting or cooling/heating loads can negatively affect those who live and work in the building. Therefore, it is important to measure the satisfactions of people who are influenced by the demand response programs.
In the previous chapters, we proposed a method to quantify thermal comfort and directly used it in the proposed mathematical models. In this chapter, we use utility theory, which measures and quantifies the preferences of users over a particular good, service, or activity. Researchers often propose different ways to infer underlying relative utilities from observed choice(s) [109, 110]. In most studies, utility functions return values between 0 and 1 representing lowest and highest preferences of the user or the decision maker. For example, Figure 5.12 shows the utility functions associated with total cost of energy (percentage of decrease in energy cost) and lighting scenarios. The x-axis represents: i) the percentage of reduction in peak hours load and ii) the percentage of decrease in total cost of energy. The left y-axis represents the utility values of both cost of energy and lighting scenarios. For example, a 25% reduction in lighting load will result in utility value of 0.82 (see blue line in figure 5.12) for lighting and utility value of 0.5 for cost of energy (see red line in figure 5.12). It is observed that as

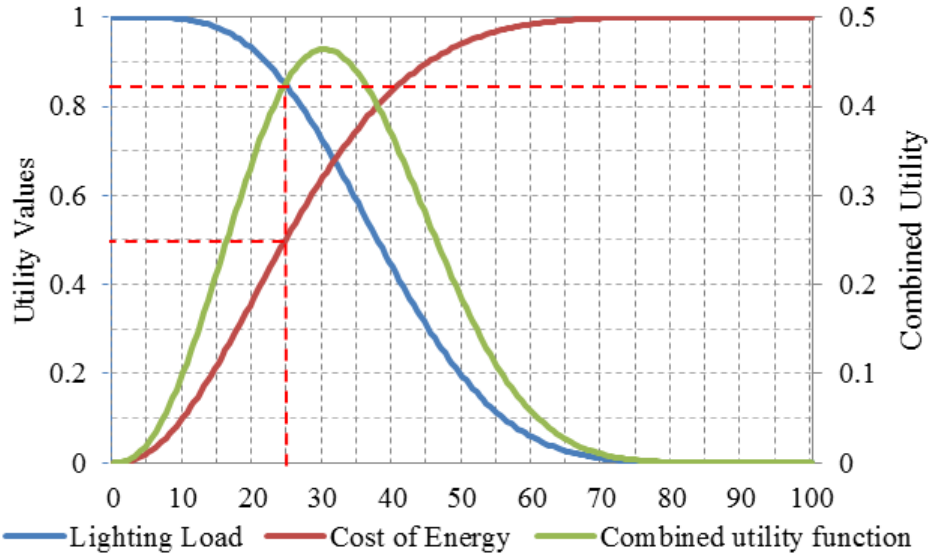

Figure 5.12: An example of utility function for amounts of reduction in cost of energy and in lighting load.

the cost of energy decreases, the utility function increases (blue line). In addition, as lighting load decreases, the utility values decreases.

The right y-axis represents the combined utility that is obtained by taking the geometric average of both utility functions of lighting and total cost of energy. For example, the combined utility value for a 25% reduction in lighting is **0.42**. If the 50%-reduction scenario is selected, then the utility function of lighting and cost would be 0.19 and 0.98, respectively. In this situation, the combined utility is **0.2**, which is less than the 25%-reduction scenario (that is **0.42**). Note that different functional forms can be proposed to build utility models. One way to find utility function is to interactively use the opinion of the user(s) (manager, decision maker etc.). Questionnaire, interview, and other forms of interactions are typically used to find the appropriate utility functions. In Figure 5.12, the maximum combined utility is obtained when 30% of the current lighting schedule is reduced. In this case, the combined utility function is 0.46. Therefore, for this functional form of utility, a 30% reduction in lighting load may not significantly decrease the user satisfaction and at the same time can save more than 2% in total daily cost of energy. A systematic way to create and calculate utility can be a direct

extension of this work.

5.6 Conclusions

The proposed framework utilizes the information of historical data to predict the future patterns of industrial loads. In addition, the risk analysis approach presented in this framework, can be implemented to calculate risk of industrial load in the day ahead. The result shows that the estimated risk is not significantly deviated from the actual cost. In addition, the proposed framework can potentially be used to evaluate different demand response programs and select program with the highest combined utility value.

Chapter 6

Concluding Remarks and Future Researches

6.1 Introduction

In the final chapter, conclusions and a number of potential future researchers are reviewed. In general, this research aims to develop and employ a set of data-driven analytical techniques to capture the behavior of energy dynamics in both building and community levels. Three main problems (questions) have been addressed in this work: i) *Modeling and Forecasting:* there are many factors (covariates) that affect building energy dynamics over time: weather-related factors, time-related factors, occupancy, equipment, building characteristics, machinery, cooling, heating systems, set points, and many other exogenous factors. The question is how to find the effect of such factors on patterns of energy dynamics over time? How to select a limited number of factors to effectively capture variability within energy data? How to develop a statistical model to forecast stochastic patterns of energy dynamics? ii) *Optimization:* Given the statistical forecast model for building energy dynamics, how to manipulate the controllable decision variables (namely, heating, cooling set points) to minimize building total cost of energy as well as total deviations from thermal comfort. iii) *Predictive Analytics/Risk Analysis:* Assuming there are extremely large industrial loads in a non-residential building, how to calculate a realistic, pessimistic and optimistic estimations of total energy costs in the day ahead? In this chapter, we provide brief conclusions for each chapter and discuss how we address the above research questions. In addition, we provide several potential researches that can be done to improve the methods proposed in this study.

6.2 Forecasting of Energy Dynamics

As we discussed in Chapter 2, our proposed forecast model is a hybrid time-series regression model that can be applied to a wide range of energy measures including cooling, heating and electricity load demands, total building energy usage, short-term or long-term community energy usage, HVAC power consumption etc. First, it fits a regression model based on several input variables such as weather data (ambient temperature, relative humidity, wind speed and direction, etc.), occupancy, equipment dynamic information, etc. Then, the residuals (the difference between actual data and predicted values) are calculated. In the next step, a time series model is fitted to explain the variability of the remaining values. The two-step hybrid model does not guarantee to obtain the least square estimation (LSE). To revise it, Cochran-Orcutt estimation algorithm is generalized to achieve LSE values. This algorithm is able to estimate the parameters of both regression component and time series component iteratively and sequentially until it gets very close to the LSE condition.

A number of direct extensions can be done to generalize our proposed forecasting model. In this study, we use a multiple linear regression to start the algorithm. It means that it is assumed the relationship between input variables and energy dynamics is linear. This assumption can be relaxed by using any non-linear models. To the best of our knowledge, Cochran-Orcutt estimation technique has not been developed for nonlinear model, since finding appropriate nonlinear transformation is often difficult. To do this, one can propose a pre-defined structure for both time-series as well as nonlinear regression model and finds the least-square estimators simultaneously for both components using a numerical minimization algorithm. Meta-heuristic and evolutionary algorithms can alternatively be employed to search for LSE estimates.

In addition, we illustrate the effectiveness of our proposed model using a set of training and testing datasets. One can also compare the performance of the proposed model with other competing methods. Gaussian process regression, wavelet transformation techniques, splines, semi-parametric models, and artificial neural network are some of

the competing methods. All of these methods fit a set of input variables to a response (energy data).

Furthermore, the proposed model is appropriate for forecasting purposes. However, for optimization purposes, users should implement it cautiously. In the process of optimization, we manipulate decision variables, to find the best setting that can optimize one or more specific objective functions e.g. total energy cost, or total power consumption. However, the relationship between decision variables and response value is only defined through the first component (regression part). It means that the optimization model can only control the first component of the forecast model. If the regression model is poor or ill-conditioned while the time series component is good, then we can still get good forecast values. However, the model may not work appropriately for optimization. This is also a case for other competing methods.

In order to avoid this problem, one should find the ratio of variability explained by the regression model to that part explained by the time series model. If this ratio is large enough, then the regression part is significantly effective in the process of optimization.

6.3 Forecasting of Energy Dynamics

In Chapters 3 and 4, a cooling/heating model was proposed to forecast the zones internal temperature and/or their corresponding cooling/heating power to reach a specific set point. The model presented in Chapter 3 was originally developed from the first law of thermodynamics. Then the model was improved through use of a statistical model to minimize the distance between the forecast and actual values. Although the proposed model was effective for short-term forecasting, for larger lag it did not perform well. Therefore, in Chapter 4, the model was revised and extended using an ordinary regression structure. The numerical example showed that the extended model was able to adequately forecast the zones internal temperature as well as the zones effective power. In addition, in the heating/cooling model presented in Chapter 3, the parameters were fixed over time. This assumption was relaxed in Chapter 4, by defining a set of time-related indicator variables. The results of the forecast model presented in Chapter 4

were promising. However, in Chapter 4, we used the simulated data to build the model and to evaluate it performance. A future potential research would be to check the result of the proposed cooling/heating data using actual (measured) data.

The model can potentially be extended using more input variables if data are available. For example, the interconnectivity between different zones, number of equipment and their operating status over time, occupancy etc. are some variables that can improve the performance of the proposed model.

6.4 Optimal Control Strategy

In Chapters 3 and 4, we proposed an optimal control strategy to minimize both building total energy cost as well as total deviation from thermal comfort. In both chapters, the decision variables were zones cooling/heating set point values for the next 24 hours.

As mentioned in Chapter 4, the proposed control strategy searched for the same optimal set points for all zones at any time. This was particularly effective when there were relatively large numbers of zones with the same functionality in a buildingsuch as offices, university buildings etc.

One potential extension is to propose a control strategy, which seeks for different set point values for different zones. This can be considered as a large-scale optimization model and the algorithm needs to search in a much bigger feasible region. For a building with r zones, and n possible set point values, at any time algorithm should search for 24nr different combinations. Considering that the process of optimization should be repeated every hour, it is not practical to do an exhaustive search method to seek for the optimal combinations of set point values.

To overcome this problem, one idea is to decrease the search spaces. There are many physical characteristics in building, which can be used to reduce the search space. For example, if there are two similar zones, both offices in a large building with almost same number of people, then it is logical to assume that their set point values should be identical. A zone selection method can be applied to divide zones into a smaller group of zones with similar characteristics.

Another potential extension of our proposed control strategy is to develop an optimization method that is able to deal with large-scale dynamic problems. Dynamic programing is typically considered as an efficient algorithm to search for optimal solution. For many cases, the algorithm process time is polynomial in the number of states (number of zones) as well as number of actions (number of available set point values). However, it is not yet practical for very large problems. Approximating methods can also be chosen to solve large-scale dynamic programming. In such methods, instead of calculating objective functions, one can use a fast approximation that is computationally efficient. In other versions, some algorithms may not search all the combinations of set point values. It means that several algorithms search for a sub-optimal strategy, which provides promising results and is yet computationally efficient.

Another potential research is related to the proposed multi-objective dynamic programing. In this thesis, we used a weighted metric method, which minimized the deviation of each objective function from its ideal value. However, in practical cases, it is not always possible to know the ideal values of objective functions. In addition, in Chapter 4, we discussed that the ideal value could significantly affect the importance of each objective function. Smaller or larger values of ideal values could potentially decrease or increase the importance of objective functions.

Therefore, another multiobjective programing methods can be proposed to deal with this problem. Multiobjective dynamic programing based on the theory of utility can be considered as an alternative. For both total building energy cost and thermal comfort, decision makers often know their preferences and as a result can use it to form a utility function structure.

6.5 Predictive Analytics

In Chapter 5, we illustrated one application of predicative analytics approach to reduce cost-based risk of load consumption in non-residential buildings. A general framework was introduced to combine predictive analytics approach and cost-based risk analysis to evaluate the demand response programs.

Furthermore, this chapter opens up a wide range of potential researches in the area of building energy analytics. Nowadays, technology allows us to extract big amount of real data from all equipment within a building. There is no limitation for the volume and type of data collected over a very short period of time. These data include patterns with assignable causes, consumption behavior, and other useful information that can effectively be used to reduce energy use. One potential extension for Chapter 6, is to develop an integrated framework that determine all input, output and methodologies to develop a data-driven recommendation system. This data-driven structure determines the type of input data, source of input data, data collection equipment, methods for analyzing datapredictive analytics, output format, reporting system, optimization techniques, list of actions and all other required information. The proposed energy-analytics structure can then collect energy data, learns the pattern, and provides optimal actions/recommendation to reduce cost of energy, deviation from thermal comfort, carbon footprint etc. The data-collector and controllers can be implemented in any buildings and can feed into the proposed energy-analytics structure. This structure can also be hosted online so that users can track their energy information in real time.

References

[1] U.S. Department of Energy. Energy Efficiency (2012) & Renewable Energy *2011 Buildings Energy Data Book* available at `http://buildingsdatabook.eren.doe.gov/docs/DataBooks/2011_BEDB.pdf`, Sep 2014.

[2] US Department of Energy (2008).*Energy Efficiency Trends in Residential and Commercial Buildings.* available at `http://apps1.eere.energy.gov/buildings/publications/pdfs/corporate/bt_stateindustry.pdf`, Sep 2014.

[3] US Department of Energy (2008).*Energy Efficiency Trends in Residential and Commercial Buildings.* available at `http://apps1.eere.energy.gov/buildings/publications/pdfs/corporate/bt_stateindustry.pdf`, Sep 2014.

[4] US Department of Energy (2005).*Annual Energy Review 2004* Washington, DC, Annual Report 061-003-01141-1, available at `http://www.eia.gov/totalenergy/data/annual/archive/038404.pdf`, Sep 2014.

[5] US Department of Energy (2003).*Grid 2030: A National Vision For Electricity's Second 100 Years.*, available at `http://energy.gov/sites/prod/files/oeprod/DocumentsandMedia/Electric_Vision_Document.pdf`, Sep 2014.

[6] Wu, D. W., & Wang, R. Z. (2006). Combined cooling, heating and power: a review.*progress in energy and combustion science*,32(5), 459-495.

[7] Jian, Y. (2010). Research on the optimization of building energy efficient measures based on incremental costs. In.*2010 2nd International Conference on Computer Engineering and Technology*, (Vol. 6).

[8] San Martn, J. I., Zamora, I., San Martn, J. J., Aperribay, V., & Egua, P. (2008). Trigeneration Systems with Fuel Cells. *POWER*, 40, 65-85.

[9] Ye, L., & Yi, L. (2011). Optimal design of distributed CCHP system. *P In Transportation, Mechanical, and Electrical Engineering (TMEE), 2011 International Conference on*, (pp. 1961-1965). IEEE.

[10] Cho, H., Mago, P. J., Luck, R.,& Chamra, L. M. (2009). Evaluation of CCHP systems performance based on operational cost, primary energy consumption, and carbon dioxide emission by utilizing an optimal operation scheme. *Applied Energy*, 86(12), 2540-2549.

[11] Liu, M., Shi, Y., & Fang, F. (2013). Optimal power flow and PGU capacity of CCHP systems using a matrix modeling approach. *Applied Energy*, 102, 794-802.

[12] Cho, H., Eksioglu, S. D., Luck, R., & Chamra, L. M. (2008). Operation of a cchp system using an optimal energy dispatch algorithm. *In ASME 2008 2nd International Conference on Energy Sustainability collocated with the Heat Transfer, Fluids*

Engineering, and 3rd Energy Nanotechnology Conferences pp. 747-754). American Society of Mechanical Engineers.

[13] Kong, X. Q., Wang, R. Z., & Huang, X. H. (2005). Energy optimization model for a CCHP system with available gas turbines. *Applied Thermal Engineering*, 25(2), 377-391.

[14] Chandan, V., Do, A. T., Jin, B., Jabbari, F., Brouwer, J., Akrotirianakis, I., Chakraborty, A. & Alleyne, A. (2012). Modeling and optimization of a combined cooling, heating and power plant system.. *American Control Conference*, pp. 3069-3074, IEEE.

[15] Mago, P. J., & Chamra, L. M. (2009).Analysis and optimization of CCHP systems based on energy, economical, and environmental considerations. Energy and Buildings. *Applied Thermal Engineering*, , 41(10), 1099-1106.

[16] Wang, J. J., Jing, Y. Y., & Zhang, C. F. (2010). Optimization of capacity and operation for CCHP system by genetic algorithm. *Applied Energy* 87(4), 1325-1335.

[17] Hu, M., & Cho, H. (2014). A probability constrained multi-objective optimization model for CCHP system operation decision support. *Applied Energy*, 116, 230-242.

[18] Box, George EP, Gwilym M. Jenkins, and Gregory C. Reinsel. *Time series analysis: forecasting and control*. John Wiley & Sons, 2013.

[19] Huang, S. J., & Shih, K. R. (2003). Short-term load forecasting via ARMA model identification including non-Gaussian process considerations. *Power Systems, IEEE Transactions on,* 18(2), 673-679.

[20] Muche, T. (2014). Optimal operation and forecasting policy for pump storage plants in day-ahead markets. *Applied Energy*, 113, 1089-1099.

[21] Taylor, J. W., McSharry, P. E., & Buizza, R. (2009). Wind power density forecasting using ensemble predictions and time series models. *Energy Conversion, IEEE Transactions on,* 24(3), 775-782.

[22] Garca-Martos, C., Rodrguez, J., & Snchez, M. J. (2013). Modelling and forecasting fossil fuels, CO2 and electricity prices and their volatilities. *Applied Energy*, 101, 363-375.

[23] Amjady, N. (2001). Short-term hourly load forecasting using time-series modeling with peak load estimation capability. *Power Systems, IEEE Transactions on*, 16(3), 498-505.

[24] Abdel-Aal, R. E., & Al-Garni, A. Z. (1997). Forecasting monthly electric energy consumption in eastern Saudi Arabia using univariate time-series analysis. *Energy,* 22(11), 1059-1069.

[25] Mbamalu, G. A. N., & El-Hawary, M. E. (1993). Load forecasting via suboptimal seasonal autoregressive models and iteratively reweighted least squares estimation. Power Systems, IEEE Transactions on, 8(1), 343-348.

[26] Goia, A., May, C., & Fusai, G. (2010). Functional clustering and linear regression for peak load forecasting. *International Journal of Forecasting*, 26(4), 700-711.

[27] Serinaldi, F. (2011). Distributional modeling and short-term forecasting of electricity prices by Generalized Additive Models for Location, Scale and Shape. *Energy Economics*, 33(6), 1216-1226.

[28] Jain, R. K., Smith, K. M., Culligan, P. J., & Taylor, J. E. (2014). Forecasting energy consumption of multi-family residential buildings using support vector regression: Investigating the impact of temporal and spatial monitoring granularity on performance accuracy. *Applied Energy*, 123, 168-178.

[29] Apadula, F., Bassini, A., Elli, A., & Scapin, S. (2012). Relationships between meteorological variables and monthly electricity demand. *Applied Energy*, 98, 346-356.

[30] Mavromatidis, L. E., Bykalyuk, A., & Lequay, H. (2013). Development of polynomial regression models for composite dynamic envelopes thermal performance forecasting. *Applied Energy*, 104, 379-391.

[31] Inman, R. H., Pedro, H. T., & Coimbra, C. F. (2013). Solar forecasting methods for renewable energy integration. *Progress in Energy and Combustion Science,*39(6), 535-576.

[32] Yang, H. T., Huang, C. M., & Huang, C. L. (1995, May). Identification of ARMAX model for short term load forecasting: an evolutionary programming approach. In Power Industry Computer Application Conference, 1995. *Conference Proceedings., 1995 IEEE* (pp. 325-330). IEEE.

[33] Yang, H. T., & Huang, C. M. (1998). A new short-term load forecasting approach using self-organizing fuzzy ARMAX models. *Power Systems, IEEE Transactions on*, 13(1), 217-225.

[34] Kalogirou, S. A. (2003). Artificial intelligence for the modeling and control of combustion processes: a review. *Progress in Energy and Combustion Science,*29(6), 515-566.

[35] Mellit, A., & Kalogirou, S. A. (2008). Artificial intelligence techniques for photovoltaic applications: A review. *Progress in Energy and Combustion Science,* 34(5), 574-632.

[36] Kankal, M., Akpnar, A., Kmrc, M. ., & zahin, T. . (2011). Modeling and forecasting of Turkeys energy consumption using socio-economic and demographic variables. *Applied Energy*, 88(5), 1927-1939.

[37] Kulkarni, S., Simon, S. P., & Sundareswaran, K. (2013). A spiking neural network (SNN) forecast engine for short-term electrical load forecasting.*Applied Soft Computing*, 13(8), 3628-3635.

[38] Kandil, N., Wamkeue, R., Saad, M., & Georges, S. (2006). An efficient approach for short term load forecasting using artificial neural networks.*International Journal of Electrical Power & Energy Systems*, 28(8), 525-530.

[39] Deihimi, A., Orang, O., & Showkati, H. (2013). Short-term electric load and temperature forecasting using wavelet echo state networks with neural reconstruction. *Energy*, 57, 382-401.

[40] Liu, H., Tian, H. Q., Pan, D. F., & Li, Y. F. (2013). Forecasting models for wind speed using wavelet, wavelet packet, time series and Artificial Neural Networks. *Applied Energy*, 107, 191-208.

[41] Lee, Y. S., & Tong, L. I. (2012). Forecasting nonlinear time series of energy consumption using a hybrid dynamic model. *Applied Energy*, 94, 251-256.

[42] Li, K., & Su, H. (2010). Forecasting building energy consumption with hybrid genetic algorithm-hierarchical adaptive network-based fuzzy inference system. *Energy and Buildings*, 42(11), 2070-2076.

[43] Lin, C. T., Chou, L. D., Chen, Y. M., & Tseng, L. M. (2014). A hybrid economic indices based short-term load forecasting system. *International Journal of Electrical Power & Energy Systems*, 54, 293-305.

[44] Kutner, M. H. (1996). Applied linear statistical models (Vol. 4). Chicago: Irwin.

[45] Cochrane, Donald, and Guy H. Orcutt. "Application of least squares regression to relationships containing auto-correlated error terms." *Journal of the American Statistical Association* 44.245 (1949): 32-61.

[46] Fu, M. C. (2002). Optimization for simulation: Theory vs. practice. *INFORMS Journal on Computing*, 14(3), 192-215.

[47] Borrelli, F., Bemporad, A., & Morari, M. (2012). Predictive control. Draft Available at: `http://www.mpc.berkeley.edu/mpc-course-material`(in preparation).

[48] Ma, Y., Matusko, J., & Borrelli, F. (2013). Stochastic Model Predictive Control for Building HVAC Systems: Complexity and Conservatism. *Control Systems Technology, IEEE Transactions on* v.99, pp.1,1 .

[49] Oldewurtel, F., Parisio, A., Jones, C. N., Gyalistras, D., Gwerder, M., Stauch, V., ... & Morari, M. (2012). Use of model predictive control and weather forecasts for energy efficient building climate control. *Energy and Buildings*, 45, 15-27.

[50] Henze, G. P., Felsmann, C., & Knabe, G. (2004). Evaluation of optimal control for active and passive building thermal storage. *International Journal of Thermal Sciences*, 43(2), 173-183.

[51] Vasak, M., Starcic, A., & Martincevic, A. (2011, May). Model predictive control of heating and cooling in a family house. In MIPRO, *2011 Proceedings of the 34th International Convention* (pp. 739-743). IEEE.

[52] Ma, Y., Kelman, A., Daly, A., & Borrelli, F. (2012). Predictive control for energy efficient buildings with thermal storage. *IEEE control systems magazine*, 32(1), 44-64.

[53] Ma, Y., Borrelli, F., Hencey, B., Coffey, B., Bengea, S., & Haves, P. (2012). Model predictive control for the operation of building cooling systems. *Control Systems Technology, IEEE Transactions on,* 20(3), 796-803.

[54] Mady, A. E. D., Provan, G., Ryan, C., & Brown, K. N. (2011, August). Stochastic Model Predictive Controller for the Integration of Building Use and Temperature Regulation In *AAAI*.

[55] Bohlin, T., & Graebe, S. F. (1995). Issues in nonlinear stochastic grey box identification. International *Journal of Adaptive Control and Signal Processing*, 9(6), 465-490.

[56] Lehmann, B., Gyalistras, D., Gwerder, M., Wirth, K., & Carl, S. (2013). Intermediate complexity model for model predictive control of integrated room automation. *Energy and Buildings*, 58, 250-262.

[57] Ma, J., Qin, J., Salsbury, T., & Xu, P. (2012). Demand reduction in building energy systems based on economic model predictive control. *Chemical Engineering Science*, 67(1), 92-100.

[58] Ma, J., Qin, S. J., & Salsbury, T. (2013, June). Experimental study of economic model predictive control in building energy systems. In *American Control Conference (ACC)*, 2013 (pp. 3753-3758). IEEE.

[59] Prvara, S., irok, J., Ferkl, L., & Cigler, J. (2011). Model predictive control of a building heating system: The first experience. *Energy and Buildings*, 43(2), 564-572.

[60] Mahdavi, A., & Prglhf, C. (2008). A model-based approach to natural ventilation. Building and Environment, 43(4), 620-627.

[61] Kolokotsa, D., Pouliezos, A., Stavrakakis, G., & Lazos, C. (2009). Predictive control techniques for energy and indoor environmental quality management in buildings. *Building and Environment*, 44(9), 1850-1863.

[62] Yang, J., Rivard, H., & Zmeureanu, R. (2005). On-line building energy prediction using adaptive artificial neural networks. *Energy and buildings*,37(12), 1250-1259.

[63] Yang, J., Rivard, H., & Zmeureanu, R. (2005). On-line building energy prediction using adaptive artificial neural networks. E*nergy and buildings*,37(12), 1250-1259.

[64] Pang, X., Wetter, M., Bhattacharya, P., & Haves, P. (2012). A framework for simulation-based real-time whole building performance assessment. *Building and Environment*, 54, 100-108.

[65] Kmpf, J. H., Wetter, M., & Robinson, D. (2010). A comparison of global optimization algorithms with standard benchmark functions and real-world applications using EnergyPlus. *Journal of Building Performance Simulation*,3(2), 103-120.

[66] Wetter, M., & Wright, J. (2004). A comparison of deterministic and probabilistic optimization algorithms for nonsmooth simulation-based optimization. *Building and Environment*, 39(8), 989-999.

[67] Wetter, M. (2011). Co-simulation of building energy and control systems with the Building Controls Virtual Test Bed. *Journal of Building Performance Simulation*, 4(3), 185-203.

[68] Kontes, G. D., Valmaseda, C., Giannakis, G. I., Katsigarakis, K. I., & Rovas, D. V. (2014). Intelligent BEMS design using detailed thermal simulation models and surrogate-based stochastic optimization. *Journal of Process Control*.

[69] Zhou, Y. P., Wu, J. Y., Wang, R. Z., Shiochi, S., & Li, Y. M. (2008). Simulation and experimental validation of the variable-refrigerant-volume (VRV) air-conditioning system in EnergyPlus. *Energy and buildings*, 40(6), 1041-1047.

[70] Melki, S., & Hayek, M. (2009, July). Building simulation tools and their role in improving existing building designs. In Advances in Computational Tools for Engineering Applications, 2009. *ACTEA'09. International Conference on* (pp. 503-507). IEEE.

[71] Regulatory Assistance Project and ICF International (2009) Standby Rates for Customer-Sited Resources, Issues, considrations and the Elements of Model Tariffs, A report prepared for U.S. Environmental Protection Agency; Office of Atmospheric Programs Climate Protection Partnerships. available `http://www.epa.gov/chp/documents/standby_rates.pdf`

[72] Eschenauer, H. A., Koski, J., & Osyczka, A. *Multicriteria Design Optimization: Procedures and Applications*. 1986. NY: Springer-Verlag.

[73] Collette, Y., & Siarry, P. *Multiobjective optimization: principles and case studies*. 2003. New York: Springer; 2003.

[74] Kasprzak, E. M., & Lewis, K. E. (2001). Pareto analysis in multiobjective optimization using the collinearity theorem and scaling method. *Structural and Multidisciplinary Optimization*, 22(3), 208-218.

[75] Deru, M., Field, K., Studer, D., Benne, K., Griffith, B., Torcellini, P., ... & Crawley, D. (2011). US Department of Energy commercial reference building models of the national building stock.

[76] Bertsekas, D. P., & Bertsekas, D. P. (1995). *Dynamic programming and optimal control* (Vol. 1, No. 2). Belmont, MA: Athena Scientific.

[77] Barto, A. G. (1998). Reinforcement learning: An introduction. MIT press.

[78] Tsitsiklis, J. N., & Van Roy, B. (1996). Feature-based methods for large scale dynamic programming. *Machine Learning*, 22(1-3), 59-94.

[79] Cai, Y., & Judd, K. L. (2010). Stable and efficient computational methods for dynamic programming. Journal of the European Economic Association, 8(23), 626-634.

[80] Judd, K. L. (1998). Numerical methods in economics. MIT press.

[81] U.S. Energy Information Administration 2014, The International Energy Outlook 2014: World Petroleum and Other Liquid Fuels, with Projection of 2040, U.S. Department of Energy, available at `http://www.eia.gov/forecasts/ieo/`

[82] US Department of Energy (2009).*Annual Energy Review 2008* Washington, DC, Annual Report 061-003-01141-1, available at `http://www.eia.gov/totalenergy/data/annual/archive/038408.pdf`, Sep 2014.

[83] Westphal, F. S., & Lamberts, R. (200). The use of simplified weather data to estimate thermal loads of non-residential buildings. *Energy and buildings*, 36(8), 847-854.

[84] Coughlin, K., Piette, M. A., Goldman, C., & Kiliccote, S. (2009). Statistical analysis of baseline load models for non-residential buildings. *Energy and Buildings*, 41(4), 374-381.

[85] Awan, S. M., Khan, Z. A., Aslam, M., Mahmood, W., & Ahsan, A. (2012, May). Application of NARX based FFNN, SVR and ANN Fitting models for long term industrial load forecasting and their comparison. In Industrial Electronics (ISIE), 2012 *IEEE International Symposium on* (pp. 803-807). IEEE.

[86] Azadeh, A., Ghaderi, S. F., & Sohrabkhani, S. (2008). Annual electricity consumption forecasting by neural network in high energy consuming industrial sectors. *Energy Conversion and Management*, 49(8), 2272-2278.

[87] Bianco, V., Manca, O., Nardini, S., & Minea, A. A. (2010). Analysis and forecasting of nonresidential electricity consumption in Romania. *Applied Energy*, 87(11), 3584-3590.

[88] Penya, Y. K., Borges, C. E., Agote, D., & Fernndez, I. (2011, June). Short-term load forecasting in air-conditioned non-residential Buildings. *In Industrial Electronics (ISIE)*, 2011 IEEE International Symposium on (pp. 1359-1364). IEEE.

[89] Vijayaraghavan, A., & Dornfeld, D. (2010). Automated energy monitoring of machine tools. *CIRP Annals-Manufacturing Technology*, 59(1), 21-24.

[90] Bruzzone, A. A. G., Anghinolfi, D., Paolucci, M., & Tonelli, F. (2012). Energy-aware scheduling for improving manufacturing process sustainability: a mathematical model for flexible flow shops. *CIRP Annals-Manufacturing Technology*, 61(1), 459-462.

[91] Grimes, D., Ifrim, G., OSullivan, B., & Simonis, H. (2014). Analyzing the Impact of Electricity Price Forecasting on Energy Cost-Aware Scheduling. *Sustainable Computing: Informatics and Systems*.

[92] Guzek, M., Pecero, J. E., Dorronsoro, B., & Bouvry, P. (2014). Multi-objective evolutionary algorithms for energy-aware scheduling on distributed computing systems. *Applied Soft Computing*.

[93] Dai, M., Tang, D., Giret, A., Salido, M. A., & Li, W. D. (2013). Energy-efficient scheduling for a flexible flow shop using an improved genetic-simulated annealing algorithm. *Robotics and Computer-Integrated Manufacturing*, 29(5), 418-429.

[94] Hastie, T., Tibshirani, R., Friedman, J., Hastie, T., Friedman, J., & Tibshirani, R. (2009). *The elements of statistical learning* (Vol. 2, No. 1). New York: Springer.

[95] Siegel, E. (2013). *Predictive analytics: the power to predict who will click, buy, lie, or die*. John Wiley & Sons.

[96] Tukey, J. W. (1977). *Exploratory data analysis*.

[97] Hartwig, F., & Dearing, B. E. (Eds.). (1979). *Exploratory data analysis*. Sage.

[98] van Dam, K. K., Lansing, C., Elsethagen, T., Hathaway, J., Guillen, Z., Dirks, J., Skorski, D. Stephan, E. Gorrissen, W. Gorton I, & Liu, Y. (2014, August). Nationwide buildings energy research enabled through an integrated data intensive. *Building Simulation* (Vol. 7, No. 4, pp. 335-343). Tsinghua University Press.

[99] Talebpour, M. R., Stewart, R. A., Beal, C., Dowling, B., Sharma, A., & Fane, S. (2011). Rainwater Tank End Usage and Energy Demand-A pilot study. *Water-Australian Water and Wastewater Association*, 38(1), 97.

[100] Qu, J., Li, L., Liu, L., Tian, Y., & Chen, J. (2013, July). Smart temperature monitoring for data center energy efficiency. In *Service Operations and Logistics, and Informatics (SOLI)*, 2013 *IEEE International Conference on* (pp. 360-365). IEEE.

[101] Bouveyron, C., & Brunet, C. (2012). Simultaneous model-based clustering and visualization in the Fisher discriminative subspace. *Statistics and Computing*,22(1), 301-324.

[102] Bouveyron, C., & Brunet-Saumard, C. (2014). Model-based clustering of high-dimensional data: A review. Computational Statistics & *Data Analysis*, 71, 52-78.

[103] Bouveyron, Charles, Stphane Girard, and Cordelia Schmid. (2007). High-dimensional data clustering. Computational Statistics & *Data Analysis* 52, no. 1 502-519.

[104] Bouveyron, C., Girard, S., & Schmid, C. (2007). High-dimensional data clustering. Computational Statistics & *Data Analysis*, 52(1), 502-519.

[105] Berg, L., Bouveyron, C., & Girard, S. (2012). HDclassif: An R package for model-based clustering and discriminant analysis of high-dimensional data. *Journal of Statistical Software,* 46(6), 1-29.

[106] Agresti, A. (2014). *Categorical data analysis*. John Wiley & Sons.

[107] Czepiel, S. A. (2002). Maximum likelihood estimation of logistic regression models: theory and implementation. Available at `http://czep.net/stat/mlelr.pdf`

[108] Venables, W. N., & Ripley, B. D. (2002). *Modern applied statistics with S*. Springer.

[109] Orsborn, S., Cagan, J., & Boatwright, P. (2009). Quantifying aesthetic form preference in a utility function. *Journal of Mechanical Design*, 131(6), 061001.

[110] Houthakker, H. S. (1950). Revealed preference and the utility function.*Economica*, 159-174.